

https://dspace.org/

Numerical investigation on aerodynamic and flight dyanamic performances of piezoelectric actuation for civil aviation aircraft

Keeka, Hemansu

2016

http://hdl.handle.net/10539/22445

Keeka, Hemansu (2016) Numerical investigation on aerodynamic and flight dynamic performances of piezoelectric actuation for civil aviation aircraft, University of the Witwatersrand, Johannesburg, <http://hdl.handle.net/10539/22445>

Downloaded from a DSpace repository. https://dspace.org/

Numerical Investigation on Aerodynamic and Flight Dynamic Performances of Piezoelectric Actuation for Civil Aviation Aircraft

Hemansu Keeka

A dissertation submitted to the Faculty of Engineering and the Built Environment, University of the Witwatersrand, Johannesburg, in fulfilment of the requirements for the degree of Master of Science in Engineering

Johannesburg, September 2016

DECLARATION

I declare that this dissertation is my own, unaided work, except where otherwise acknowledged. It is being submitted for the degree of Master of Science in Engineering in the University of the Witwatersrand, Johannesburg. It has not been submitted before for any degree or examination at any other university.

Signed this 15th day of September 2016

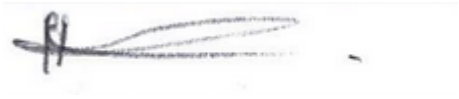

_____

Hemansu Keeka

"I dedicate this Master's dissertation to my loving family:

***Kanti**, my Father,*

***Damyanti**, my Mother,*

***Yagnash**, my Brother,*

*And **Rakhee**, my Fiancée.*

Thank you for all your support, patience and continual encouragement for this milestone."

ACKNOWLEDGEMENTS

I would like to sincerely thank my supervisor, Professor J. O. Pedro for the patience, guidance and assistance throughout this research.

I would like to thank Shawn Sampson, Business Process Manager from Textron Aviation for providing the Cessna Citation V flight and operating manuals.

ABSTRACT

The work in this dissertation presents the analysis of developing a novel means of flight trajectory alteration of a civil aircraft. Piezoelectric actuators have been advancing in the aerospace industry with uses in structural, vibrational and sensing applications. However, they have not been considered as a primary control method like an elevator, aileron and rudder. The analysis performed in this research involved developing an actuation model which is designed such that various changes in flight trajectory are brought about. The analysis began by building a base rigid aircraft model, where other analyses were appended to. The rigid aircraft model was developed using the aerodynamics of both Roskam (2001) and DATCOM. The DATCOM model was found to compensate for additional aircraft positions outside the flight envelope, whereas Roskam (2001) did not adequately provide the aerodynamics for when the aircraft would experience stall conditions, for example. The research then lead into developing the piezoelectric actuation model. This involved utilizing piezoelectric actuators on the wing of the aircraft, which was set to create vertical and twisting deformations, without altering the wing's camber. Two novel methods of actuation are discussed. A wing - twist mode which consisted of three types of actuation, viz. linear twist, inverse linear twist, and linear twist symmetric. The second was the bending mode which altered the aircraft's dihedral, and consisted of two types of actuation, viz. linear bending and linear bending symmetric. Effects of these two modes on the aerodynamics were depicted. Added to the overall model was the analysis of elastic aerodynamic effects. This was conducted by performing vibrational analysis on the individual components of the aircraft, viz. wing, horizontal tail and vertical tail. The results found that the elastic aerodynamic effects on the rigid model were significant only in lift. The rest were not significant because of the high frequency of the beams under consideration. Conclusively, the novel actuation methodology developed in this research yielded results demonstrating the viability of it being used above conventional methods such as elevator, rudder and ailerons. This was found by noting that various trajectory alterations were perceived without input from the conventional actuation methods. Increase in the rotational motions, as well as the translational motion was found, but did not cause any dynamic instabilities in the aircraft model. Thus, the actuation model was seen to operate well above the conventional methods, and situation specific uses were described for the actuation modes. These include uses in take-off and landing, cruise optimization and coordinated turns.

CONTENTS

DECLARATION i
ACKNOWLEDGEMENTS iii
ABSTRACT iv
CONTENTS v
LIST OF FIGURES viii
LIST OF TABLES xi
NOMENCLATURE xii
1. INTRODUCTION 1
1.1. Background 2
1.1.1. Flexible Wing 2
1.1.2. Smart Materials: Piezoelectric Actuator 4
1.2. Literature Review 7
1.2.1. Actuation Mechanisms on Aircraft 7
1.2.2. Smart Materials: Piezoelectric Actuators 10
1.2.3. Effects of Flexible Wings 19
1.2.4. Why Piezoelectric Actuation Over Conventional Methods? 20
1.2.5. Research Gaps in the Literature 21
1.3. Motivation 21
1.4. Research Objectives 22
1.5. Design Assumptions 23
1.6. Research Question 23
1.7. Research Strategy and Methodology 23
1.7.1. Flight Conditions 24
1.7.2. Rigid Aircraft Model 24
1.7.3. Piezoelectric Actuation Model 25
1.7.4. Effects of Elastic Deformation on the Aerodynamic Forces and Moments 25
1.7.5. Results 26
1.7.6. Flight Conditions Identified 26
1.8. Contributions to Knowledge 27
1.9. Layout of Dissertation 28
2. RIGID AIRCRAFT MODEL 30
2.1. Coordinate System 30

2.2. Equations of Motion 32
2.3. Aerodynamic Forces and Moments 34
2.4. Aerodynamic Coefficients 37
2.5. Atmospheric Properties 42
2.6. Trim Conditions 43
2.7. Rigid Model Simulation 44
3. PIEZOELECTRIC ACTUATION MODEL 50
3.1. Assumptions 50
3.2. Actuation Methods 51
3.2.1. Twisting Actuation 52
3.2.2. Bending Actuation 61
3.3. Piezoelectric Actuator Simulation 70
4. EFFECTS OF ELASTIC DEFORMATION ON THE AERODYNAMIC FORCES AND MOMENTS 73
4.1. Vibration of a Cantilever Beam 73
4.1.1. Initial Conditions 76
4.2. Elastic Effects on the Aircraft Aerodynamics 79
4.2.1. Lift 80
4.2.2. Side Force 81
4.2.3. Pitching Moment 81
4.2.4. Rolling Moment 83
4.2.5. Yawing Moment 84
4.3. Simulation of Deformation Effects 85
5. RESULTS 88
5.1. Conventional Actuation 88
5.2. Rigid Aircraft Model + Piezoelectric Actuation 91
5.3. Rigid Aircraft Model + Piezoelectric Actuation + Effects on Aerodynamics due to Elastic Deformation 97
6. CONCLUSIONS 102
6.1. Conclusions 102
6.2. Recommendations for Future Work 103
REFERENCES 105
APPENDIX A – Aircraft Properties 110
APPENDIX B – Aircraft Mass Data 111

APPENDIX C – DATCOM Model 115

LIST OF FIGURES

Figure 1: Active Aeroelastic Wing Operation 4
Figure 2: Smart Structure Method of Operation [Akhras (2000)]. 5
Figure 3: Piezoelectric Actuator Configuration showing simple Deformation 6
Figure 4: Fly-by-wire Flight Control System [Collinson (1999)] 9
Figure 5: Orientation of Piezoceramic Layers on the Smart Fin in Correlation to the Passive Structural Layers [Nir and Abramovich (2010)] 11
Figure 6: Piezoelectric Actuator Placement with Fin Mode Shapes: a) First Bending, b) First Torsional, c) Second Bending [Mehrabian and Yousefi-Koma (2007)] 12
Figure 7: Piezoelectric Actuator Panel Positioning [Li *et al.*, (2011)] 12
Figure 8: High Aspect Ratio Piezoelectric Actuator Positioning on a Cessna Citation Wing [Tuzcu and Meirovitch (2006)] 13
Figure 9: Wing of the Cessna Citation V Researched [Martindale (2011)] 14
Figure 10: Solid State Control Surfaces with Piezoelectric Actuators of an Unmanned Aerial Vehicle (Remote Control Plane) [Bilgen *et al.*, (2013)] 15
Figure 11: Flight Vehicle Demonstrator with Piezoelectric Actuator Position [Suleman and Costa (2004)] 15
Figure 12: Parallel and Serial Configuration of a Bimorph [PI (2004)] 16
Figure 13: Cantilever Bimorph Showing Dimensions. a) Top View, b) Side View 18
Figure 14: Phases of Flight 27
Figure 15: Dissertation Layout Showing Connections between Various Chapters 29
Figure 16: Body Axis Coordinate System for the Aircraft 30
Figure 17: Notation for angle of Attack and Sideslip 31
Figure 18: Rotational Rates showing Instability of the Initial Rigid Model 42
Figure 19: Aircraft Body Axis Velocity U with Earth Fixed Velocity X_E 45
Figure 20: Body Axis Velocity W with Earth Fixed Velocity Z_E 45
Figure 21: Aircraft Velocity Vector V_∞ with Angle of Attack α 46
Figure 22: Aircraft Pitching Moment M 46
Figure 23: Aircraft Lift Force L and Drag Force D 47
Figure 24: Aircraft Body Axis Forces F_X and F_Z 47
Figure 25: Aircraft Body Axis Pitch Rate Q 48
Figure 26: Aircraft Euler Pitch Angle θ 48
Figure 27: Aerodynamic Coefficients of Lift (C_L), Drag (C_D) and Pitching Moment (C_M) 49
Figure 28: Mode Shape Deflections of a Simple Cantilever I-Beam 51
Figure 29: Wing Profile Showing Placement of Piezoelectric Bender Actuators 52
Figure 30: Wing Profile Showing Vertical Displacements due to Positive Twist 53
Figure 31: Wing Planform Showing Actuator Placement 54
Figure 32: Twist Reference Frame 55
Figure 33: Twist Actuation as an External Input in Simulink. a) Rotary Switch for Actuation Type, b) Knob for Magnitude of Twist 56
Figure 34: Relation between θ and y-coordinates 59
Figure 35: Starboard Wing Planform Showing Actuator Placements for Bending 62
Figure 36: Bending Actuation Deflection on Starboard Wing 63

Figure 37: Bending Actuation as an External Input in Simulink. a) Rotary Switch for Actuation Type, b) Knob for Magnitude of Dihedral 64
Figure 38: Resulting Side Force on a Linear Bending mode Actuation 69
Figure 39: Linear Twist Mode Showing the Various Aerodynamic Coefficients 70
Figure 40: Inverse Linear Twist Mode showing Various Aerodynamic Coefficients 71
Figure 41: Linear Twist Symmetric Mode Showing Various Aerodynamic Coefficients 71
Figure 42: Linear Bending Mode Showing Various Aerodynamic Coefficients 72
Figure 43: Linear Bending Symmetric Mode Showing Various Aerodynamic Coefficients 72
Figure 44: Deflection of a Cantilever Beam Showing Bending with a Point Load of 'F' 73
Figure 45: Deflection of a Cantilever beam showing Twist with a Moment 'M' 75
Figure 46: Description of Distance between Locus of Aerodynamic Centers and COG of the Wing 82
Figure 47: Description of Distance between Locus of Aerodynamic Centers and COG of the Vertical Tail 83
Figure 48: Summation of the Lift Force from all Four Vibration Modes in Bending and Twisting 85
Figure 49: Summation of the Side Force from all Four Vibration Modes in Bending and Twisting. Period of One Second Shown 86
Figure 50: Summation of the Rolling Moment from all Four Vibration Modes in Bending and Twisting. Period of One Second Shown 86
Figure 51: Summation of the Pitching Moment from all Four Vibration Modes in Bending and Twisting 87
Figure 52: Summation of the Yawing Moment from all Four Vibration Modes in Bending and Twisting.. 87
Figure 53: Graph Showing Velocity and Angle of Attack with Step Input at five seconds with Elevator at, a) +5° and b) -5° 88
Figure 54: Graph Showing Lift and Drag with Step Input at five seconds with Elevator at, a) +5° and b) -5° 89
Figure 55: Graph Showing Lift, Drag and Pitching Moment Coefficient with Step Input at five seconds with Elevator at, a) +5° and b) -5° 89
Figure 56: Graph showing Velocity, Angle of Attack and Sideslip Angle with Step Input at 5 Seconds to a magnitude of +5° of the actuators, a) Linear Twist, b) Inverse Linear Twist, c) Linear twist Symmetric, d) Linear Bending and e) Linear Bending Symmetric 91
Figure 57: Graph showing Roll, Pitch and Yaw Rate with Step Input at 5 Seconds to a magnitude of +5° of the actuators, a) Linear Twist, b) Inverse Linear Twist, c) Linear twist Symmetric, d) Linear Bending and e) Linear Bending Symmetric 92
Figure 58: Graph showing Lift, Side Force and Drag with Step Input at 5 Seconds to a magnitude of +5° of the actuators, a) Linear Twist, b) Inverse Linear Twist, c) Linear twist Symmetric, d) Linear Bending and e) Linear Bending Symmetric 93
Figure 59: Graph showing Rolling, Pitching and Yawing Moment with Step Input at 5 Seconds to a magnitude of +5° of the actuators, a) Linear Twist, b) Inverse Linear Twist, c) Linear twist Symmetric, d) Linear Bending and e) Linear Bending Symmetric 94
Figure 60: Graph Showing Velocity, Angle of Attack and Side Slip Angle with a Step Input at 5 Seconds to a Magnitude of +5°, a) No actuation, b) Linear Twist, c) Inverse Linear Twist, d) Linear Twist Symmetric, e) Linear Bending and f) Linear Bending Symmetric 97
Figure 61: Graph Showing Roll, Pitch and Yaw Rate with a Step Input at 5 Seconds to a Magnitude of +5°, a) No actuation, b) Linear Twist, c) Inverse Linear Twist, d) Linear Twist Symmetric, e) Linear Bending and f) Linear Bending Symmetric 98

Figure 62: Graph Showing Lift, Side Force and Drag with a Step Input at 5 Seconds to a Magnitude of +5°, a) No actuation, b) Linear Twist, c) Inverse Linear Twist, d) Linear Twist Symmetric, e) Linear Bending and f) Linear Bending Symmetric 99
Figure 63: Graph Showing Rolling, Pitching and Yawing Moment with a Step Input at 5 Seconds to a Magnitude of +5°, a) No actuation, b) Linear Twist, c) Inverse Linear Twist, d) Linear Twist Symmetric, e) Linear Bending and f) Linear Bending Symmetric 100
Figure 64: DATCOM AC3D Model Utilised for Rigid Body Simulation 116

LIST OF TABLES

Table 1: Advantages and Disadvantages of a Flexible Wing [Ifju *et al.,* (2002) and Hu *et al.,* (2010)] 3
Table 2: Advantages and Disadvantages of the Current Mechanisms on Aircraft 8
Table 3: Units of Bimorph Modelling Equations 18
Table 4: Initial Flight Conditions 27
Table 5: Aerodynamic Coefficients of the Rigid Aircraft 34
Table 6: Description of Coefficients for Lift 38
Table 7: Description of Coefficients for Side Force 38
Table 8: Description of Coefficients for Rolling Moment 39
Table 9: Description of Coefficients for Pitching Moment 40
Table 10: Description of Coefficients for Yawing Moment 40
Table 11: Comparison between Roskam (2001) Values and DATCOM Values 41
Table 12: Trim Setting for Angle of Attack and Elevator Deflection 44
Table 13: Variation of Wing Twist γ through Various Modes of Twist 57
Table 14: Affected Aerodynamic Properties Due to Twist Geometry Alterations on the Wing 58
Table 15: Variation of Dihedral Angle Γ through Various Modes of Bending 65
Table 16: Affected Aerodynamic Properties Due to Dihedral Geometry Alterations on the Wing 65
Table 17: Mode shape equations of Twist and Bending showing Constants 78
Table 18: Concluding uses for Piezoelectric Actuation above conventional Methods 104
Table 19: Aircraft Data 110

NOMENCLATURE

Symbol	Description
$C_{l_{\alpha_\Gamma}}$	Altered Lift Curve Slope Due to Dihedral
$C_{l_{\beta_\Gamma}}$	Roll Stability Derivative Due to Dihedral
C_{l_α}	Lift-Curve Slope
C_{s_Γ}	Side Force Coefficient Due to Dihedral
A_n	Trigonometric Series Coefficients
C_{d_i}	Induced Drag
C_{l_p}	Rolling Moment Due to Roll Rate P
$C_{l_{roll_\Gamma}}$	Roll Coefficient Due to Dihedral
$C_{l_{roll}}$	Rolling Moment
C_{l_β}	Roll Stability Derivative
C_{n_i}	Induced Yawing Moment
C_{n_p}	Yawing Moment Due to Roll Rate P
C_{s_p}	Side Force Coefficient Due to Roll Rate P
C_L	Lift Coefficient
C_m	Pitching Moment Coefficient
$F_X F_Y F_Z$	Forces in the Body Fixed Axis
$I_{\cdot\cdot}$	Tensor of Inertia
S_{ref}	Wing Reference Area
V_∞	Velocity Vector
$X_E Y_E Z_E$	Earth Fixed Coordinate
a_i	Distance Between Beam and Mass Element
$\bar{c}$	Geometric Chord
c_l	Sectional Lift Coefficient
c_m	Sectional Pitching Moment Coefficient
m_i	Mass Element Number i
$\bar{x}$	Rearward longitudinal Distance Between COG and MAC
α_i	Induced Angle of Attack

$\boldsymbol{\delta_{z_{m_i}}}$	Mass Element Deflection
$\boldsymbol{\delta_{z_B}}$	Aft Actuator Deflection
$\boldsymbol{\delta_{z_C}}$	Fore Actuator Deflection
$\boldsymbol{\eta_m}$	Asymmetric Lift Distribution Multiplier
$\boldsymbol{\eta_{ms}}$	Symmetric Lift Distribution Multiplier
$\boldsymbol{\sigma_m}$	Asymmetric Lift Distribution Moment Multiplier
$\boldsymbol{\sigma_{ma}}$	Anti-symmetric Lift Distribution Moment Multiplier
$\boldsymbol{\frac{\partial C_{l_p}}{\partial \Gamma}}$	Rate of Change of C_{l_p} With Respect to Dihedral
$\boldsymbol{\frac{\partial C_{n_p}}{\partial \Gamma}}$	Rate of Change of C_{n_p} With Respect to Dihedral
$\boldsymbol{\frac{\partial C_{s_p}}{\partial \Gamma}}$	Rate of Change of C_{s_p} With Respect to Dihedral
$\boldsymbol{AR}$	Aspect Ratio
$\boldsymbol{B}$	Length of Fore Actuator
$\boldsymbol{C}$	Length of Aft Actuator
$\boldsymbol{COG}$	Centre of Gravity
$\boldsymbol{D}$	Drag Force
$\boldsymbol{L}$	Lift Force
$\boldsymbol{L_{roll}}$	Rolling Moment
$\boldsymbol{M}$	Pitching Moment
$\boldsymbol{N}$	Yawing Moment
$\boldsymbol{MAC}$	Mean Aerodynamic Chord
$\boldsymbol{P}$	Roll Rate
$\boldsymbol{Q}$	Pitch Rate
$\boldsymbol{R}$	Yaw Rate
$\boldsymbol{S}$	Side Force
$\boldsymbol{U}$	Translational Velocity in the X-direction
$\boldsymbol{V}$	Translational Velocity in the Y-direction
$\boldsymbol{W}$	Translational Velocity in the Z-direction
$\boldsymbol{XYZ}$	Body Fixed Axis
$\boldsymbol{b}$	Wing Span

c	Sectional Chord
q	Dynamic Pressure
z	Vertical Distance Between Root Chord and COG
Γ	Dihedral Angle
Λ	Wing Sweep
α	Angle of Attack
β	Angle of Sideslip
γ	Twist Angle
θ	Euler Pitch Angle
λ	Taper Ratio
ψ	Euler Yaw Angle
ϕ	Euler Roll Angle

1. INTRODUCTION

In the advancements of the aviation industry, there are continual optimizations for greater efficiencies in every aspect of an aircraft. These advancements often include weight and aerodynamic efficiencies. Aircraft are built with lighter and stronger materials (composite materials) which reduce weight drastically, increasing the fuel efficiency and range. Aerodynamic advancements are made for the same purpose, often changing and adapting the structure of the aircraft for flight.

Aerodynamic and flight dynamic advancements have led investigations into aircraft flexibility and how this can be used to the advantage of an aircraft's flight efficiency. Control of an aircraft's dynamics have also been thoroughly researched, and often linked to the aircraft's aerodynamics and flight dynamics with active control, and vibration control being some of the main considerations as the fields of study.

One of the recent advancements being applied to the aviation industry is the use of smart materials. Smart materials, as described by Lightman *et al*., (2003), are usually compounds of different types of materials, treated in a specific way to perform and react in a particular manner. They remember configurations and can conform to them when given a specific stimulus.

The research presented in this paper seeks to understand the aerodynamic and flight dynamic aspects of a civil aircraft, by using smart materials as a means of aircraft control. The intended application is the integration of a smart material within a highly flexible wing (aeroelastic wing) of a civil aircraft, to perform as a control mechanism to bring about aircraft trajectory alterations. The investigation into this new means of actuation seeks to replace the current form of actuation which exists within the aviation industry. These current actuation methods include the use of hydraulic, fly-by-wire systems and numerous other methods, which bring about control surface changes to alter the aircraft's flight trajectory.

The smart material in question here is the piezoelectric actuator (PA). It is designed to be sandwiched within the skin of the aircraft, and actuated only by applying an electric field to it. Once actuated, the aerofoil and the wing undergo deformation. This will be explained in greater detail later. Due to these deformations (twisting, bending etc.), an aeroelastic wing has to be utilised.

This new means of actuation is highly advantageous in that it will enable greater weight reduction due to exclusion of the hydraulics and other actuation components, and provide smoother, uninterrupted airflow across the aerofoil due to the wing's aeroelastic properties, that is, the wing becomes aerodynamically cleaner.

1.1. Background

Control surface actuation induces aircraft alterations in its trajectory, in a similar fashion to a motor vehicle experiencing changes in movement caused by changes in inputs such as the steering wheel, throttle, brakes etc. Motor vehicles are accompanied by handling and performance characteristics, which include, but are not limited to: ride comfort, traction or grip, ease of manoeuvrability etc. On aircraft, the handling characteristics are highly dependent on factors like the position of the centre of gravity, the values of the static and manoeuvre margins, and many other factors based on performance criteria.

This research aims at determining a civil aircraft's performance characteristics based on actuation by the use of PAs. Its use here requires an analysis of an elastic or flexible aircraft, as twisting and bending of the wing will be executed to accomplish alterations in the flight trajectory.

It is to be noted here that the research is limited to the wing only to determine the PAs ability and controllability to perform as a control surface actuator, where the control surface is the entire wing. The functions of the slats, ailerons and flaps are researched to be imitated by altering the wing's geometry (twisting and bending etc.) by the PAs. The following provides a background on the uses of flexible (aeroelastic) wings, operation of PAs and performance requirements for this research that will be used to determine flight characteristics.

1.1.1. Flexible Wing

Finding the stability of a rigid-winged aircraft is much easier compared to that of a flexible-winged aircraft, as it is known that a flexible winged aircraft contains a constantly changing stiffness and geometry. The basic rigid wing is exceptional in its use as it is easy to design, but has many challenges such as: weight, aerodynamics, flying capabilities and range of operation. Conventional rigid aircraft wings are flexible to a certain degree, but are still considered rigid because of their structural properties being constant. A flexible wing has large deflections or changes in shape, and the structural properties do not remain constant. The methodology in rigid bodies is such that the aerodynamic forces are calculated from the effects of the body, however in aeroelastic conditions, the shape of the body is determined by the aerodynamic loads [Hodges and Pierce (2014)]. Table 1 presents the advantages and disadvantages of a flexible wing [Ifju *et al.,* (2002) and Hu *et al.,* (2010)]. It will be shown later how the disadvantages stated in Table 1 can be overcome by implementing PAs within the skin of the aircraft.

There are numerous manners in which aeroelastic wings can be utilised to perform a desired function, and be used in modelling the real-life situation. Nguyen and Tuzcu (2009) looked at the flight dynamics of

a flexible aircraft with aeroelastic and inertial force interactions. The key consideration in their research was to include the effects of the actual physics of flight in which inertial, propulsive and aerodynamic forces exist and are significant. This way, the model is believed to be highly realistic and the effects from a flexible wing could be coupled to determine the flight dynamic effects. The exact method used here was the combination of structural dynamics of an equivalent beam model of a flexible wing, where the flight dynamics used accounted for the respective rigid body motion, aeroelastic, propulsive and inertial forces.

Table 1: Advantages and Disadvantages of a Flexible Wing [Ifju *et al.,* (2002) and Hu *et al.,* (2010)]

Advantages	**Disadvantages**
• The ability to adapt the airflow to provide smoother flight (increasing performance). • Ability to alleviate the effects of gust winds. • Delay airfoil stall. • Have enhanced agility (increased flight maneuverability).	• Constant shape changes decrease the lift efficiency of the airfoil (lift to drag ratio). • Thrust or input power required would have to be large, as compared to a rigid wing aircraft due to the decreased lift. • Decreases the stiffness of the wing.

Flick *et al.,* (1999) looked at the impact of a particular type of aeroelastic wing, called an Active Aeroelastic Wing (AAW) Technology, on conceptual aircraft design. AAWs use the effects of aeroelasticity as a net benefit during manoeuvring. Flick *et al.,* (1999) further explained that this type of wing does not require smart actuation or adaptive control law techniques, but rather can complement them.

An AAW uses the structural flexibility of the wing, by the operation of leading and trailing edge (LE and TE respectively) control surfaces to aeroelastically shape the wing (see Figure 1). An AAW can be utilised to produce large control authority at higher dynamic pressures, and enable the manoeuvring of load control for both symmetric and asymmetric manoeuvres.

Flick *et al.,* (1999) researched the conceptual design of using AAW on a fighter jet aircraft. The major consideration with regard to this actuation type would be the addition of weight, as well as additional design for internal load conditions (structural analysis). It must be pointed out here that the conceptual design was done on a small fighter jet, hence sizing would prove to be problematic for this situation; however, one cannot negate the attribute of weight penalties as this is also an important factor with larger aircraft.

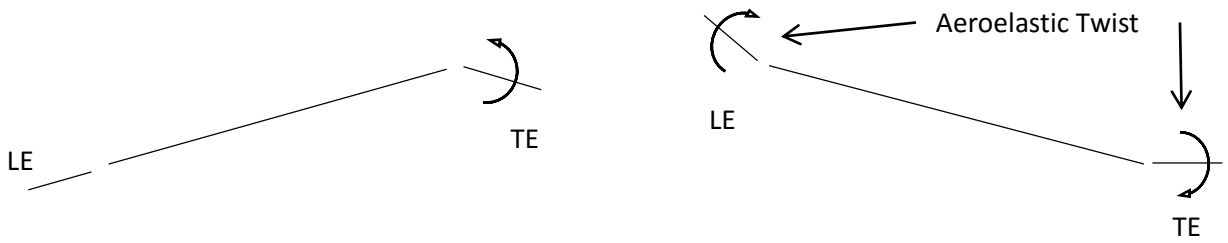

Figure 1: Active Aeroelastic Wing Operation

1.1.2. Smart Materials: Piezoelectric Actuator

As explained earlier, smart materials have unique reactions when given a specific stimulus. The following are the characteristics of smart materials [Addington and Schodek (2005)], they demonstrate the following:

- Immediacy – they respond in real-time.
- Transiency – they respond to more than one environmental state.
- Self-actuation – intelligence is internal rather than external to the 'material'.
- Selectivity – their response is discrete and predictable.
- Directness – the response is local to the 'activating' event.

Of importance is the characteristic of self-actuation for this research. Actuation is always accompanied by a sensing device, which computes the error between the desired and the output performance, where the material is guided accordingly for the relevant changes. For some materials which have self-actuation, the material itself senses the changes and reacts accordingly, hence the term, smart material.

Numerous types of smart materials are available, with various uses. Though there is a basic list of smart materials categorised according to their method of operation, the most important are:

- Magnetostrictive – these materials undergo mechanical changes when they are in a magnetic field.
- Shape Memory Alloys – these undergo phase transformations when they are in a thermal field.
- Piezoelectric materials – these undertake a mechanical change when they are in an electric field.

Of importance to this research project is the application of smart materials. That is, how are they applied into the overall configuration of the final design? Integrating smart materials to the system necessitates

the use of sensors and actuators. The term actuator is used here as describing the system that would actuate the smart material (e.g.: an electric field etc.), subsequently, it will be shown that the smart material is used as an actuator as well. This whole subsystem is referred to as a smart structure [Akhras (2000)]. There are five basic components to a smart structure (see Figure 2).

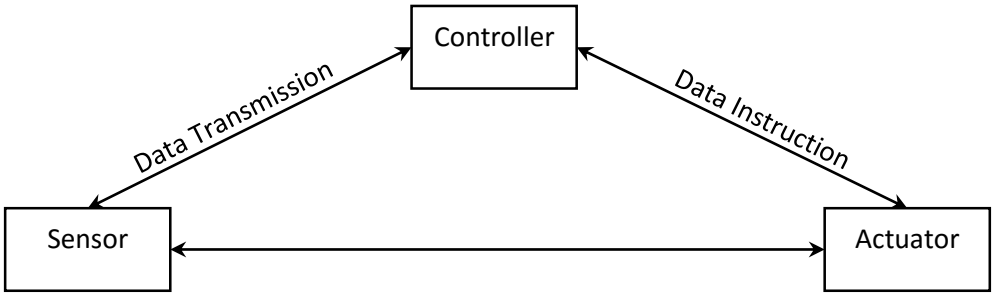

Figure 2: Smart Structure Method of Operation [Akhras (2000)].

Data is obtained from the actuator, by the sensor, to determine if the desired output is met. The sensor then transmits the data to the controller (known as data transmission). The controller assesses the data transmitted from the sensor, and computes the appropriate adjustment or change, which is given back to the actuator (known as data instruction). This smart structure comprises of a smart material that can act as an actuator, and/or another smart material that can be utilised as a sensor. A focal feature of smart materials is their ability to be used as a sensor and/or as an actuator, intensifying their range and method of usage.

The key advantages of smart materials are their variability in application in substantially specific and demanding environments, environments where common materials cannot adequately be designed to fit the purpose. A specific few smart materials are much easier to manufacture as opposed to normal materials, which may require significant energy and time for production, hence decreasing production costs.

The major disadvantage of smart materials is that the uses are so specific that their application needs to be highly researched, with numerous tests, which can be costly. Albeit normal materials are also pre-requisitely tested, their reactions can be predicted in many modes of use, and their stability and reliability are known. The same however cannot be said of smart materials.

There are numerous types of piezoelectric materials that have been researched. Piezoelectric actuators are commonly known as Macro Fibre Composites (MFC's) [Nir and Abramovich (2010)]. These materials

were developed by NASA at the Langley Research Centre. It is produced in various forms, ranging from monolithic, directed or fibrous piezoelectric smart materials and can be configured with materials such as graphite [Rabinovitch and Vinson (2003) and Zareie and Zabihollah (2011)].

The method of operation of PAs is such that a current is supplied through an external electrical power source, which deforms the piezoceramic. Figure 3 shows a description of a simple setup of the piezoelectric actuator. Depending on the manner in which the electric field is applied (through a positive or negative voltage), the piezoceramic deforms as shown in Figure 3. It must be noted that this is a basic configuration of the actuator; the conducting wire in the piezoceramic can be orientated in different manners to bring about different deformation modes. Each of these actuators can be arranged in series or in parallel, and at different angles to a reference setting, to bring about different modes of deformation.

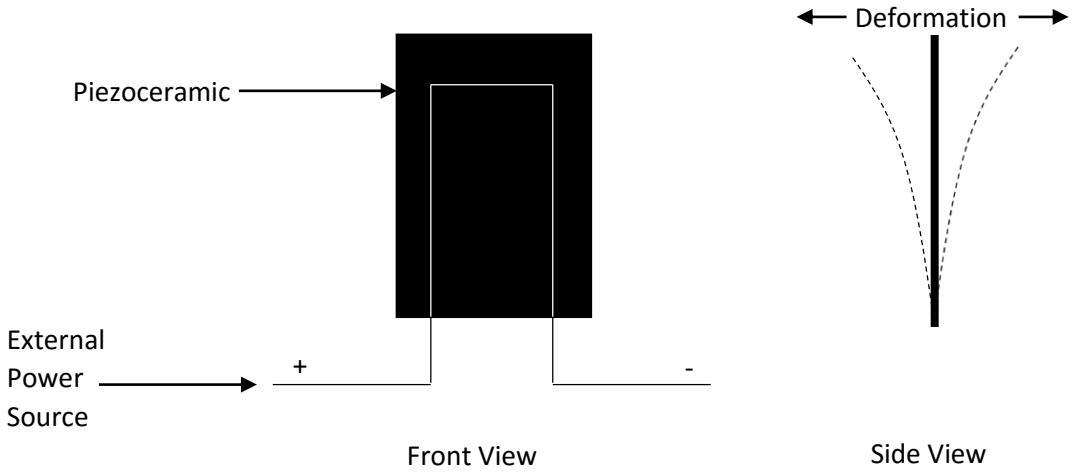

Figure 3: Piezoelectric Actuator Configuration showing simple Deformation

Nir and Abramovich (2010) and Rabinovitch and Vinson (2003) show the manner in which the piezoelectric actuators are arranged and create the different modes of deformation for a smart fin utilising PAs.

The advantages of PAs are that they allow for small displacements of minute strains (0.001-0.002 strain), hence with proper choice of controller, they can be used for active control. They have a low thermal coefficient (and maximum operating temperature of close to 300°C), and a large bandwidth of operation [Gandhi and Thompson (1992)].

The disadvantages are that high voltages are required for operation (in the range of kilo-volts), they are brittle due to their ceramic composition, and have high levels of hysteresis [Huang and Tan (2011)] and chattering.

Control has also been a major research area of PAs. It has been done to avoid the foremost disadvantages stated above. The most prominent disadvantage is that of hysteresis. Thus, a controller is required to calculate and compensate for, and/or even negate the effects of hysteresis. Huang and Tan (2011) researched the different forms of control, while considering different forms of mathematical modelling for hysteresis. They concluded that sliding mode control is a worthy choice of control in high frequency environments, and they are simple and easily implemented within the overall system. Another form of control that had been more complex, the adaptive control, was found to reduce the chattering phenomena, and could achieve multiple control objectives like tracking error and control energy.

1.2. Literature Review

The following will encompass the current means of control surface actuation on aircraft in the industry, and highlight the progress of PAs and their application on aircraft.

1.2.1. Actuation Mechanisms on Aircraft

The actuation mechanisms on aircraft are those components that bring about the desired deflection of the primary and secondary control surfaces. Logically, the larger the aircraft, the more powerful the actuation mechanism required. The current forms of actuation mechanisms on aircraft are:

- Mechanical.
- Hydraulic and servomotors.
- Fly-by-wire.

The characteristic advantages and disadvantages of the above stated actuation types are presented in Table 2. Of importance to this research project is fly-by-wire actuation. It can be seen that active control can be achieved, which is a property that PAs are shown to have as well.

Figure 4 shows the typical setup configuration for a fly-by-wire control system [Collinson (1999)]. As the figure shows, the flight computer inputs data from the aircraft's dynamics, the pilot's stick movements and the sensors for the atmosphere conditions. One can notice the similarity between Figure 2 and Figure 4. This research project will operate using a similar flow of work as these two figures. From Table 2, the major disadvantage for heavy aircraft is weight due to the actuation mechanisms. Saving on all this weight allows the aircraft to increase its performance, range, payload, and flight efficiency.

Table 2: Advantages and Disadvantages of the Current Mechanisms on Aircraft

Actuation Type	Advantages	Disadvantages	Description
Mechanical	• Light. • Easy to assemble and replace. • Pilot feels actual aerodynamic forces.	• Simple connection points, highly susceptible to failure • Large stick forces may prevail.	Perfect for light aircraft.
Hydraulic and Servomotors	• Able to withstand large aerodynamic loads. • Minimal time delay for actuation.	• Increases weight due to hydraulic fluid, fluid lines and pump. • Damage and loss of control due to hydraulic fluid leakage. • Costly maintenance and repair.	Used on large aircraft. Methods have been introduced to prevent fluid leakage, which adds weight.
Fly-by-wire	• No hydraulic fluid, less weight. • Active control for better performance. • Ability to reduce tail-plane natural stability [Collinson (1999)].	• Weight due to many miles of cables. • Electrical failures result in loss of control. • Costly maintenance and repair.	Redundant methods have been introduced to compensate for electrical failures, which adds weight.

The present research project is to be used for application on large civil aviation aircraft, hence mechanical actuators will not be weighed accordingly in its advantages and disadvantages. Piezoelectric actuators that can be implemented on aircraft skin can save a considerable amount of weight. The use of hydraulics, pumps, servomotors etc., can be completely removed, enabling more space and the use of less strengthening material, shaving the weight of the aircraft even further. The major disadvantage is the voltage required to generate the electric field, and hysteresis.

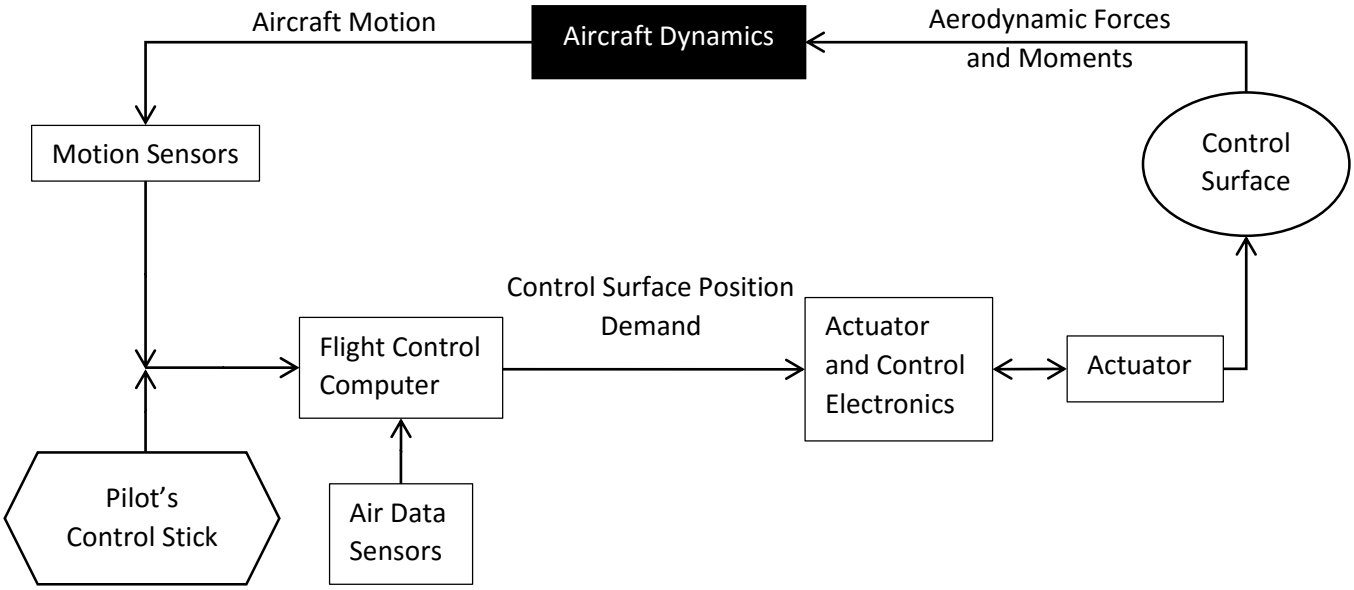

Figure 4: Fly-by-wire Flight Control System [Collinson (1999)]

Fly-by-wire introduces electrical signal conditioning, which aids in transmission of desired outputs, as opposed to mechanical configurations. Due to this easier and lighter means of actuation, the progression towards hybrid actuation ensued. Cochoy *et al.,* (2007) explains that hybrid actuation seeks to introduce electromechanical actuators into primary flight controls. These actuators include the electrohydraulic servoactuator (EHSA) and electromechanical actuator (EMA). They are introduced in demand of a full electric aircraft. Some advantages of hybrid actuation in comparison to Table 2 are [Jänker *et al.,* (2008)]:

- Better energy efficiency.
- Better actuator dynamics.
- Weight benefit.

PAs fall into the category of hybrid actuation, providing complete electrical actuation, with the added benefit of a greater weight reduction compared to EMA and EHSA. Jänker *et al.,* (2008) distinctively state that EMA's can be used for primary flight controls on aircraft, whereas PAs are more suitable for active rotor and vibration control on helicopters. The following will show how vibration control has been adapted for use on aircraft, and other novel forms of application, in addition to rotor vibration control.

1.2.2. Smart Materials: Piezoelectric Actuators

PAs have been utilised for many applications on aircraft. One of the main applications is vibration control. An aircraft often experiences vibration in flight which has a detrimental effect on the structure. Thus PAs are utilised to act as vibration dampers, or stiffening structures which are activated to provide rigidity without the extra added weight of aircraft skin material and/or structural members.

Vibration analysis and control has been carried out on helicopter rotors actuators [Duquette and Fu-Shang (2007) and Prechtl (1994)], also with focus on the twist of helicopter rotor blades [Park and Kim (2005)]. The analyses often considered control of the high-frequency vibrations brought about by the rotor blades.

The research into smart fins was also conducted, considering the buffet loads that occur, especially in the F/A 18 [Ulker *et al.,* (2009), Nir and Abramovich (2010), Moses *et al.,* (2005), Rabinovitch and Vinson (2003), Chen *et al.,* (2009)]. Vibration suppression has not only been focused on the aircraft tail and the rotor of the helicopter, but also on the hull [Sohn *et al.,* (2011)] and wing of the aircraft [Otiefy and Negm (2011)].

The aim of this research project is not vibration control, but rather, viewing the resultant flight dynamic properties of a PA incorporated wing in comparison to the basic wing of a civil aviation aircraft. Based on this, the following depicts the various novelties and aspects to consider on aircraft control surface actuation with the use of PAs.

One of the problems to be encountered with this research project is the placement of the PAs on the wing. The PAs must be placed in such a manner that the actuation is efficient in that the relevant movement of the wing is brought about in the most ideal form. Researching the placement of the PAs in itself could become a project on its own, thus methods used by various other projects on PAs will be shown here, and the desired form will be chosen as the need arises.

Nir and Abramovich (2010) conducted research on the design, analysis and testing of a smart fin. They used PAs in the skin of a fin which had been intended for use on Unmanned Aerial Vehicles (UAVs). Their study presented various lamination and actuation methods through finite element and analytical modelling. Their fin used PAs in a manner such that they would sandwich the structural layer (the skin of the aircraft) while orienting the PAs in dissimilar angular configurations (see Figure 5).

The three actuations that resulted due to their orienting of the PAs were:

- *Pure Shear Strain*: Resulted in the twisting of the airfoil.

- *Skew Bending*: Resulted in the wing demonstrating bending.
- *Single Active Layer*: Resulted in a combination of pure shear strain and skew bending.

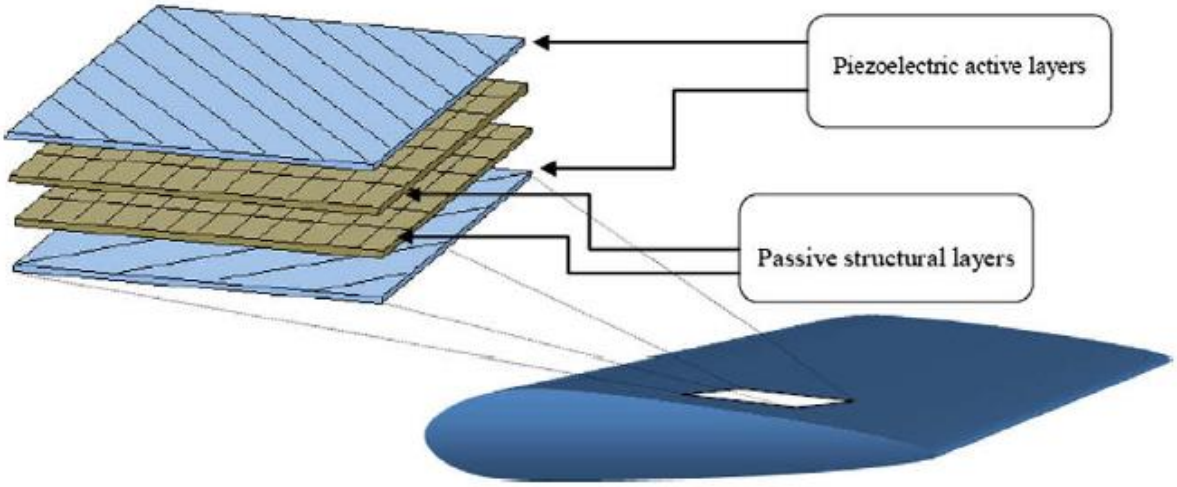

Figure 5: Orientation of Piezoceramic Layers on the Smart Fin in Correlation to the Passive Structural Layers [Nir and Abramovich (2010)]

The conclusion was that the single active layer showed the least amount of effectiveness, the pure shear strain achieved the greatest twist intensity and skew bending improved the airfoil's performance, but this was only the case if the trailing edge had an open section, which understandably decreased the structural rigidity. The recommendation here was to take this reduced rigidity into consideration for future work.

In a similar project to the smart fin developed by Nir and Abramovich (2010), Mehrabian and Yousefi-Koma (2007) looked at the optimal positioning of PAs on a smart fin by bio-inspired algorithms. The project had been conducted for vibration suppression of the fin of an F/A18 aircraft. The placement of the PAs resulted in similar displacements as Nir and Abramovich (2010), but with clearer distinction between the modes of bending. Figure 6 shows these bending modes with respect to the placement of the PAs.

Given that these methods of placement and mode shapes are for a smart fin, the methodology can also be applied for a wing. Research conducted on the wing by Li *et al.,* (2011) on a rectangular wing contained a different setup of the PAs. Their approach was that of adding PA panels in a uniform pattern, as shown in Figure 7**.** The objectives set by Li *et al.,* (2011) were to increase lift force, provide roll maneuver assistance, decrease induced drag and decrease wing root moment.

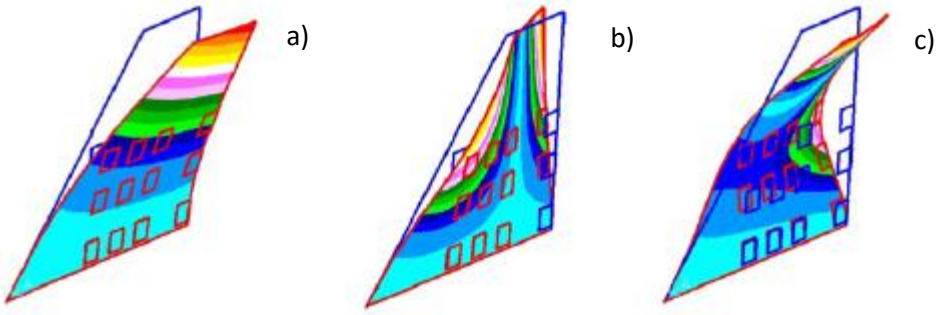

Figure 6: Piezoelectric Actuator Placement with Fin Mode Shapes: a) First Bending, b) First Torsional, c) Second Bending [Mehrabian and Yousefi-Koma (2007)]

The results were compared to a basic wing, but it must be noted that the research had been conducted for a rectangular wing only. The major outcome of the research was that a better control effect would have resulted if the PAs were utilised on a high aspect ratio wing.

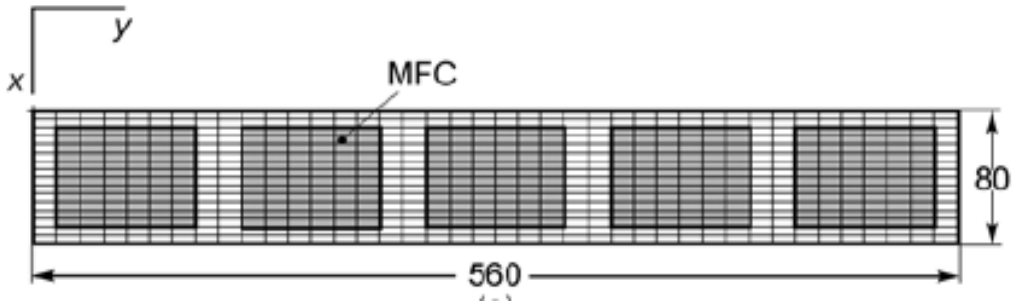

Figure 7: Piezoelectric Actuator Panel Positioning [Li *et al*., (2011)]

In comparison to Li *et al.,* (2011) method of actuation, Tuzcu and Meirovitch (2006) apply PAs on a civil aircraft wing to analyse vibration with the aim of active damping. The placement process used here was of high aspect ratio PA panels at various locations (see Figure 8).

It is important to note that the configurations on the wings/fins that required vibration control are not necessarily the best configuration for altering the wing's geometry, as these are strategically placed for buffet load and vibration suppression, not for actuation.

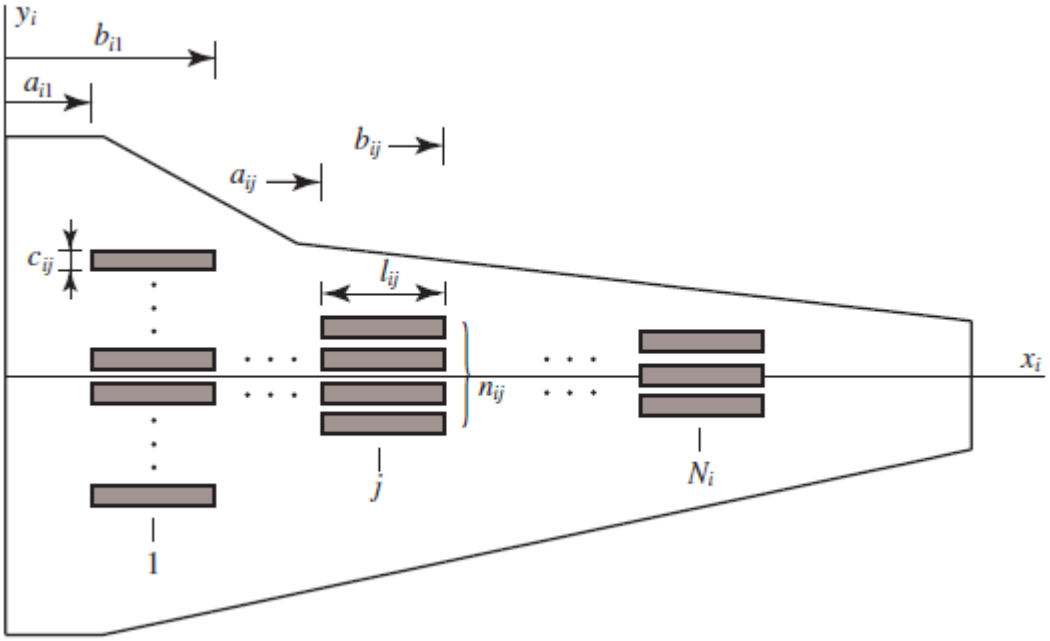

Figure 8: High Aspect Ratio Piezoelectric Actuator Positioning on a Cessna Citation Wing [Tuzcu and Meirovitch (2006)]

In relation to the wing used by Tuzcu and Meirovitch (2006), Martindale (2011) conducted research on a first-order model on a variable camber wing of a Cessna Citation V. The wing was a NACA 5 series, upon which the camber was variably changed to bring about smooth deformations along the span of the wing. Martindale (2011) further explained that there would be a means of actuation to bring about this variable change of camber. It is seen as an opportunity here that PAs can be utilised to bring about these camber changes, however, the desired camber changes were intended to be brought about internally, as opposed to external actuation. The investigation by Martindale (2011) considered roll authority, and validation of static and dynamic behavior and was limited in such a way that they could be compared to a conventional rigid wing. It must be noted here that the comparison made was between the camber control technique of a flexible wing and a rigid wing. Figure 9 shows the wing of the Cessna Citation V that was researched for the first-order variable camber calculations.

Other novel research projects which consider the use of PAs as a means of control surface actuation were conducted by Bilgen *et al.,* (2013) and Suleman and Costa (2004). Bilgen *et al.,* (2013) through a group called the Virginia Tech Morphing Design Team, built the first smartly-actuated, remotely-controlled aircraft (RC aircraft). The RC aircraft had been composed of a type of PA called the Macro Fibre Composite

(MFC). The team conducted theoretical analyses on the aerodynamics of the RC aircraft, and built a model for testing.

Through the actual flight experiment, the RC aircraft was found to be sluggish on the controls and resembled a “slow flyer” as opposed to basic aerobatic aircraft. A unique finding in the flight experiment was the damage on the RC when it experienced a crash-landing. The fuselage was extensively damaged; however, the control surfaces containing the MFC material were damage-resistant, hence showing the capability of energy absorption during impact. The team recommended that the aircraft be studied further in its dynamic stability and control. Figure 10 shows the concept.

Suleman and Costa (2004) used PAs on a flight vehicle demonstrator concept to research aeroelastic vibration suppression. Their research considered gust response alleviation and flutter suppression amongst other research requirements. The flight vehicle demonstrator is shown in Figure 11. The flight vehicle underwent wind tunnel tests as well, to show the feasibility of the concept. The results showed that the PAs worked well in suppressing the flutter.

Using the wing researched by Tuzcu and Meirovitch (2006) in correlation to Martindale (2011), the study can be taken further due to the fact that the PA configuration by Tuzcu and Meirovitch (2006) was intended for flight trajectory alteration, and not vibration suppression. Bilgen *et al.,* (2013) RC aircraft had been designed with PAs positioned in the simplest and structurally feasible form, as it was of a small size. The research to be conducted for this project seeks for a strategic placement of PAs to bring about the best form of aircraft trajectory alterations, as given by Tuzcu and Meirovitch (2006).

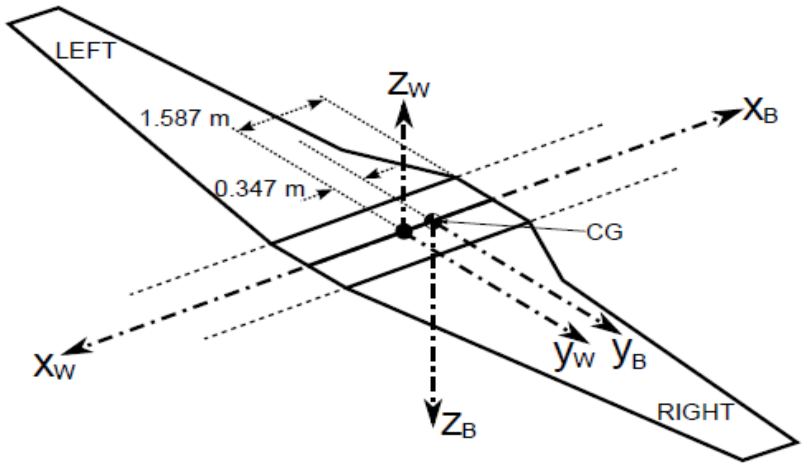

Figure 9: Wing of the Cessna Citation V Researched [Martindale (2011)]

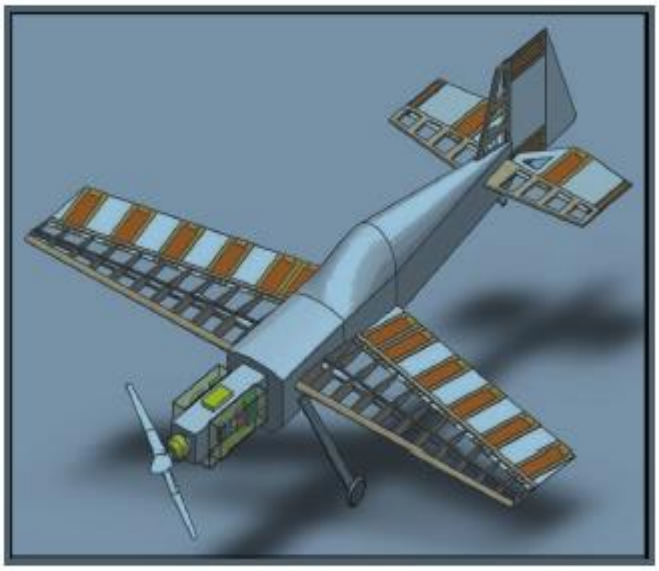

Figure 10: Solid State Control Surfaces with Piezoelectric Actuators of an Unmanned Aerial Vehicle (Remote Control Plane) [Bilgen *et al*., (2013)]

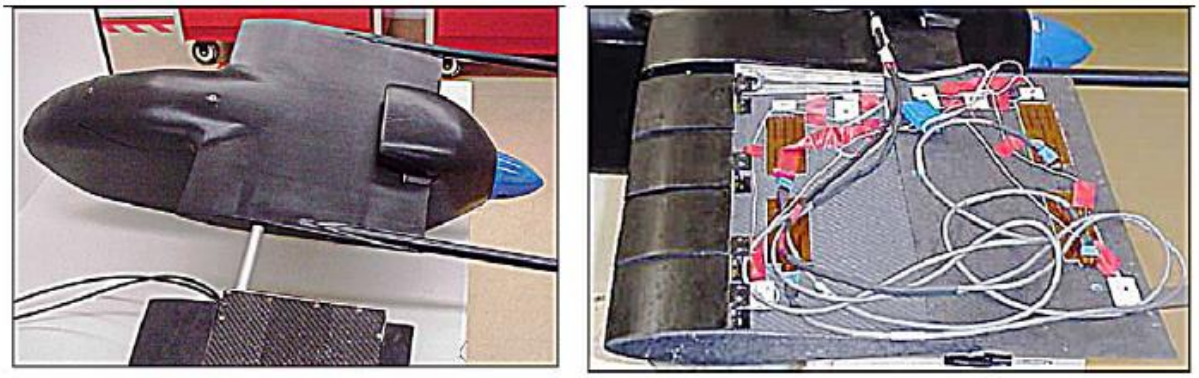

Figure 11: Flight Vehicle Demonstrator with Piezoelectric Actuator Position [Suleman and Costa (2004)]

1.2.2.1. Modelling of a Piezoelectric Actuator

The two most common configurations for PAs are stack actuators and bender actuators. Stack actuators are consisted of ceramic wafers stacked on top of each other, creating a mechanical series, but parallel electrically due to the connection of electrodes. Stacked actuators are commonly used for applications where compression/tension is the resulting type of load. For the application of this research, bender actuators are the desired types of PAs, as bending and twisting are the resultant type of loads. See Figure 3 for a description of a simple bender actuator [PI (2004)].

There are many configurations of a bender actuator. The most common configuration involves the attachment of two layers of material, known as a Bimorph. These two layers are commonly steel and a piezoelectric ceramic actuator (known as PZT). However, a lighter configuration can be achieved by attaching two layers of PZT. This configuration allows the setting of one layer to contract, and the other layer to expand [PI (2004)].

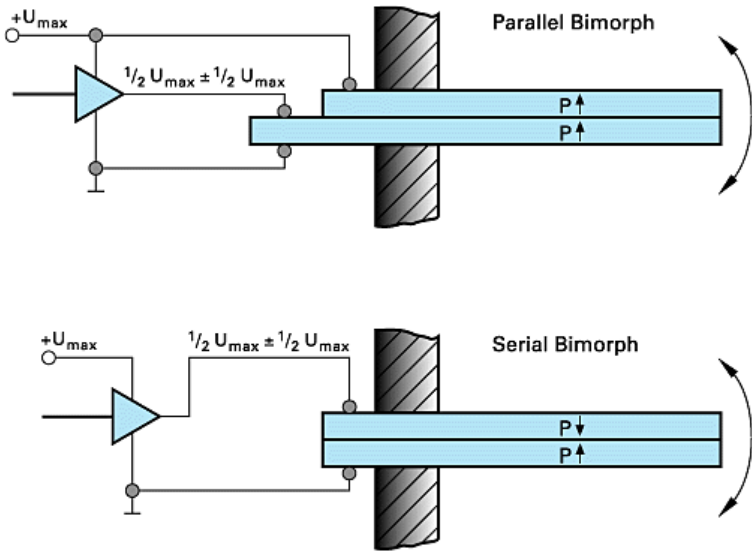

Figure 12: Parallel and Serial Configuration of a Bimorph [PI (2004)]

The Bimorph actuators are available in two electrical configurations: serial bimorph, and parallel bimorph. The serial bimorph has a two-electrode configuration, while the parallel bimorph has a three-electrode configuration, as shown in Figure 12. In the serial configuration, one of the two ceramic layers is always operated opposite to the direction of polarization. Serial bimorphs are utilised mainly as force and acceleration sensors [PI (2004)]. The intention for this research would be to use a three-electrode configuration bimorph, as this allows for a blocking force as well as a desired deflection with a voltage input. A blocking force is the ability of the bimorph to withstand a deflection from external inputs excluding the electrical input.

For this research, the modelling of these bimorph actuators will not be covered in detail, as control of these actuators will not be considered due to a large amount of control theory existing for such an

actuator. Modelling for this research will encompass dimensions of the actuators, voltage inputs and deflections, and blocking forces.

It must be noted here that in the current stage of PA development, there are limitations to the sizes and applications of these actuators. The intention for the research would be to extrapolate from these available actuators and utilise them for a much larger scale in terms of application and size. Given that this is not practically possible at this stage of PA development, the scaling is purely conceptual.

The basic governing equations used to model a bimorph are as follows [PI (2004)] (Figure 13 shows the relevant dimensions of a cantilever bimorph configuration):

$$bending = \frac{7 \times 10^{-11}.l^3}{w.t^3} \tag{1.1}$$

$$deflection = \frac{9 \times 10^{-10}.l^2}{w^2} \tag{1.2}$$

$$charge\ output = \frac{8 \times 10^{-8}.l^2}{t^2} \tag{1.3}$$

$$resonant\ frequency = \frac{400.t}{l^2} \tag{1.4}$$

$$capacitance = \frac{8 \times 10^{-8}.l_t.w}{t} \tag{1.5}$$

$$voltage\ output = \frac{10^{-2}.l^2}{t.l_t.w} \tag{1.6}$$

$$blocking\ force = \frac{10.t.w}{l} \tag{1.7}$$

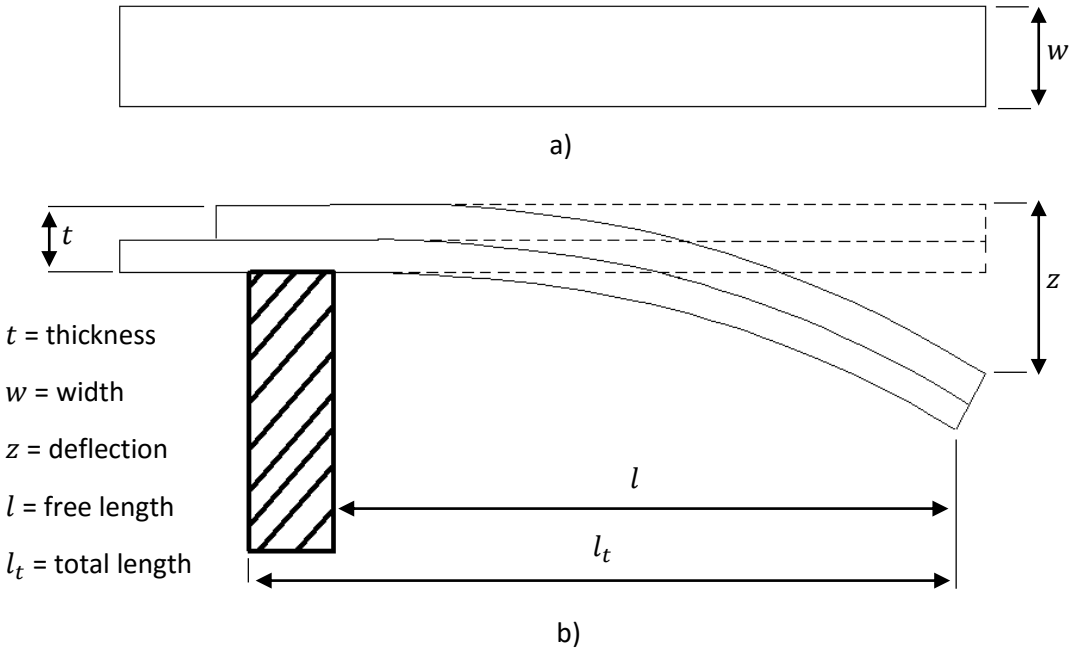

Figure 13: Cantilever Bimorph Showing Dimensions. a) Top View, b) Side View

Table 3: Units of Bimorph Modelling Equations

bending	m/N
deflection	m/V
charge output	C/N
resonant frequency	Hz
capacitance	F
voltage output	V/N
blocking force	N/V

The units of the above mentioned equations are shown in Table 3. It can be seen that deflection and blocking force are dependent on the voltage input. The larger the voltage input, the greater these two values.

1.2.3. Effects of Flexible Wings

In effect, the disadvantages for flexible wings stated in Table 1 can be overcome by PAs in the following manner. Considering the disadvantage of the constant changes decreasing the lift efficiency, PAs can be implemented within the skin of the aircraft, in a similar manner to Nir and Abramovich (2010), to make the required changes, with active control, to ensure that the aircraft flies at its maximum lift efficiency. Using control by the implementation of PAs in this manner, and by considering that a flexible wing can undergo large deformations, the lift efficiency can be extended much further as opposed to conventional rigid wing aircraft, by increasing the flight envelope.

The flight envelope stipulates the domain in which the aircraft is flyable. For rigid wing aircraft, the flight envelope has its limits narrowed rapidly, depending on the relative air velocity. The aircraft can only maintain flight when it is aligned to the relative air velocity (that is, the air flows over the relevant lifting surfaces to produce adequate lift). However, a flexible wing aircraft can adapt to the reference air direction (example, a large gust wind). It can be noted here that there is an opportunity for PAs to be utilized to control the shape of the wing and bring about the necessary changes.

Control in the form of PAs for when the reference air direction is not aligned to the aircraft can prove to be highly advantageous for the pilot and the aircraft. In cases when an aircraft may enter a flat spin (aircraft maintaining its level attitude, but falling while spinning about its vertical axis) the reference air direction is now nowhere close to providing lift to any lifting surface to escape the danger. By using PAs to change the airfoil geometry through the wings flexibility, the airfoil can be altered in the direction of the prevailing air reference direction, and lift can be restored, and the aircraft can recover. This is but one of the situations the aircraft experiences, there are many other situations like stalls, adverse yaw effects, adverse aileron effects, weathercock flight etc. which create difficulty in controlling the aircraft, but can be overcome through the appropriate use of a non-rigid wing and PAs (another opportune use of PAs).

Referring to the large thrust required, piezoelectric actuators can deform the wing in the desired sense, restoring the lift and decreasing the need to increase thrust. The other major disadvantage for flexible wings stated above is the decrease in the stiffness. Large aerodynamic loads require that the wing is as strong as possible to handle them. Carbon fibre composite wings are extensively researched in terms of their flexibility and strength and the application thereof. They are light but strong at the same time, making them exceptionally viable for use in aeroelastic configurations. PAs have also been researched in their integration within the system. Logically, it would be ineffective to use PAs and not consider that they can also be used as stiffening members. Rabinovitch and Vinson (2003) and Zareie and Zabihollah (2011)

have considered manners in which PAs can be integrated into the wing of an aircraft. Different configurations can be considered, with different materials, for example graphite, to increase the stiffness of the wing.

Usually, aircraft with a flexible wing, like NASA's Helios [Gibson *et al.,* (2011)], are accompanied by a high aspect ratio. Having a high aspect ratio increases the elasticity of the wing and also increases the performance (lift efficiency). Physically, a structure that is longer and thinner has more flexibility than a structure that is shorter and thicker, the only problem with this is that the space available for control surfaces is decreased. Once again, another opportune use for PAs to negate such a disadvantage, as they can be used in the skin of the aircraft, and making the whole wing become the deflecting control surface, as opposed to being a compensating surface area for control surfaces.

Another advantage of a flexible wing is that it allows for smoother airflow. Not having linkages such as flaps and slats allows for uninterrupted airflow. Thus briefly, a non-rigid wing has a positive aerodynamic effect. The negative effects of this is the loss of handling. Flexible wings limit the amount of control surfaces (and their surface areas) that can be attached, which inherently affects the handling.

1.2.4. Why Piezoelectric Actuation Over Conventional Methods?

The intended use of PAs for this research project is to place them on the skin of the aircraft, possibly following an analogous approach as proposed by Tuzcu and Meirovitch (2006). The prevailing questions about this new form of actuation are: why use it? Why develop a whole new means of actuation when servomotors and fly-by-wire are in perfect working condition, and have been used ever since their implementation in the 1970's? The answers and reasoning are as follows.

Weight is the major consideration. The more weight the aircraft can save, the more efficient the aircraft is. The logic here is: can the numerous numbers of cables and motors, and/or hydraulics be completely replaced by a single actuation mechanism, Piezoelectric Actuators? If all this weight can be saved, the aircraft becomes vastly lighter, increasing its performance, payload, saving on fuel etc. This single reduction creates a chain effect of aircraft aspects that suddenly become advantageous or pose no threat at all to aircraft design. If an aircraft's actuation mechanisms can be replaced by PAs, there are fewer moving components, hence chances of failure decrease immensely. However, when single components fail, they lead to more dramatic changes in the system's performance. It is also known that PAs are

cheaper to manufacture, hence decreasing the cost of production. These are all however secondary advantages.

A question arises here, why use a non-rigid wing when a rigid wing has been the only convention on aircraft thus far? Non-rigid wings are the aviation industry's most modern research development. Aerodynamically, a non-rigid wing has its advantages of allowing smoother airflow versus a rigid wing. It was stated earlier that rigid wings need separate moving control surfaces to bring about aerodynamic changes, hence creating breaks in the airflow.

1.2.5. Research Gaps in the Literature

The research gaps in the existing literature are:

- PA application has mainly been considered in terms of structural and vibration feasibility and incorporation into the system in which it is to be applied, often performing its role as a sensor and load suppressor (vibration and buffet loads) respectively, as opposed to an actuator.
- Due to the active control characteristic often ascribed to PAs, applications have primarily been on propellers of fixed-wing aircraft and swashplates on helicopter rotor blades since these components experience active twisting in their application.
- Numerous concepts examined buffet loads on the vertical tail plane, especially in the occurrences of a double tail-plane however buffet loads were not researched for on the main wing of the aircraft in the literature.

A thorough study of dynamic stability and control has not been extensively researched due to the hysteresis and lag of PAs in operation.

1.3. Motivation

The majority of the research related to PAs is based on structural, or pure control techniques. The combination of the two has considerably been carried out on rotating-wing aircraft [Duquette and Fu-Shang (2007), Prechtl (1994), Park and Kim (2005)]. They have also been implemented on the fin of conventional aircraft, often considering buffet loads and vibration control [Ulker *et al.,* (2009), Nir and Abramovich (2010), Moses *et al.,* (2005), Rabinovitch and Vinson (2003)]. Added to this list are control

and aerodynamic properties on the aircraft wing with the use of PAs [Tuzcu and Meirovitch (2006), Li *et al.,* (2011)].

Bilgen *et al.,* (2013) developed a remotely controlled aircraft incorporating PAs as an actuating mechanism on the wing and tailplane. Their investigation included comparisons between the PA configuration and the basic configuration in terms of the wing's lift to drag ratio and other performance properties. Flight test results were also compared with wind tunnel results, aided by Vortex Lattice Method simulations.

Martindale (2011) investigated a first-order model of a variable camber wing for a civil aircraft. It is seen as an opportunity here to enhance this first-order model of variable camber by implementing PAs as the actuating mechanism. Martindale's research focused solely on the aerodynamic and structural results of utilising variable camber. The gap that can be filled in here is the flight dynamic characteristics of such a wing. The civil aircraft on which the research was conducted was the Cessna Citation V. It must be noted that Martindale (2011) desired internal actuation for camber control, but it can be performed externally as well.

It was noted from the available literature that no comparison had been made of the effectiveness of PAs compared to basic actuation techniques on civil aircraft. Thus, an opportunity exists to utilise PAs on a civil aircraft wing as a means of flight trajectory control, and compare this to that of the current form of actuation on aircraft. This comparison can be conducted in terms of the aerodynamic and flight dynamic properties resulting from each type of actuation.

1.4. Research Objectives

The main objective of this research project is to determine the flight dynamic and aerodynamic properties of a flexible civil aircraft wing numerically, which utilises piezoelectric actuators as a means of flight trajectory alteration.

The following are sub-objectives of this research project:

1. A comparison must be made between the uses of a fully flexible wing with PAs to that of conventional actuation methods.
2. The numerical model must examine the following cases:
    a. Case 1: actuation of the conventional methods (aileron, rudder, elevator).
    b. Case 2: actuation of the conventional methods (aileron, rudder, elevator) with the piezoelectric actuator.

c. Case 3: actuation of the piezoelectric actuator.

1.5. Design Assumptions

Overarching assumptions were made to set ideal conditions for developing the research. These conditions made it easier to conceptually develop the novel actuation model being developed in this dissertation. These assumptions are as follows:

1. The aircraft to be used in this research is assumed to be fully flexible, without any structural limitations.
2. The aircraft does not experience variable mass within the intended time frame. The analysis in the intended short time frame will not show significant changes in aircraft mass, thus the mass is fixed at maximum take-off weight.
3. The atmosphere is assumed to be at International Standard Atmosphere conditions.
4. Any control system additions to the aircraft are appended without structural considerations. The primary focus of this research is to understand the aerodynamic and flight dynamic properties. Structural changes due to control system additions do occur, but assumption 1 is invoked here to allow for a degree of flexibility in the development of the novel actuation model.

1.6. Research Question

The research question this dissertation addresses is the viability of a new means of actuation for future use in the aircraft industry. Can elasticity of an aircraft be utilized in conjunction with smart materials as a primary/secondary flight trajectory alteration mechanism independent of conventional control methods, and if so, how? This research addresses this two-part question by designing a method for smart materials to be utilized as a trajectory altering mechanism, as well as a look into the flight dynamics and aerodynamics to determine its viability.

1.7. Research Strategy and Methodology

The purpose of this research is to investigate the aerodynamics and flight dynamics of a flexible civil aircraft under piezoelectric actuation.

The proposed conceptual analysis is designed to integrate the piezoelectric actuators into the skin of the wing, which will then be controlled strategically to alter the wing's geometry, and ultimately the flight trajectory of the aircraft. Simultaneously, elastic properties are added to the aircraft, permitting flexible analysis alongside rigid analysis.

In nominal cases, flexible aircraft analysis is accompanied by vibration and finite element analysis of the aircraft [Waszak *et al.,* (1987), Li (2010), Andrews (2011), Meirovitch and Tuzcu (2003), Tuzcu and Meirovitch (2006)]. Due to the complexity and range of this analysis, a slightly different approach is adopted in this research, which will be explained later.

The layout and method of analysis is presented below, depicting the various chapters leading towards a model which incorporates the rigid vehicle, piezoelectric actuation and finally elastic effects.

1.7.1. Flight Conditions

Each phase of flight is analyzed under different conditions as the aircraft experiences different forces. For this research, analysis will require concentrating on mainly the longitudinal dynamics of the aircraft, with a look at lateral dynamics as well. The following details the method of identifying the flight conditions required for this research.

1. Review the various flight phases.
2. Identify critical points in flight relative to objectives.
3. Develop time frame for flight analysis.
4. Develop flying conditions (speed, altitude, aircraft state etc.).

1.7.2. Rigid Aircraft Model

The rigid aircraft model is the base of this research. The research is constructed such that various extended analysis requirements are added onto the dynamics of the rigid aircraft model. Thus validation requires that the rigid aircraft model performs in both small and large scale time frames.

The intended approach to developing the rigid model is to ensure that the model accounts for as many nominal properties of flight as possible. Gust models, pilot models and stability augmentation systems are not included here, as they are required for analysis outside the scope of this dissertation. Notwithstanding this statement the model has been developed such that additions may be appended as required.

The layout and methodology for the rigid aircraft model is detailed below:

1. Identify coordinate system.
2. Develop equations of motion.
3. Account for various aerodynamic forces and moments, defined in aerodynamic coefficients.
4. Detail the atmospheric properties.

1.7.3. Piezoelectric Actuation Model

Piezoelectric actuation provides the novelty in this research such that it differs from the usual usage of PAs. Stated earlier, the current applications of PAs are under significant consideration in vibration analysis, and as a stiffening material, as well as sensory applications [Sosnicki *et al.,* (2006), Prechtl (1994)]. Having these uses, PAs can now add a third dimension by performing as an actuating mechanism, which is detailed in this research. Some applications for flight actuation considerations have been researched by Li *et al.,* (2004), Tuzcu and Meirovitch (2006), Li *et al.,* (2011), and more importantly by Bilgen *et al.,* (2013). Although these authors worked on various niche applications to further develop piezoelectric actuation on aircraft, the work presented in this research aims at encompassing and providing a holistic solution that seeks to provide an alternative to current means of trajectory alterations.

In this research, where the focus is primarily on the aerodynamics and flight dynamics, the level of detail for piezo-modeling is limited to application in a hypothetical sense, and does not consider control modelling, the effects caused on the actuator as well as the effects of the actuator itself, and aircraft structural conditions.

The layout and methodology for developing the piezoelectric actuation model is given as follows:

1. Develop assumptions to favour extrapolation of a PA for hypothetical use in this research.
2. Analyze and develop actuation methods based on desired trajectory alterations.
3. Formulate aerodynamic analysis of the actuation methodologies.
4. Develop means of attaching the system (aerodynamic properties) to the rigid aircraft model.

1.7.4. Effects of Elastic Deformation on the Aerodynamic Forces and Moments

As described earlier, the elastic effects on the aircraft's aerodynamics in this research have been broken down for the aircraft into three components, viz. the wing, horizontal tail and vertical tail. It was decided

not to consider the full aircraft in vibration due to the complexity of the model. In applying this decision, the aircraft was deemed completely flexible, and not having to analyze one mode of vibration as done by Meirovitch and Tuzcu (2003).

The layout and methodology for appending the elastic aerodynamics are detailed below:

1. Conduct separate vibrational analysis of each of the three components of the aircraft model. This is a decoupled analysis.
2. Formulate an elastic structure resulting in an aerodynamic model that can be appended to the rigid aircraft model, alongside piezoelectric actuation.

1.7.5. Results

The results which will be primarily displayed in graphs is broken down into piecewise information. As the flight conditions will be set, results will be provided for various inputs by the system model. These results will be displayed with other data made available.

The layout and methodology is to develop:

1. Results of conventional actuation.
2. Results of rigid aircraft + piezoelectric actuation.
3. Results of rigid aircraft + piezoelectric actuation + effects on aerodynamics due to elastic deformation.

1.7.6. Flight Conditions Identified

There are various stages in flight, each presenting differing aircraft states. Some states may require more use of the aircraft throttle, others more use of the aircraft control surfaces. Figure 14 shows the various stages of flight [Boeing (2013)].

As the figure depicts, 57% of the flight occurs during the cruise phase. Here the throttle is set to a constant, and the aircraft experiences straight and level flight. If flight can be made efficient, the cruise phase would be the optimal choice for this consideration. In terms of this research, longitudinal flight is the primary concern, which is best viewed at the cruise phase where the aircraft experiences a net propelling force, with other forces in equilibrium with each other.

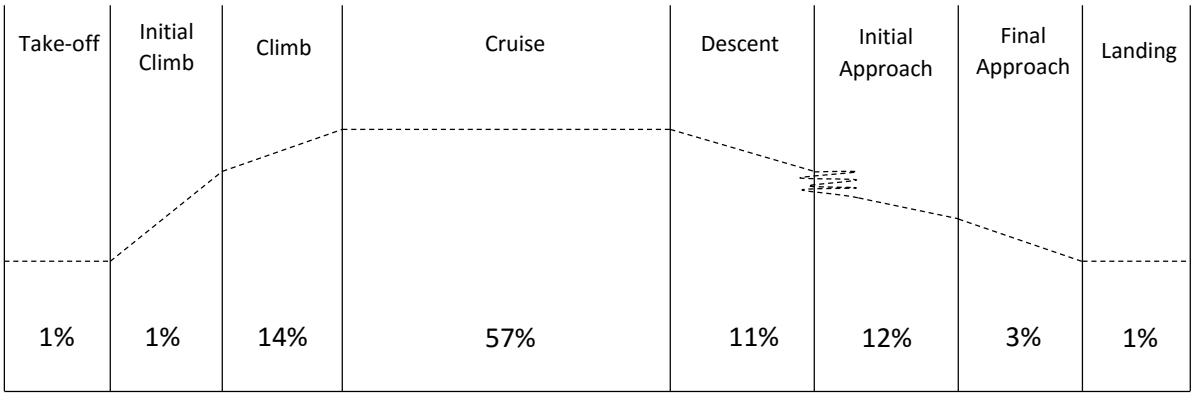

Figure 14: Phases of Flight

Before determining the various models for this research, the flight conditions for cruise, or in technical terms, straight and level flight must be laid out. These are stated in Table 4.

Table 4: Initial Flight Conditions

Item	**Value**
Initial Altitude	8000 m
Initial Velocity	220 m/s
Throttle Setting	100 %
Simulation Time (Max)	10 s

1.8. Contributions to Knowledge

The contribution to knowledge are as follows:

1. A novel actuation methodology on an existing civil aviation aircraft, without the use of conventional aircraft controls.
2. A novel use of smart materials on a fixed-wing aircraft.

1.9. Layout of Dissertation

A description of the layout of this dissertation is provided in Figure 15. Chapter 1 deals with identifying the niche area of study that this dissertation forms part of. The literature details the research conducted in the fields of study of flexible aircraft, flight control systems and smart materials. This then leads into the objectives, where, based on the literature, research gaps are identified and objectives set to fill those gaps.

From the objectives, the flight conditions are identified to set the requirements on which the models were based on. This leads into chapter 2 where the rigid aircraft model is developed. The rigid aircraft model required identification and derivation of the coordinate system and the equations of motions accompanied by the aerodynamic forces and moments respectively.

Chapter 3 involves the design of the novel actuation model intended for this research. The method and logic used to design the actuation system is shown, accompanied by the aerodynamics involved with the necessary flight trajectory changes that would be made by the system.

Chapter 4 deliberates on the elastic effects on the aerodynamic forces and moments. In this chapter, a vibrational analysis similar to that of a cantilever beam is conducted, accompanied by an aerodynamic analysis of this vibration on an aircraft.

To complete the analysis set out by the objectives, the piezoelectric actuation model was appended to the rigid aircraft model. The aerodynamics were analyzed by control deflections only by the novel actuation model. From here, the elastic effects were appended to the rigid model and actuation model, with an analysis once again conducted by control deflections only for the novel actuation model.

Chapter 5 illustrates the results, with comparisons to each model described above, viz.:

1. Rigid model.
2. Rigid model + piezoelectric actuation.
3. Rigid model + piezoelectric actuation + effects on aerodynamic forces and moments due to elastic deformation.

Chapter 6 contains the conclusions based on the novel actuation model developed. The uses for the novel actuation model are tabulated and the objectives set out for the dissertation are addressed. Recommendations are provided to account for assumptions made in this research as well as extended research to further develop the idea.

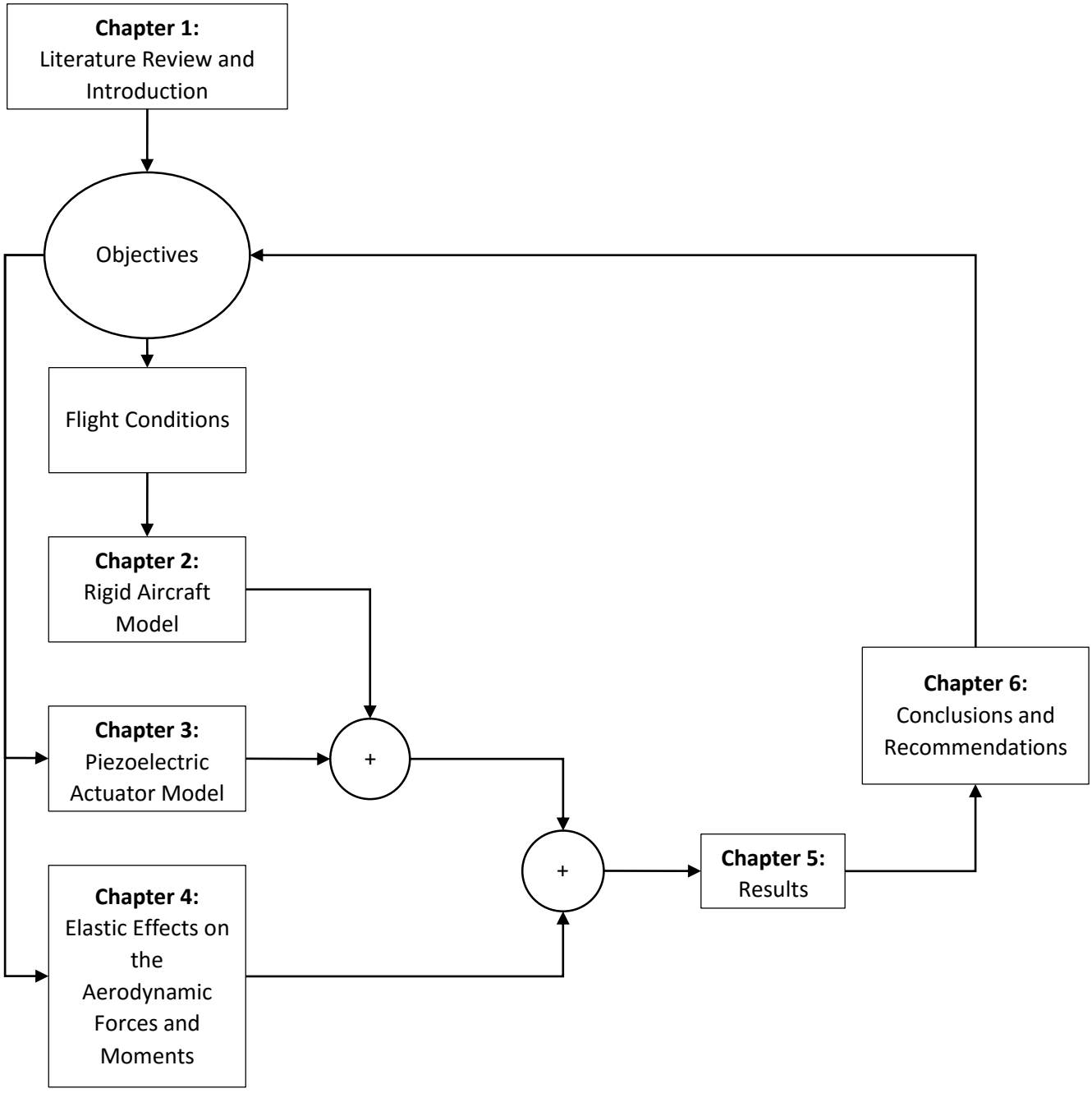

Figure 15: Dissertation Layout Showing Connections between Various Chapters

2. RIGID AIRCRAFT MODEL

The rigid flight dynamics of the aircraft under consideration, the Cessna Citation V, forms the base of the research. As the rigid flight dynamics model develops, the elastic aerodynamics and actuation will be appended, forming a complete model.

2.1. Coordinate System

The coordinate system utilized for the vehicle frame is the body axis system, where the axis origin is situated at the center of gravity (COG) of the vehicle, as shown in Figure 16.

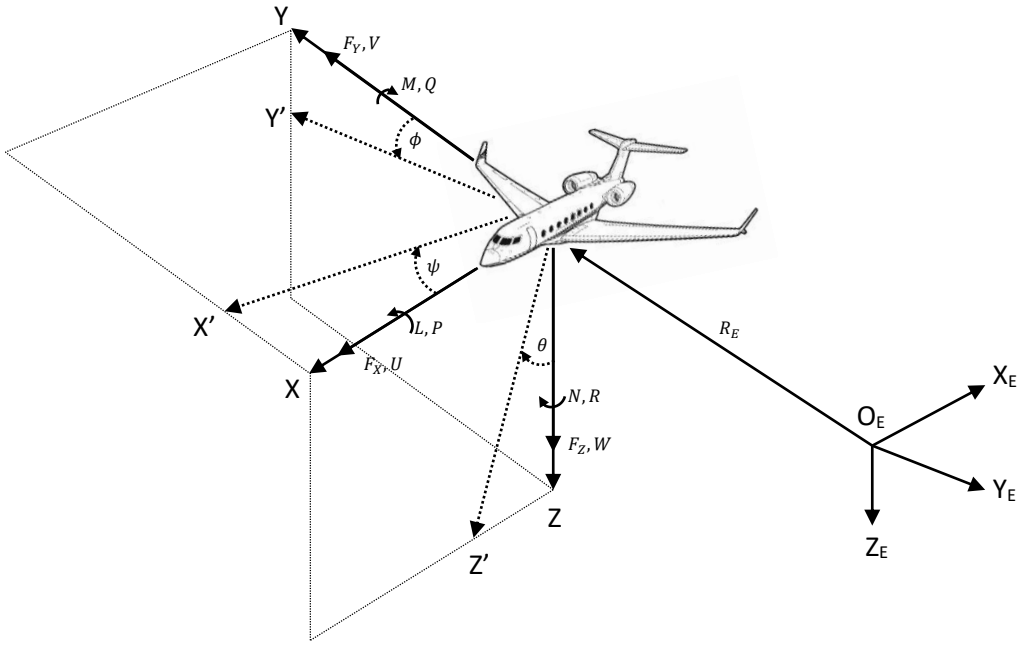

Figure 16: Body Axis Coordinate System for the Aircraft

The body axis breaks down to the coordinates XYZ, where X faces in the direction of the nose, and lies in the symmetry plane of the vehicle (cutting the aircraft in such a way that the left half is symmetrical to the right), Y points in the direction of the right wing, and finally Z is oriented downwards, completing a right-handed orthogonal axis system. This symmetry allows for simplification of the equations of motion, which will be described later. The aircraft forces and moments in the XYZ coordinates are respectively given by F_X, F_Y, F_Z and L, M, N (Roll, Pitch, Yaw). The instantaneous translational velocities in the XYZ coordinates are described by U, V, W, whilst instantaneous rotational velocities by P, Q, R. The positive directions of the vectors are indicated by the direction of the arrows.

The Euler angles (ϕ, θ, ψ) are rotation angles which are measured relative to a previous or equilibrium state of the aircraft. An equilibrium state can be defined as XYZ, and the rotation to the new state through the Euler angles by X'Y'Z'.

O_E is the origin of an Earth Fixed frame, where X_E points in the northerly direction (to the poles), Y_E to the East, and Z_E to the center of the earth. R_E is the vector relating the vehicle fixed frame to the Earth-Fixed frame. To obtain the relation between the vehicle fixed frame and the Earth-Fixed frame, a transformation vector is utilized. The transformation vector requires rotating the Euler angles sequentially to successfully obtain a relation between the vehicle and Earth-Fixed frames. To go from the Earth-Fixed frame to the vehicle-fixed frame, the aircraft is firstly rotated through a bank angle ϕ, then a pitch angle θ, and finally a yaw angle of ψ. The resulting matrix is given as:

$$T_{Earth \to Vehicle} = \begin{bmatrix} 1 & 0 & 0 \\ 0 & cos\phi & sin\phi \\ 0 & -sin\phi & cos\phi \end{bmatrix} \begin{bmatrix} cos\theta & 0 & -sin\theta \\ 0 & 1 & 0 \\ sin\theta & 0 & cos\theta \end{bmatrix} \begin{bmatrix} cos\psi & sin\psi & 0 \\ -sin\psi & cos\psi & 0 \\ 0 & 0 & 1 \end{bmatrix}$$
$$= \begin{bmatrix} (cos\theta cos\psi) & (cos\theta sin\phi) & (-sin\theta) \\ (sin\phi sin\theta cos\psi - cos\phi sin\psi) & (sin\phi sin\theta sin\psi + cos\phi cos\psi) & (sin\phi cos\theta) \\ (cos\phi sin\theta cos\psi + sin\phi sin\psi) & (cos\phi sin\theta sin\psi - sin\phi cos\psi) & (cos\phi cos\theta) \end{bmatrix} \quad (2.1)$$

To obtain a conversion from vehicle fixed frame to Earth-Fixed frame, the inverse of this transformation matrix may be applied.

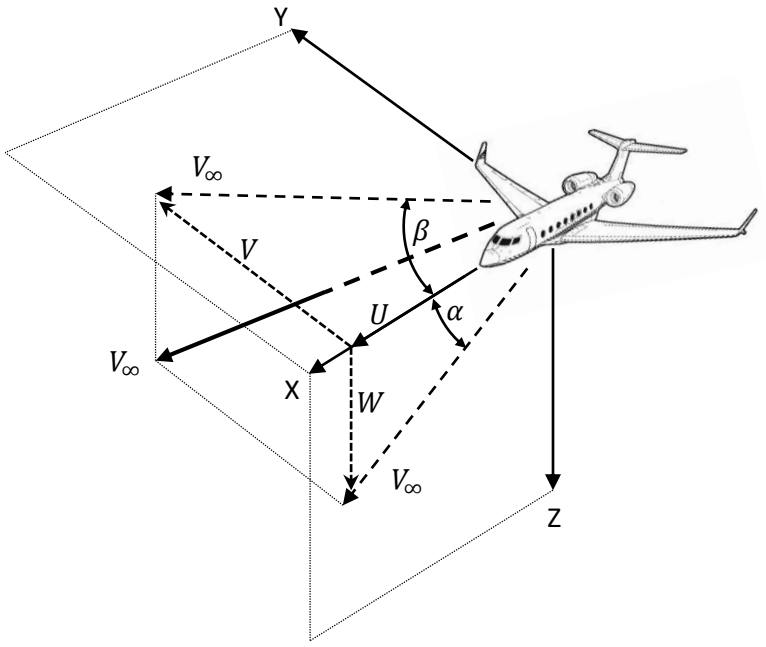

Figure 17: Notation for angle of Attack and Sideslip

The velocity vector, V_∞, described in Figure 17, is the resultant velocity contributed by the three translational velocity components U, V, W. The equation is given by:

$$V_\infty = \sqrt{U^2 + V^2 + W^2} \tag{2.2}$$

The translational velocity components are broken down to formulate the local angle of attack, α, and local sideslip angle, β. These are given by:

$$\alpha = \cos^{-1}\frac{U}{V_\infty} = \tan^{-1}\frac{W}{U}$$
$$\beta = \sin^{-1}\frac{V}{V_\infty} \tag{2.3}$$

2.2. Equations of Motion

The equations of motion for the vehicle have been derived from Schmidt (2012) and Etkin (1959). The equations are nonlinear in nature, and encompass the following assumptions:

- The Earth is considered flat and non-rotating.
- The vehicle is symmetric across the XZ plane (Figure 16).
- The effects of rotating machinery, such as propellers, are ignored as the aircraft under research is a business jet with two jet engines, one placed on either side of the fuselage.
- The effects of variable mass are non-existent. The time frame for simulations do not require adjustment of fuel used and ultimately the dynamics resulting from a changing vehicle mass.

The nonlinear equations governing rigid body translation are given by:

$$\dot{U} = -QW + VR - gsin\theta + \frac{\left(F_{A_X} + F_{P_X}\right)}{m}$$
$$\dot{V} = -RU + PW + gcos\theta sin\phi + \frac{\left(F_{A_Y} + F_{P_Y}\right)}{m} \tag{2.4}$$
$$\dot{W} = -PV + QU + gcos\theta cos\phi + \frac{\left(F_{A_Z} + F_{P_Z}\right)}{m}$$

g is the acceleration due to gravity, set at 9.81 $m.s^{-2}$, and m is the mass of the aircraft. F_A is the aerodynamic forces in the respective coordinate directions XYZ, and F_P the propulsive force due to the jet engines.

Before calculating the rigid body rotations, the moments and products of inertia need to be defined with respect to the body axis of the vehicle. These are given by:

$$\begin{aligned} I_{xx} &= \int_m (y^2 + z^2)dm & I_{xy} &= I_{yx} = \int_m xy\, dm \\ I_{yy} &= \int_m (x^2 + z^2)dm & I_{xz} &= I_{zx} = \int_m xz\, dm \\ I_{zz} &= \int_m (x^2 + y^2)dm & I_{yz} &= I_{zy} = \int_m yz\, dm \end{aligned} \tag{2.5}$$

The mass element dm is the various mass points along the spans of the aircraft .Given that the rigid vehicle is symmetrical about the XZ plane, both $I_{xy} = I_{yx}$ and $I_{yz} = I_{zy}$ are zero. Thus the resulting nonlinear equations for rigid body rotation are given by:

$$\begin{aligned} \dot{Q} &= \frac{1}{I_{yy}}(PR(I_{zz} - I_{xx}) + I_{xz}(R^2 - P^2) + M_A + M_P) \\ \begin{Bmatrix} \dot{P} \\ \dot{R} \end{Bmatrix} &= \frac{1}{I_{xx}I_{zz} - I_{xz}^2}\begin{bmatrix} I_{zz} & I_{xz} \\ I_{xz} & I_{xx} \end{bmatrix}\begin{Bmatrix} I_{xz}PQ + RQ(I_{yy} - I_{zz}) + L_A + L_P \\ -I_{xz}RQ + PQ(I_{xx} - I_{yy}) + N_A + N_P \end{Bmatrix} \end{aligned} \tag{2.6}$$

It can be seen that the rotation rates $\dot{P}$ and $\dot{R}$ are coupled. Thus adverse yaw effects are built into these equations of motion. L_A, M_A, N_A are the aerodynamic moments of roll, pitch and yaw respectively. Those with subscripts 'P' denote the resultant moments due to the propulsive forces.

The body rates described by P, Q, R must be related to the Euler angles given by ϕ, θ, ψ. They are provided by the kinematic equations of motion relating the inertial rotation rates to the Euler angle rates, which are given by:

$$\begin{aligned} \dot{\phi} &= P + Qsin\phi tan\theta + Rcos\phi tan\theta \\ \dot{\theta} &= Qcos\phi - Rsin\phi \end{aligned} \tag{2.7}$$

$$\dot{\psi} = (Qsin\phi + Rcos\phi)sec\theta$$

Integrating these equations will give the Euler angles.

The last of the equations of motion relate the vehicle fixed frame to the Earth-Fixed frame. These are the navigational equations relating the inertial velocity of the aircraft to a reference on the Earth. These equations describe how a reference on the Earth would view the movement of the aircraft in their coordinate system of $X_E Y_E Z_E$, and are given by:

$$\begin{aligned} \dot{X}_E &= Ucos\theta cos\psi + V(sin\phi sin\theta cos\psi - cos\phi sin\psi) + W(cos\phi sin\theta cos\psi + sin\phi sin\psi) \\ \dot{Y}_E &= Ucos\theta sin\psi + V(sin\phi sin\theta sin\psi + cos\phi cos\psi) + W(cos\phi sin\theta sin\psi - sin\phi cos\psi) \\ \dot{Z}_E &= Usin\theta - Vsin\phi cos\theta - Wcos\phi cos\theta \end{aligned} \quad (2.8)$$

Thus concluding the twelve equations of motion for the rigid vehicle. The following describes the equations to obtain the aerodynamic forces and moments.

2.3. Aerodynamic Forces and Moments

The aerodynamic forces and moments are developed by utilizing coefficients [Schmidt (2012) and Etkin (1959)]. The coefficients provide a direct means of relating the aerodynamic properties to the aerodynamic forces.

Table 5: Aerodynamic Coefficients of the Rigid Aircraft

Coefficient	Description	Control Component
$\boldsymbol{C_L}$	Total Lift (wing + body + horizontal tail)	Elevator
$\boldsymbol{C_s}$	Side Force	Rudder + Aileron
$\boldsymbol{C_D}$	Total Drag	-
$\boldsymbol{C_{L_{roll}}}$	Rolling Moment	Rudder + Aileron
$\boldsymbol{C_M}$	Pitching Moment	Elevator
$\boldsymbol{C_N}$	Yawing Moment	Rudder + Aileron

Table 5 outlines the six aerodynamic coefficients, including the control components which cause the greatest effect on that coefficient.

The equation for the lift coefficient is described by:

$$C_L = C_{L_0} + C_{L_\alpha}\alpha + C_{L_Q}Q + C_{L_{\dot{\alpha}}}\dot{\alpha} + C_{L_{i_H}}i_H + C_{L_{\delta_e}}\delta_e \tag{2.9}$$

The respective coefficients in the given equations and those to follow will be explained at a later stage. Here, $\dot{\alpha}$ is the angle of attack derivative, i_H the angle setting for the tail with respect to the fuselage, and δ_e the elevator deflection.

The equation for the side force coefficient is given by:

$$C_S = C_{S_\beta}\beta + C_{S_P}P + C_{S_r}R + C_{S_{\delta_A}}\delta_A + C_{S_{\delta_R}}\delta_R \tag{2.10}$$

Here, δ_A and δ_R are the aileron and rudder deflections respectively.

The equation for the drag coefficient is given by:

$$C_D = C_{D_0} + \left(\frac{C_{L_W}^2}{\pi A_W e_W} + \frac{C_{L_H}^2}{\pi A_H e_H}\frac{q_H}{q_\infty}\frac{S_H}{S_{ref}} + \frac{C_{S_V}^2}{\pi A_V e_V}\frac{q_H}{q_\infty}\frac{S_V}{S_{ref}}\right) \tag{2.11}$$

Here, C_{D_0} is the drag coefficient at zero lift, and the term in brackets is the sum of the induced drag of all three components (viz. wing, horizontal tail and vertical tail). $A_{component}$ is the Aspect Ratio, calculated by the square of the component span, divided by the component reference area, S_{ref} for the wing. The other two are reference areas of the horizontal tail and vertical tail (S_H and S_V respectively). q_H is the dynamic pressure at the tail, which is set to 0.9 of the dynamic pressure, q_∞. The dynamic pressure is a function of air density and aircraft velocity, V_∞ and is given as $\frac{1}{2}\rho V_\infty^2$. The Oswald efficiency number is given by $e_{component}$, which is dependent on the shape of the wing, and has magnitude one for an elliptical wing shape.

The components C_{L_W}, C_{L_H} and C_{S_V} are given by the following equations:

$$C_{L_W} = C_{L_{\alpha_W}}(\alpha + i_W - \alpha_{0_W}) \tag{2.12}$$

$$C_{L_H} = C_{L_{\alpha_H}}\left(\left(1 - \frac{d\epsilon}{d\alpha}\right)(\alpha + i_W) + \frac{d\epsilon}{d\alpha}\alpha_{0_W} + i_H - \alpha_{0_H} + \alpha_\delta \delta_E\right)$$

$$C_{S_V} = C_{S_{\beta_V}}(\beta + \beta_\delta \delta_R)$$

The coefficients in the above equations differ from those described earlier as these are component intensive and require correct geometrical and aerodynamic data for evaluation. Here, i_W is the wing angle setting relative to the fuselage, α_{0_W} and α_{0_H} the zero lift angle of attack. $\frac{d\epsilon}{d\alpha}$ is the downwash factor, which can be applied for both the horizontal tail and vertical tail. The lift curve slopes for each component are given by $C_{L_{\alpha_{component}}}$ for the wing and horizontal tail, and $C_{S_{\beta_V}}$ for the vertical tail.

The effectiveness of the elevator and rudder are given by α_δ and β_δ respectively. These are percentages which dictate how effective the control surfaces are in relation to the lift and drag they produce. The setting applied here is of 0.65 [Schmidt (2012)].

The equation for the rolling moment coefficient is given by:

$$C_{L_{roll}} = C_{L_\beta}\beta + C_{L_P}P + C_{L_r}R + C_{L_{\delta_A}}\delta_A + C_{L_{\delta_R}}\delta_R \tag{2.13}$$

Finally, the equations for the pitching and yawing moment coefficients are given by:

$$C_M = C_{M_{\alpha=\delta_E=i_H=0}} + C_{M_\alpha}\alpha + C_{M_{\dot{\alpha}}}\dot{\alpha} + C_{M_Q}Q + C_{M_{i_H}}i_H + C_{M_{\delta_E}}\delta_E \tag{2.14}$$

$$C_N = C_{N_\beta}\beta + C_{N_P}P + C_{N_r}R + C_{N_{\delta_A}}\delta_A + C_{N_{\delta_R}}\delta_R \tag{2.15}$$

The lift, side force and drag coefficients may be related to their respective forces by:

$$\begin{aligned} L &= C_L q_\infty S_W \\ S &= C_S q_\infty S_W \\ D &= C_D q_\infty S_W \end{aligned} \tag{2.16}$$

These forces are finally placed in the XYZ directions for the aerodynamic forces, $F_{A_X}, F_{A_Y}, F_{A_Z}$, and are given by:

$$F_{A_X} = -Dcos\alpha cos\beta - Scos\alpha sin\beta + Lsin\alpha \tag{2.17}$$

$$F_{A_Y} = -Dsin\beta + Scos\beta$$
$$F_{A_Z} = -Dsin\alpha cos\beta - Ssin\alpha sin\beta - Lcos\alpha$$

The roll, pitch and yaw coefficients are related to their aerodynamic forces by:

$$\begin{aligned} L_{roll_A} &= C_{L_{roll}} q_\infty S_W b_W \\ M_A &= C_M q_\infty S_W \bar{c}_W \\ N_A &= C_N q_\infty S_W b_W \end{aligned} \tag{2.18}$$

Here, b_W is the wingspan, and $\bar{c}_W$ the mean aerodynamic chord of the wing, or MAC. This ultimately provides a relation and means of obtaining the aerodynamic forces through the coefficient method. Next, the coefficients in the above equations will be discussed further, and their means of calculation.

2.4. Aerodynamic Coefficients

The aerodynamic coefficients for the forces and moments presented in the previous section are functions of various other coefficients which constitute the aircraft aerodynamics. Most of the coefficients stated are functions of the aircraft state, mainly the angle of attack. Work from Roskam (2001) and the utilization of DATCOM were compared to obtain the resulting coefficients. Firstly, material from Roskam (2001) is presented.

Table 6 describes the various coefficients which constitute the lift coefficient. Here, $C_{L_{\alpha_{component}}}$ is the lift curve slope of that component, and $\left(X_{AC_H} - X_{ref}\right)$ is the distance between the aerodynamic center of the horizontal tail and the COG. $\bar{V}_H$ is the horizontal tail volume coefficient, and is given by $\frac{S_H}{S_{ref}} \frac{\left(X_{AC_H} - X_{ref}\right)}{\bar{c}_W}$.

Table 7 describes the various coefficients which constitute the side force coefficient. Here, $\frac{d\sigma}{d\beta}$ is the side wash derivative, and is set as 0.1. $Z_{S_{MAC}}$ is the vertical distance between the mean aerodynamic chord of the vertical tail and the aircraft COG, and $X_{S_{MAC}}$ between the horizontal distance of the same two properties.

Table 8 describes the various coefficients which constitute the rolling moment coefficient.

Table 6: Description of Coefficients for Lift

Coefficient	Description	Equation	Equation No.
C_{L_0}	Zero Angle of Attack (AOA) Lift	Obtained from Airfoil Data	
C_{L_α}	AOA Lift Effectiveness	$C_{L_{\alpha_W}} + C_{L_{\alpha_H}} \frac{q_H S_H}{q_\infty S_{ref}} \left(1 - \frac{d\epsilon}{d\alpha}\right)$	(2.19)
C_{L_Q}	Pitch Rate Effectiveness	$2C_{L_{\alpha_H}} \frac{\left(X_{AC_H} - X_{ref}\right)}{\bar{c}_W} \frac{q_H S_H}{q_\infty S_{ref}}$	(2.20)
$C_{L_{\dot{\alpha}}}$	AOA Rate Lift Effectiveness	$2C_{L_{\alpha_H}} \frac{q_H}{q_\infty} \frac{d\epsilon}{d\alpha} \bar{V}_H$	(2.21)
$C_{L_{i_H}}$	Tail Incidence Lift Effectiveness	$C_{L_{\alpha_H}} \frac{q_H S_H}{q_\infty S_{ref}}$	(2.22)
$C_{L_{\delta_e}}$	Elevator Lift Effectiveness	$C_{L_{\alpha_H}} \frac{q_H S_H}{q_\infty S_{ref}} \alpha_\delta$	(2.23)

Table 7: Description of Coefficients for Side Force

Coefficient	Description	Equation	Equation No.
C_{S_β}	Side Slip Effectiveness	$-C_{L_{\alpha_V}} \frac{q_H S_V}{q_\infty S_{ref}} \left(1 - \frac{d\sigma}{d\beta}\right)$	(2.24)
C_{S_P}	Roll Rate Side Force Effectiveness	$-2C_{L_{\alpha_V}} \frac{q_H S_V}{q_\infty S_{ref}} \frac{Z_{S_{MAC}}}{b_W}$	(2.25)
C_{S_r}	Yaw Rate Side Force Effectiveness	$C_{L_{\alpha_V}} \frac{q_H S_V}{q_\infty S_{ref}} \frac{2X_{S_{MAC}}}{b_W}$	(2.26)
$C_{S_{\delta_R}}$	Rudder Side Force Effectiveness	$C_{L_{\alpha_V}} \frac{q_H S_V}{q_\infty S_{ref}} \beta_\delta$	(2.27)

Table 8: Description of Coefficients for Rolling Moment

Coefficient	Description	Equation	Equation No.
C_{L_β}	Side Slip Rolling Moment Effectiveness	Read off Data Tables	
C_{L_P}	Roll Rate Rolling Moment Effectiveness	Read off Data Tables	
C_{L_r}	Yaw Rate Rolling Moment Effectiveness	$C_{L_{\alpha_V}}\left(\frac{2X_{S_{MAC}}Z_{S_{MAC}}}{b_W^2}\right)\frac{q_H S_V}{q_\infty S_{ref}}$	(2.28)
$C_{L_{\delta_A}}$	Aileron Rolling Moment Effectiveness	$C_{L_{\alpha_V}}\frac{q_H S_V}{q_\infty S_{ref}}\frac{X_{S_{MAC}}}{b_W}\beta_\delta$	(2.29)
$C_{L_{\delta_R}}$	Rudder Rolling Moment Effectiveness	Read off Data Tables	

Coefficients that could not be calculated were utilized from data tables provided by Roskam (2001). Table 9 describes the various coefficients which constitute the pitching moment coefficient, and constituents of the yawing moment coefficient in Table 10. To add a degree of certainty and comparison to the equations provided by Roskam (2001), a DATCOM Model was utilized for the aircraft. DATCOM is specialized software which develops directional stability derivatives, as well as aerodynamic information with the most recent versions. The DATCOM model utilized here does not account for rudder input, and thus these values cannot be measured. Table 11 displays the data calculated using the equations from Table 9 and Table 10 and the values developed by DATCOM. It must be noted here that DATCOM develops the aerodynamics by a range of angle of attack values, thus for this case, the values at an angle of attack of zero degrees have been chosen. Roskam (2001) equations do not take into account change of angle of attack. Concurrently, the coefficients for aileron and rudder are both given as a function of angle of attack and deflection of that control surface.

Table 9: Description of Coefficients for Pitching Moment

Coefficient	Description	Equation	Equation No.
$C_{M_{\alpha=\delta_E=i_H=0}}$	Zero Setting Pitching Moment Effectiveness	Read Off Data Tables	
C_{M_α}	AOA Pitching Moment Effectiveness	$C_{L_{\alpha_W}} \frac{(X_{ref} - X_{AC_W})}{\bar{c}_W} - C_{L_{\alpha_H}} \frac{q_H S_H}{q_\infty S_{ref}} \left(\frac{X_{AC_H} - X_{ref}}{\bar{c}_W}\right)\left(1 - \frac{d\epsilon}{d\alpha}\right)$	(2.30)
$C_{M_{\dot{\alpha}}}$	AOA Rate Pitching Moment Effectiveness	$-C_{L_{\alpha_H}} \bar{V}_H \frac{q_H}{q_\infty} \left(\frac{X_{AC_H} - X_{ref}}{\bar{c}_W}\right) \frac{d\epsilon}{d\alpha}$	(2.31)
C_{M_Q}	Pitch Rate Pitching Moment Effectiveness	$-2.2 C_{L_{\alpha_H}} \bar{V}_H \frac{q_H}{q_\infty} \left(\frac{X_{AC_H} - X_{ref}}{\bar{c}_W}\right)$	(2.32)
$C_{M_{i_H}}$	Tail Setting Pitching Moment Effectiveness	$-C_{L_{\alpha_H}} \frac{q_H S_H}{q_\infty S_{ref}} \left(\frac{X_{AC_H} - X_{ref}}{\bar{c}_W}\right)$	(2.33)
$C_{M_{\delta_E}}$	Elevator Pitching Moment Effectiveness	$-C_{L_{\alpha_H}} \frac{q_H S_H}{q_\infty S_{ref}} \bar{V}_H \beta_\delta$	(2.34)

Table 10: Description of Coefficients for Yawing Moment

Coefficient	Description	Equation	Equation No.
C_{N_β}	Side Slip Yawing Moment Effectiveness	$C_{L_{\alpha_V}} \left(1 - \frac{d\sigma}{d\beta}\right) \frac{q_H S_V}{q_\infty S_{ref}} \frac{X_{S_{MAC}}}{b_W}$	(2.35)
C_{N_P}	Roll Rate Yawing Moment Effectiveness	$2 C_{L_{\alpha_V}} \left(\frac{X_{S_{MAC}} Z_{S_{MAC}}}{b_W^2}\right) \frac{q_H S_V}{q_\infty S_{ref}}$	(2.36)
C_{N_r}	Yaw Rate Yawing Moment Effectiveness	$-C_{L_{\alpha_V}} \left(\frac{2X_{S_{MAC}}^2}{b_W^2}\right) \frac{q_H S_V}{q_\infty S_{ref}}$	(2.37)
$C_{N_{\delta_A}}$	Aileron Yawing Moment Effectiveness	Read Off Data Tables	
$C_{N_{\delta_R}}$	Rudder Yawing Moment Effectiveness	Read Off Data Tables	

Table 11: Comparison between Roskam (2001) Values and DATCOM Values

Coefficient	Roskam Equations	DATCOM Model	% Error
C_{L_α}	6.32	5.73	9.33
C_{L_Q}	8.56	7.96	7.01
$C_{L_{\dot{\alpha}}}$	3.54	2.70	23.7
$C_{L_{i_H}}$	1.34	Not available	-
$C_{L_{\delta_e}}$	0.872	Function of α and δ_E	-
C_{S_β}	-0.527	-0.722	-37.0
C_{S_P}	-0.155	-0.111	28.4
C_{S_r}	0.413	Not available	-
$C_{S_{\delta_R}}$	0.380	Not Available	-
C_{L_β}	-0.0328	-0.142	-333
C_{L_P}	-0.400	-0.498	-24.5
C_{L_r}	0.0546	0.0716	-31.1
$C_{L_{\delta_A}}$	-0.142	Function of α and δ_A	-
$C_{L_{\delta_R}}$	0.134	Not Available	-
$C_{M_{\alpha=\delta_E=i_H=0}}$	-0.1	Not Available	-
C_{M_α}	1.02	2.25	-121
$C_{M_{\dot{\alpha}}}$	-0.761	-0.1327	82.6
C_{M_Q}	-2.02	-3.54	-75.2
$C_{M_{i_H}}$	-0.288	Not Available	-
$C_{M_{\delta_E}}$	-2.78	Function of α and δ_E	-
C_{N_β}	0.186	0.0693	62.7
C_{N_P}	0.0546	-0.0156	129
C_{N_r}	-0.146	-0.112	23.3
$C_{N_{\delta_A}}$	-0.0259	Function of α and δ_A	-
$C_{N_{\delta_R}}$	-0.0414	Not Available	-

The DATCOM values have been referenced against those developed by the Roskam (2001) equations. Upon thorough analysis, the differences are fairly significant and dictate large errors. It can be argued that the values by Roskam (2001) equations do not account for continually changing aircraft state, and provide an average and value to be utilized for all aircraft conditions. To test which of the two aerodynamic properties were viable for use, both data were utilized, and those of Roskam (2001) were found to be highly unsuitable. Mainly due to the fact the aircraft would uncontrollably rotate about all its axes for the duration of the simulation, as shown in Figure 18. It was realized that no measures to condition the aircraft

were present by the equations of Roskam (2001), i.e., in cases of high angle of attacks, effectiveness of the control surfaces and other coefficients would be virtually non-existent. DATCOM provided this feature, and upon application, the aircraft would automatically stabilize itself in flight.

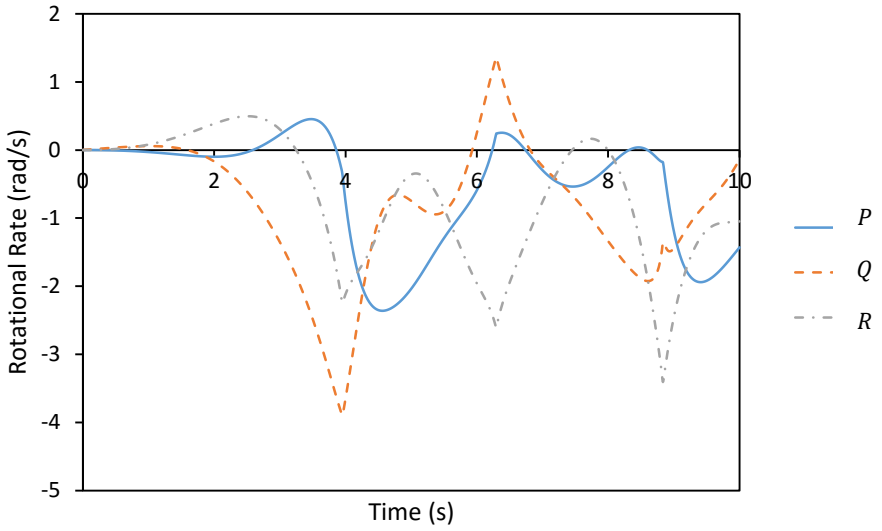

Figure 18: Rotational Rates showing Instability of the Initial Rigid Model

2.5. Atmospheric Properties

The atmosphere is constituted of several layers, of which the aircraft is assumed to only fly in the troposphere, which has a maximum altitude of 10 997 m. [Andrews (2011)]. The pressure at a given altitude Z_E is given by [Anonymous (1955)]:

$$P_s = 10332(1 - (2.2256E - 05)Z_E)^{5.256} \tag{2.38}$$

The temperature and density is given by, respectively

$$T_s = 288.16 - 0.0065Z_E \tag{2.39}$$

$$\rho = \rho_0 \left(\frac{T_s}{T_0}\right)^{4.2561} \tag{2.40}$$

where $\rho_0 = 1.225\ kg/m^3$ for sea level density, and $T_0 = 288.16K$ for sea level temperature. The dynamic viscosity is given by:

$$\mu_{air} = (1.46E-06)\frac{T_s^{1.5}}{T_s + 114} \tag{2.41}$$

2.6. Trim Conditions

Before the model can be simulated, the aircraft needs to be trimmed to allow for straight and level flight. The aircraft trim conditions require that thrust equals drag, lift equals weight and the sum of moments about the aircraft's y-axis must equal zero, as follows [Roskam (2001), Chattot and Hafez (2015)]:

$$\begin{aligned} Thrust &= Drag \\ Lift &= Weight \\ \sum M_y &= 0 \end{aligned} \tag{2.42}$$

The trim condition unknowns for this rigid model are only elevator deflection (δ_e) and pitch angle which is equal to the aircraft angle of attack ($\theta = \alpha$). The third unknown is commonly thrust, however thrust has already been set to 100% as described in Table 4, and thus the third trim condition will be excluded. The derivation for the trim condition is described as follows.

For thrust equals to drag, drag is substituted by Eq. 2.16:

$$Thrust = C_D q_\infty S_W$$

The coefficient of drag, C_D, is then substituted by Eq. 2.11.

$$Thrust = q_\infty S_W \left(C_{D_0} + \left(\frac{C_{L_W}^2}{\pi A_W e_W} + \frac{C_{L_H}^2}{\pi A_H e_H} \frac{q_H}{q_\infty} \frac{S_H}{S_{ref}} \right) \right)$$

The term C_{S_V} has been omitted from the equation as there is no lateral motion of the aircraft. The respective values for C_{L_W} and C_{L_H} are substituted (Eq. 2.12) to create the following trim equation due to thrust equaling drag, with the two unknowns $\theta = \alpha$ and δ_e:

$$Thrust = q_\infty S_W \left(C_{D_0} + \frac{\left(C_{L_{\alpha_W}} \left(\alpha + i_W - \alpha_{0_W} \right) \right)^2}{\pi A_W e_W} \right) \tag{2.43}$$

$$+q_\infty S_W \left(\frac{\left(\left(1-\frac{d\epsilon}{d\alpha}\right)(\alpha+i_W)+\frac{d\epsilon}{d\alpha}\alpha_{0_W}+i_H-\alpha_{0_H}+\alpha_\delta \delta_E\right)^2}{\pi A_H e_H} \right)$$

For lift equal to weight, lift is substituted by Eq. 2.16:

$$W = mg = C_L q_\infty S_W$$

The coefficient of lift is now substituted by Eq. 2.9:

$$mg = q_\infty S_W \left(C_{L_0} + C_{L_\alpha}\alpha + C_{L_Q} Q + C_{L_{\dot{\alpha}}}\dot{\alpha} + C_{L_{i_H}} i_H + C_{L_{\delta_e}} \delta_e \right)$$

The terms Q and $\dot{\alpha}$ are zero, thus the equation for trim, with the two unknowns $\theta = \alpha$ and δ_e is:

$$mg = q_\infty S_W \left(C_{L_0} + C_{L_\alpha}\alpha + C_{L_{i_H}} i_H + C_{L_{\delta_e}} \delta_e \right) \quad (2.44)$$

Now, Eqs. 2.44 and 2.43 are solved simultaneously to obtain $\theta = \alpha$ and δ_e. The resulting trim conditions are shown in Table 12.

Table 12: Trim Setting for Angle of Attack and Elevator Deflection

Trim Variable	Value
$\theta = \alpha$	-1.12°
δ_e	0.458°

2.7. Rigid Model Simulation

As the equations for the rigid aircraft model have now been developed, implementing them into a Simulink model and observation of the base results are required. The results presented below depict the mechanics of how the model regulates itself as it follows a cruise flight condition with no control input, stated in section 1.7.6 Flight Conditions Identified. Figure 19 displays the aircraft body-axis velocity U and Earth-Fixed axis relative velocity $\dot{X}_E$.

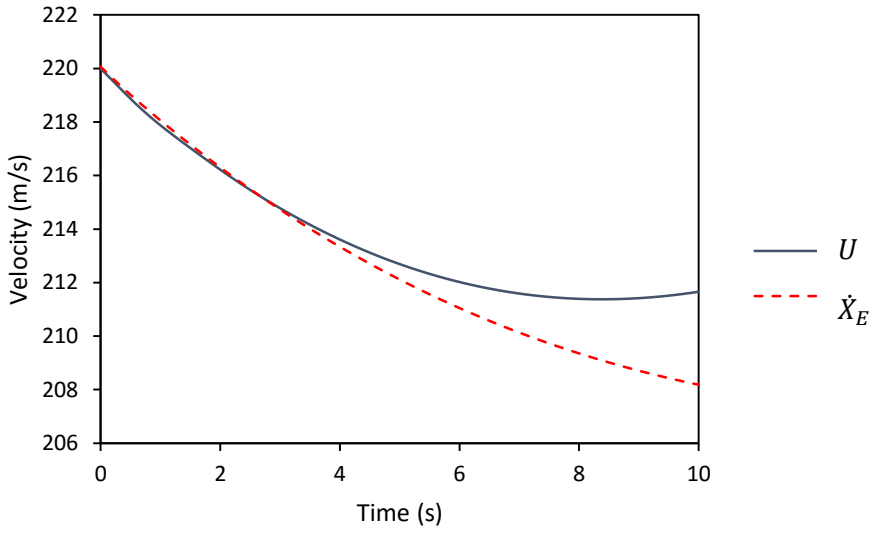

Figure 19: Aircraft Body Axis Velocity U with Earth Fixed Velocity $\dot{X}_E$

It can be noted that the aircraft experiences a decrease in velocity, in both reference frames. Of particular importance is the similarity between the two curves. Figure 20 displays both the body and Earth-Fixed axis vertical velocities.

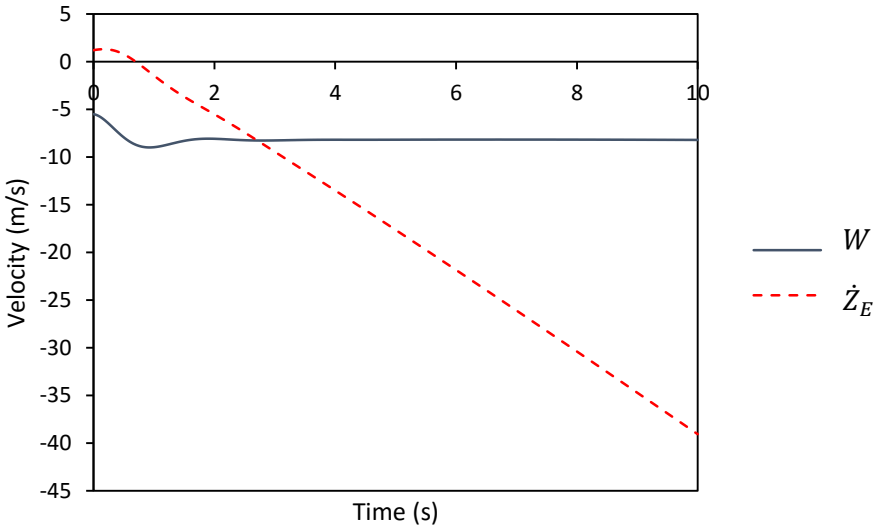

Figure 20: Body Axis Velocity W with Earth Fixed Velocity $\dot{Z}_E$

With regard to W, the model finds its equilibrium and tends to linearly decrease to -8 m/s. The negative magnitude of these two entities describes an upward motion of the aircraft model. Figure 21 displays the

velocity vector and the angle of attack of the aircraft. As it can be seen, the aircraft regulates itself and finds its equilibrium position within the time frame under the given flight conditions.

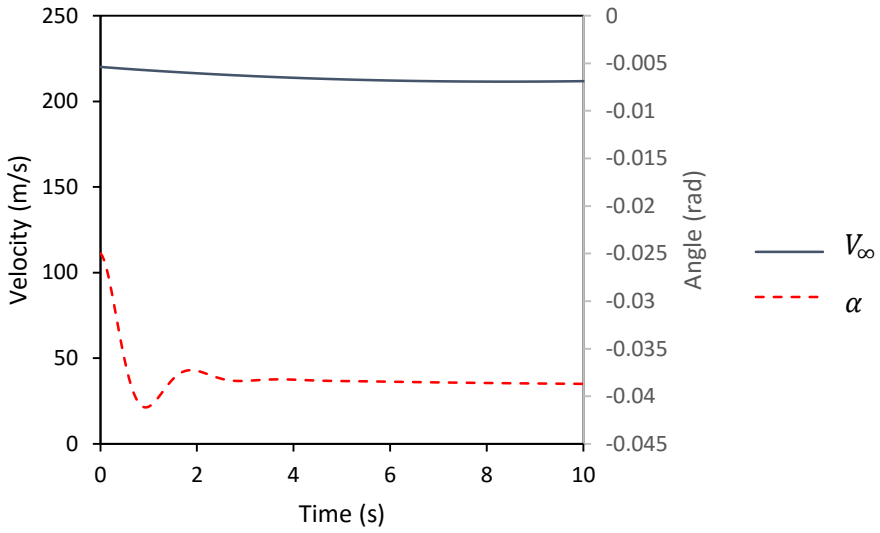

Figure 21: Aircraft Velocity Vector V_∞ with Angle of Attack α

Figure 22 shows the moment of the aircraft. Under the given conditions the aircraft fluctuates and pitches upwards and downwards until it finds its equilibrium position, which is slightly below zero, showing the aircraft pitches downwards.

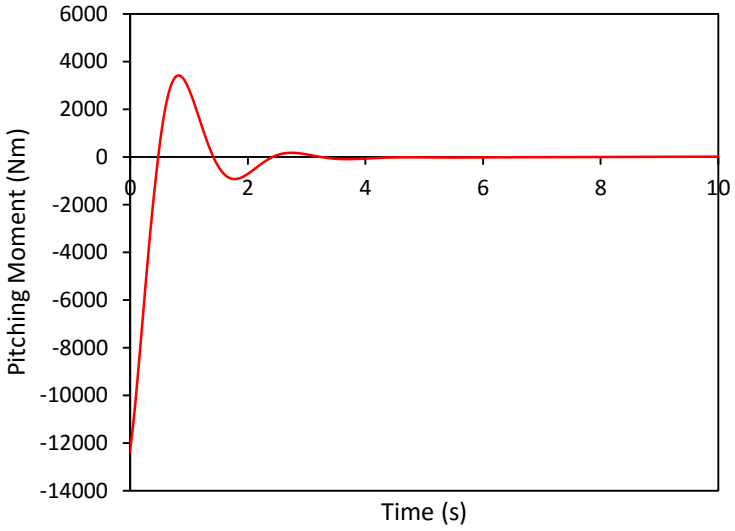

Figure 22: Aircraft Pitching Moment M

This is advantageous for stall conditions, as a net pitching down moment prevents the aircraft stall, adding safety to the system.

Figure 23 to Figure 26 provide details on other flight properties. It can be noted that the aircraft has a net downward force and pitching entities.

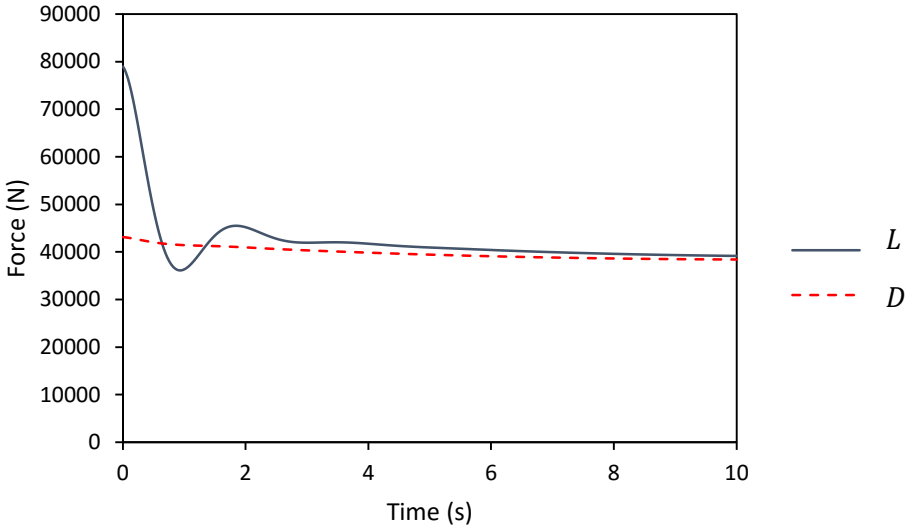

Figure 23: Aircraft Lift Force L and Drag Force D

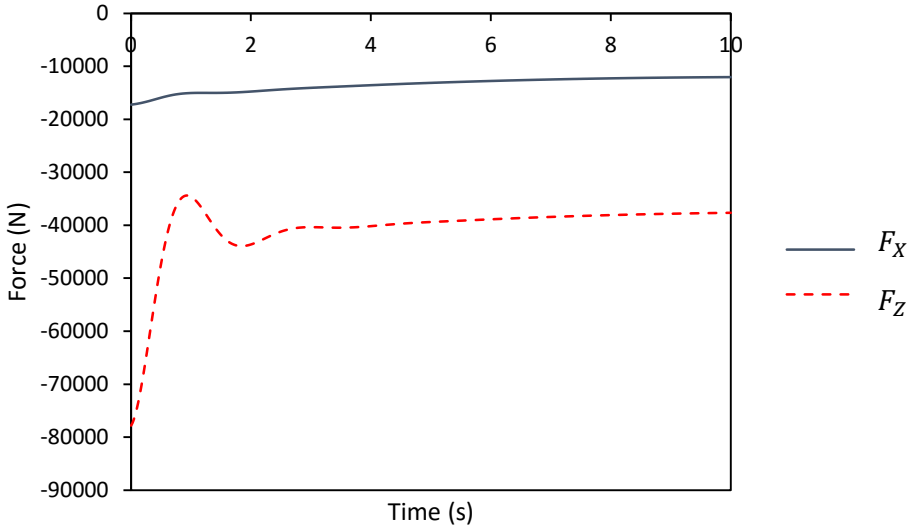

Figure 24: Aircraft Body Axis Forces $F_X$and F_Z

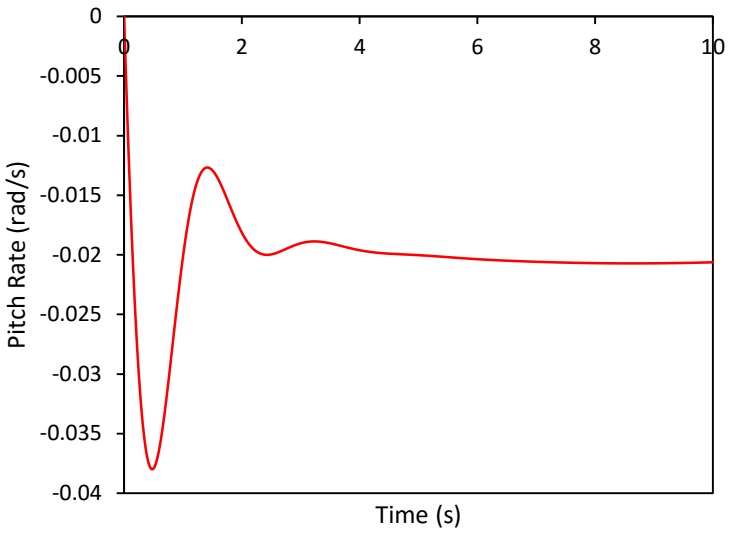

Figure 25: Aircraft Body Axis Pitch Rate Q

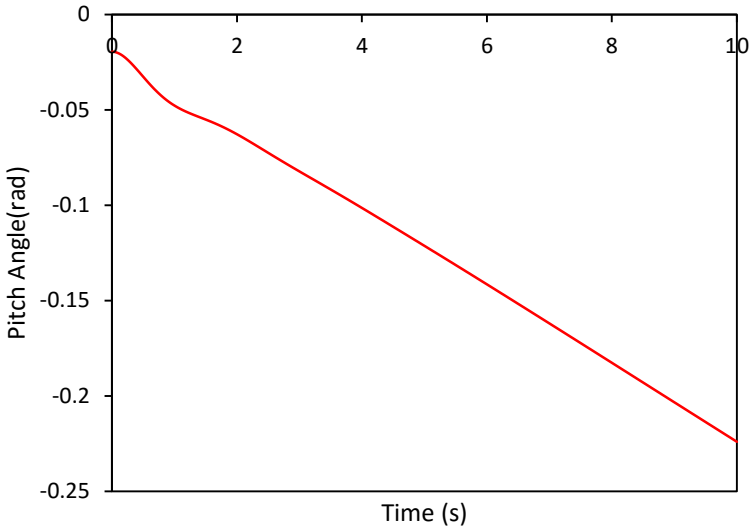

Figure 26: Aircraft Euler Pitch Angle θ

Figure 26 shows that the pitch angle continuously decreases linearly. This correlates to the negative pitching moment displayed in Figure 22 and constant negative pitch rate after a few seconds shown in Figure 25. These results indicate the model's tendency to aerodynamically become nose heavy, constantly pitching downwards. In terms of stability, it is a positive attribute for the aircraft to constantly want to pitch downwards. This, as explained earlier, prevents the aircraft from reaching stall, but simultaneously

requires trim control to ensure straight and level flight. The tendency to continuously pitch downwards is slightly higher than anticipated in this model.

Figure 27 displays the various aerodynamic coefficients of the aircraft model. Other coefficients are not shown as the aircraft is in straight and level flight rendering them a zero magnitude.

With a lift to drag ratio of roughly 1.85, the aircraft does not display positive characteristics in terms of efficiency. However, the model displays longitudinal static stability characteristics if a pitching disturbances is added.

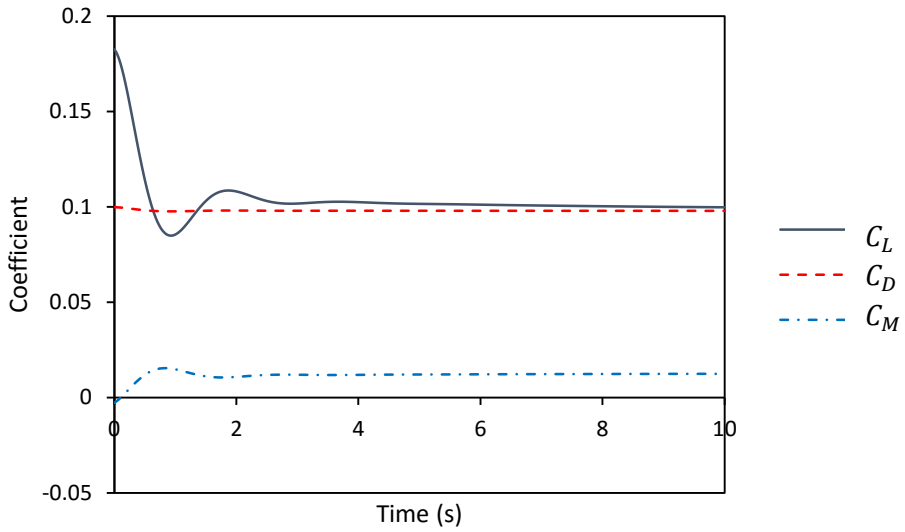

Figure 27: Aerodynamic Coefficients of Lift (C_L), Drag (C_D) and Pitching Moment (C_M)

3. PIEZOELECTRIC ACTUATION MODEL

The process of developing flight trajectory alterations using piezoelectric actuators is unique and vastly different to the usual application of PAs. The usual applications include flutter suppression, vibration suppression and the use of PAs as a stiffening structure for added structural advantage. In this research however, PAs will not be approached as described above, where they will be utilised is altering the structure of the aircraft, specifically the wing, to geometrically alter the shape, causing aerodynamic disturbances, and thus flight trajectory alterations.

During the course of developing and simulating the actuation process, there was a constant debate on whether to confirm the actuation as a primary (similar to aileron, elevator and rudder) or secondary application (similar to flaps, slats, tabs etc.). This will be further discussed in the discussions of the results.

It must be noted here that the design of the actuation mechanism is mostly conceptual, and does not consider vibrational, structural and any control design research. This actuation methodology is used to determine the aerodynamics of the aircraft.

The following highlights assumptions and methods for producing the flight trajectory alterations.

3.1. Assumptions

A few assumptions were made to examine the scope of the actuation methodology and simplify the system for research and implementation.

1. The structural components such as the stiffeners, spars, ribs and beams are flexible and maintain their structural integrity. It is assumed the structural rigidity can be adjusted by the actuators, but has not been calculated for this research.
2. The camber at each station of the wing remains constant. This is assumed as the change in camber relates to a completely different scope of analysis, increasing the complexity of the system.
3. The placement of the actuators is hypothetical, and does not disturb the placement of the primary and secondary control surfaces. Thus, the PAs and conventional control surfaces are set to work individually or in unison.
4. The PAs are scaled and enlarged from those that are currently available. It is assumed the actuators follow the same method of operations, essentially assuming that up-scaling of the actuators is linear.

5. The deflections of the actuators are linear. This is assumed as the scope of this research is not actuation modelling analysis and control, but rather using an actuation method to analyse the aerodynamics and flight dynamics of the aircraft.

3.2. Actuation Methods

The most convenient method of altering the wings geometry, without creating extra structural issues, is to follow the flexibility of the structural beam used in a conventional wing. This is done as the structural beam is used in performing flexible aircraft flight dynamic analysis, and all mass centers can be referred to this point by transfer of mass and moments. To apply this methodology, assumption 1 is utilised to render the beam as flexible as possible, but at the same time maintaining structural integrity. Figure 28 shows the three types of deflections for various modes of vibration of a flexible I-beam.

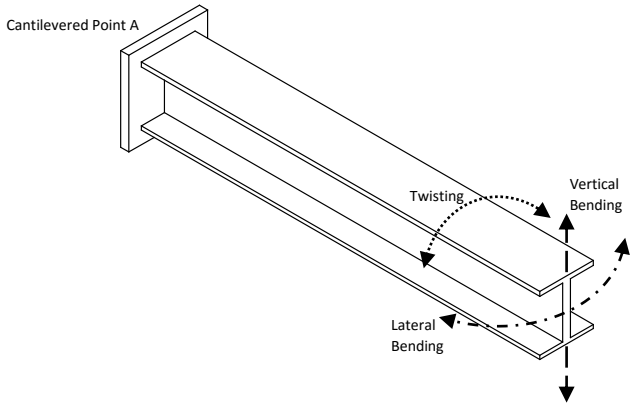

Figure 28: Mode Shape Deflections of a Simple Cantilever I-Beam

As the figure shows, there are three deflection types, and each deflection has its own vibration mode. The beam is cantilevered at one end, and free on the other. The beam experiences a maximum in twist, vertical bending and lateral bending at the free end only for the first mode of vibration for the given deflections. The modes of vibration of importance for this research are the twisting and vertical bending modes. Lateral bending was not chosen here as it results in a change in the sweep angle, which has been excluded in the aerodynamic analysis.

Thus, adapting these modes of vibration as deflections of an aircraft wing, cantilevered point 'A' can be set as the wing root, and the free end as the wing tip. Thus the twisting deflection is set as the wash-out or wash-in of the wing, and the vertical bending mode is set as the dihedral or anhedral of the wing.

The following describes the details of each actuation type being researched for use on the aircraft wing, i.e. twisting actuation and bending actuation.

3.2.1. Twisting Actuation

The twisting actuation is the more important of the two actuation methods described. This is because the twisting actuation results in the majority of the aerodynamic disturbances in the longitudinal stability of the aircraft. Current literature utilises PAs to be strategically positioned for vibration and flutter suppression, for this research however, the actuators are strategically positioned to bring about the maximum desired geometric deflection.

3.2.1.1. Actuator Positioning and Deflections

The twisting actuation is brought about by utilising the twisting motion of the beam in the wing, as described in Figure 28. This is possible by placing the actuators as shown in Figure 29.

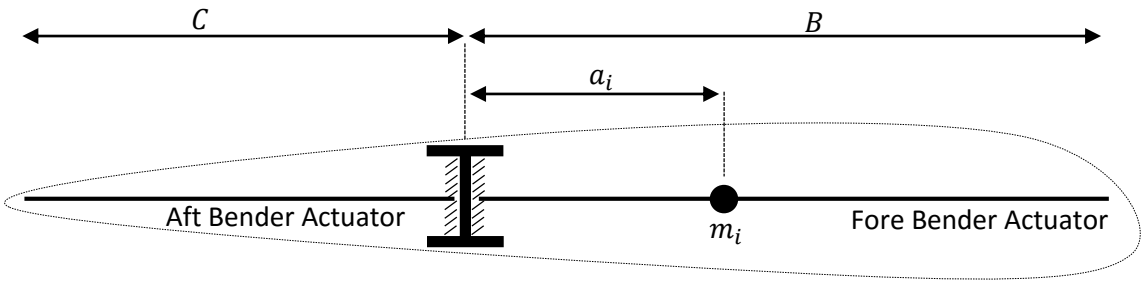

Figure 29: Wing Profile Showing Placement of Piezoelectric Bender Actuators

The bender actuators utilised for this application are split into two lengthwise pieces, the aft and fore actuators, which have dimensions C and B respectively. It is to be noted that due to the position of the beam utilised with referenced to data provided by Tuzcu and Meirovitch (2006), $C < B$, in other words the aft bender actuator is always smaller than the fore bender actuator. These actuators are fixed at the ends at the I-beam as shown in Figure 29. The addition of the lengths of the two bender actuators results

in the chord of that particular section. The distance from the beam and the mass element of the section, m_i, is a_i.

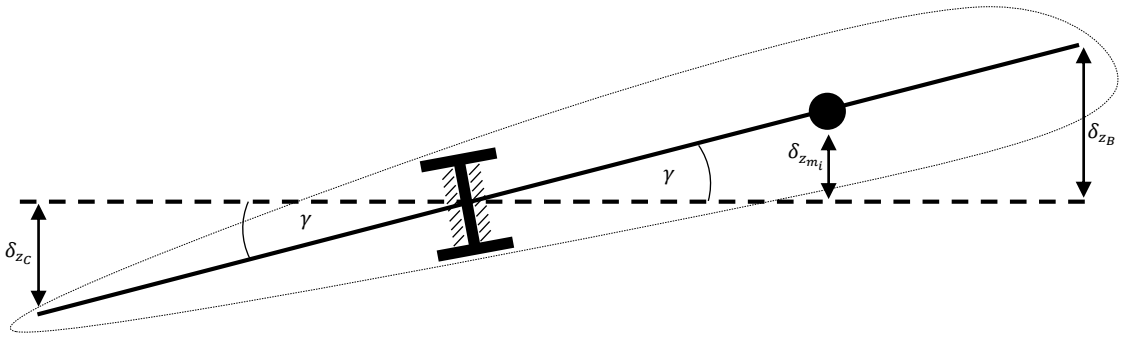

Figure 30: Wing Profile Showing Vertical Displacements due to Positive Twist

Figure 30 shows the resulting twist from the bender actuators. The fore and aft bender actuators deflect in unison, causing a twist angle of γ. Utilising assumption 5, the actuators experience a linear deflection. As the fore actuator deflects at a positive angle γ upwards, the aft actuator experiences the same deflection downwards. This helps to preserve the shape of the airfoil. The vertical deflections experienced by the aft tip, mass element and fore tip are δ_{z_C}, $\delta_{z_{m_i}}$ and δ_{z_B} respectively.

The mass element of the section, m_i, that is shown here is highly important and will be explained further. Thus far, the sectional view of the bender actuators inside the airfoil of the wing have been shown. Figure 31 illustrates the wing planform with actuator distribution. At first glance, it can be noted that the actuator widths are not consistent. The reason for this is to simplify the calculations for inertia when considering flexibility of the aircraft, each actuator has been placed such that the various mass elements on the wing are centred on that actuator. Calculating the deflection of the three components mentioned above, viz. δ_{z_C}, $\delta_{z_{m_i}}$ and δ_{z_B} requires simple trigonometry.

$$\delta_{z_C} = C.\sin(\gamma) \tag{3.1}$$

$$\delta_{z_{m_i}} = a_i.\sin(\gamma) \tag{3.2}$$

$$\delta_{z_B} = B.\sin(\gamma) \tag{3.3}$$

The vertical displacement of each mass element, $\delta_{z_{m_i}}$, is referenced back to the COG, noting that the wing is placed higher than the COG of the entire aircraft.

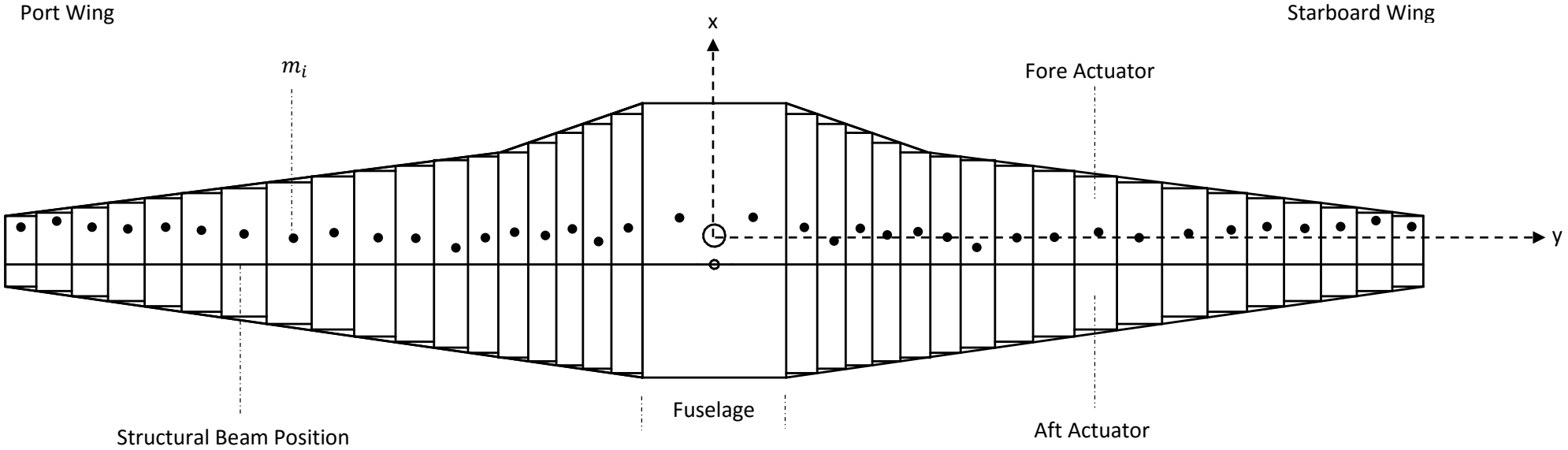

Figure 31: Wing Planform Showing Actuator Placement

3.2.1.2. Modes of Twisting Actuation

Upon thorough inspection, three modes of operation were selected for the twisting actuation. These are linear twist, inverse linear twist and linear twist symmetric. Before each mode is described, a reference frame to describe positive and negative twist is stipulated.

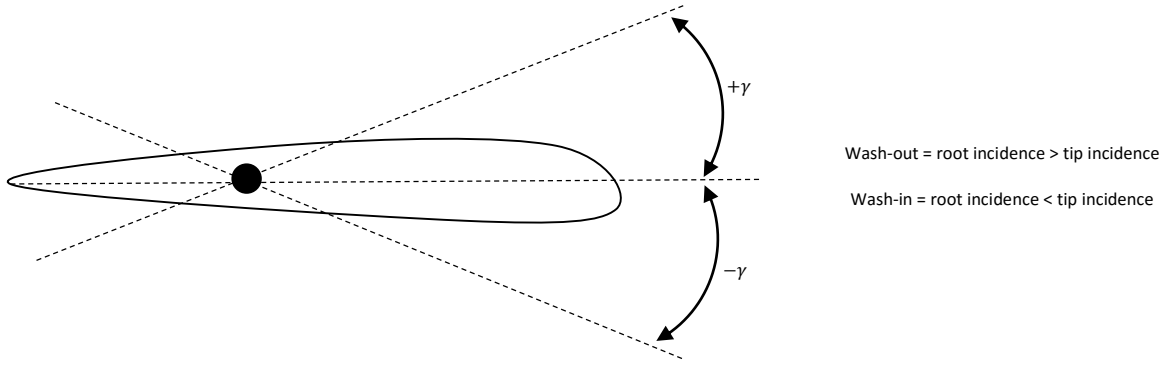

Figure 32: Twist Reference Frame

Figure 32 depicts the reference frame for twisting. If the airfoil twists upwards, it is considered a positive twist, and vice versa for negative. If the incidence angle, or the angle with respect to the fuselage, is greater at the root than at the tip, it is considered a wash-out, and vice versa for a wash-in. A wash-out would result if the twist angle at the root is positive, and smaller or negative at the tip. Coinciding with the body axes of the aircraft, the starboard wing is referred to as the positive, and the port wing as the negative section.

Actuation of twist in the Simulink model was set as an external input which could be initiated at any time during the simulation. Two dashboard items were utilised in the Simulink library for the twist actuation modes, viz. a “Rotary Switch” and a “Knob”.

In Figure 33 a), the twist mode is pre-selected, or can be changed while the simulation is running. The bending modes are described later in bending actuation. Figure 33 b) shows the magnitude of twist to be set. It is important to note that a magnitude of γ refers to a setting on the starboard wing. All references are made to the starboard wing, the positive y-axis in the body axes system of the entire aircraft, whilst the port wing automatically follows the opposite magnitude in certain scenarios, which will now be explained. It must be noted that the actuation descriptions to follow are purely conceptual and may seem physically impossible, which is where the assumptions mentioned are brought in to simplify the system for analysis.

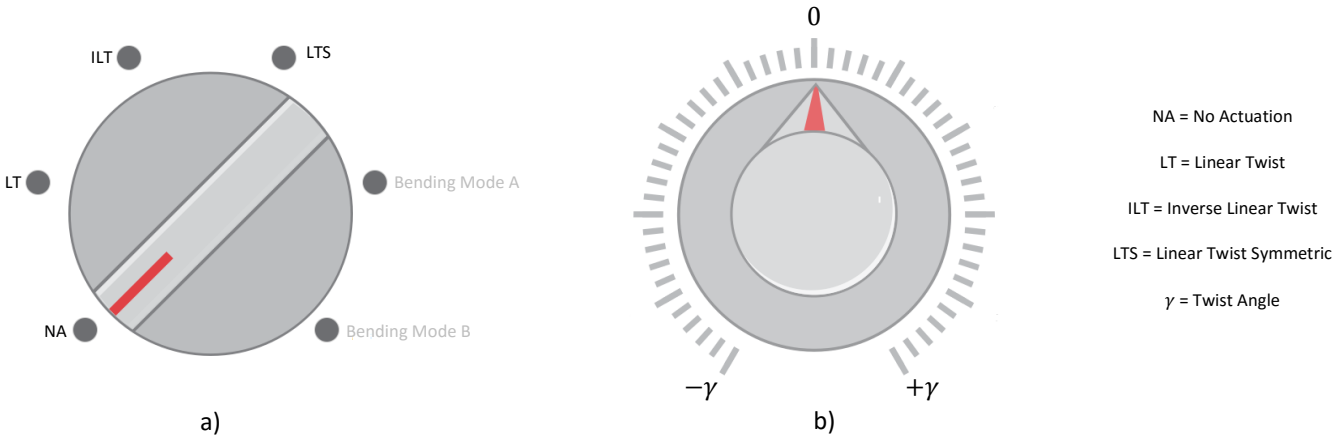

Figure 33: Twist Actuation as an External Input in Simulink. a) Rotary Switch for Actuation Type, b) Knob for Magnitude of Twist

Linear Twist: This mode of twist initiates a linear change in γ from the tip of the starboard wing to the tip of the port wing. For example, if a twist setting of $+\gamma$ is initiated, the tip of the starboard wing is set at $+\gamma$, decreasing linearly to zero at the root, and linearly altering to $-\gamma$ to the tip of the port wing.

Inverse Linear Twist: This mode of twist sets the root at γ and linearly changes to zero at both tips of the starboard and port wing. For example, if a twist setting of $+\gamma$ is initiated, the root of the wing is set at $+\gamma$, which linearly alters to zero at both tips of the wing. Depending on the magnitude of γ selected, this could create either a wash-out or wash-in configuration.

Linear Twist Symmetric: This mode of twist sets the root at zero, and the tips of both wings to γ. For example, if a twist setting of $+\gamma$ is initiated, both tips of the wing are set as $+\gamma$, linearly altering to zero at the root. Depending on the magnitude of γ selected, this could create either a wash-out or wash-in configuration.

Table 13 illustrates the modes of twist with the relative setting of γ, and the resulting geometric configuration of the wing. Upon initial inspection, it can be noted that a Linear Twist mode causes an imbalance of lift on the wing. The effects of this imbalance will be described in the next section. The other two modes maintain the symmetric structure of the wing.

3.2.1.3. Aerodynamics Due to Twist

Altering twist in the modes described above, certain aerodynamic properties are affected. These are shown in Table 14. The method used for obtaining these aerodynamic changes was that of the work by

Sivells and Neely (1947). Their work described that results would not achieve desired accuracy on low aspect ratio and large sweep aircraft.

Table 13: Variation of Wing Twist γ through Various Modes of Twist

Twist Type	Twist Value	Graphs Showing γ Variation along the Wingspan
LT (Linear Twist)	$+\gamma$	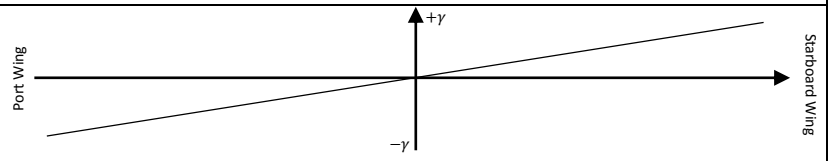
	$-\gamma$	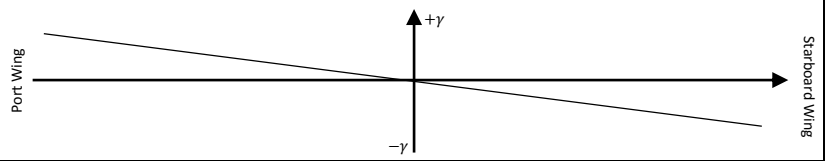
ILT (Inverse Linear Twist)	$+\gamma$	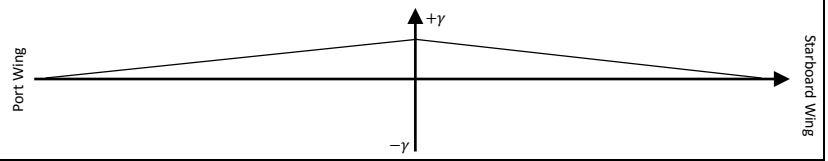
	$-\gamma$	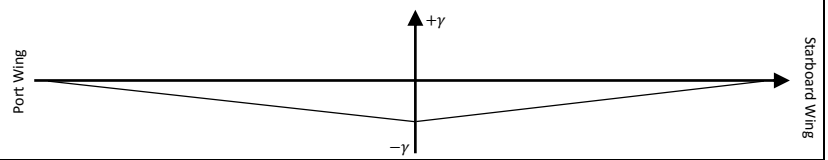
LTS (Linear Twist Symmetric)	$+\gamma$	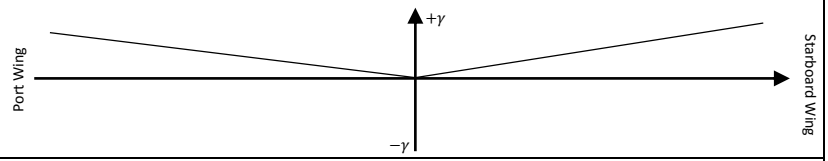
	$-\gamma$	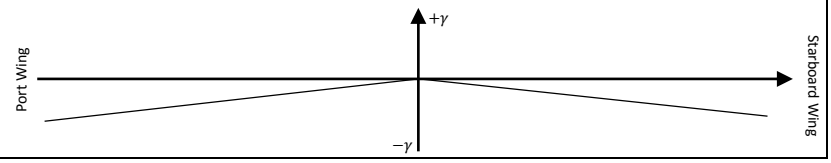

This statement fits the design of the Cessna Citation used in this research quite aptly, as the Cessna has a high aspect ratio and low sweep angle wing. Lifting line theory was utilised by the authors, whilst building on the theory of concepts from other sources, such as Multhopp (1950). The method of multipliers used by Multhopp (1950) accompanied by analysis methods of Sivells and Neely (1947) were used to obtain an induced angle of attack when span wise lift distribution is available. Sivells and Neely's (1947) method was found to be useful as it considered cases in symmetric, asymmetric and anti-symmetric lift distributions.

Table 14: Affected Aerodynamic Properties Due to Twist Geometry Alterations on the Wing

Variable	Name	Description
C_l	Lift Coefficient	Change of lift across the span of the wing
C_m	Moment Coefficient	Slight change of pitching moment due to differing lift on each wing
α_i	Induced Angle of Attack	The change of angle of attack at any point on the wing produces and induced angle of attack
C_{d_i}	Induced Drag	An induced angle of attack results in an induced drag coefficient
C_{n_i}	Induced Yawing Moment	An induced drag coefficient results in an induced yawing moment coefficient
$C_{l_{roll}}$	Rolling Moment	Roll results from asymmetric lift distribution

Following the procedure described by Multhopp (1950) and Sivells and Neely (1947), the spanwise lift distribution is given as:

$$\left(\frac{c_l . c}{b}\right)_m = \sum_{n=1}^{r-1} A_n . \sin\left(n\frac{m\pi}{r}\right) \tag{3.4}$$

Here, A_n are the coefficients of the trigonometric series, c_l the section lift coefficient, c the section chord and b the wing span. The variables r, n, m are count variables for the trigonometric series. It is of importance to note the r must be even, and the series may only be limited to $r-1$, which basically counts from the centre of the chordwise section. Also, $\theta = \frac{m\pi}{r}$ breaks the wing into equally spaced points, where θ goes from $0 < \theta < \pi$. Following the convention of the body axes system of the aircraft, θ relates to the y-positions of the chordwise sections in Figure 34.

With:

$$y = \frac{b}{2}\cos(\theta) \tag{3.5}$$

As the trigonometric coefficients of A_n are not readily available, they can be obtained by rearranging Eq. 3.4. This is done as section lift data is available, and can be used otherwise to calculate A_n.

$$A_n = \frac{2}{r}\sum_{m=1}^{r-1}\left(\frac{c_l.c}{b}\right)_m.\sin\left(n\frac{m\pi}{r}\right) \tag{3.6}$$

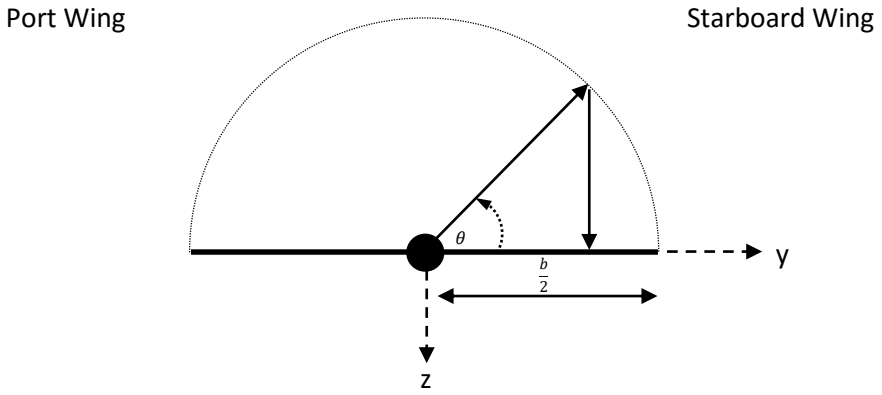

Figure 34: Relation between θ and y-coordinates

From the availability of A_n, the induced angle of attack at each section of the wing can be determined.

$$\alpha_i(\theta) = \frac{180}{4\pi}\sum_{n=1}^{r-1} n.A_n\left(\frac{\sin(n\theta)}{\sin(\theta)}\right) \tag{3.7}$$

Multipliers, which are independent of wing geometry and configuration, are utilised to aid in the calculation of the aerodynamic coefficients. Following the lengthy derivation by Sivells and Neely (1947), the multipliers are listed as stated in the following

For asymmetric lift distribution:

$$\eta_m = \frac{\pi}{2r}.\sin\left(\frac{m\pi}{r}\right) \tag{3.8}$$

If the lift distribution is symmetrical:

$$\eta_{ms} = 2\eta_m \tag{3.9}$$

For moment of an asymmetric distribution:

$$\sigma_m = \frac{\pi}{8r} . \sin\left(\frac{2m\pi}{r}\right) \tag{3.10}$$

If the moment results from an anti-symmetric distribution:

$$\sigma_{ma} = 2\sigma_m \tag{3.11}$$

Once the multipliers have been obtained, they are substituted in the various aerodynamic properties, which will then be replaced or added to the rigid aircraft coefficients.

The wing lift coefficient for asymmetric and symmetric conditions respectively are:

$$C_l = AR \sum_{m=1}^{r-1} \left(\frac{c_l . c}{b}\right)_m . \eta_m \tag{3.12}$$

$$C_l = AR \sum_{m=1}^{r/2} \left(\frac{c_l . c}{b}\right)_m . \eta_{ms} \tag{3.13}$$

AR is the aspect ratio of the wing. For symmetric conditions of lift distribution, it can be noted that summation is limited to only half of the wing described by $r/2$. Symmetric conditions in twist will prevail if the ILT or LTS modes are selected (Table 13).

The induced drag coefficient for asymmetric and symmetric conditions respectively:

$$C_{d_i} = \frac{\pi AR}{180} \sum_{m=1}^{r-1} \left(\frac{c_l . c}{b} . \alpha_i\right)_m \eta_m \tag{3.14}$$

$$C_{d_i} = \frac{\pi AR}{180} \sum_{m=1}^{r/2} \left(\frac{c_l . c}{b} . \alpha_i\right)_m \eta_{ms} \tag{3.15}$$

Once again, note the summation limits for each equation. The wing is situated closer to the center of gravity compared to the other lifting surfaces, thus the effect on the pitching moment coefficient is not as profound, but still present in cases of altercations and differing lift. The pitching moment coefficient for asymmetric and symmetric conditions respectively:

$$C_m = \sum_{m=1}^{r-1} \left(\frac{c_m . c^2}{GC . MAC} \right)_m \eta_m \tag{3.16}$$

$$C_m = \sum_{m=1}^{r/2} \left(\frac{c_m . c^2}{GC . MAC} \right)_m \eta_{ms} \tag{3.17}$$

Here, c_m is the sectional pitching moment coefficient, GC and MAC the geometric chord and mean aerodynamic chord respectively.

The rolling moment coefficient for anti-symmetric and asymmetric conditions respectively:

$$C_{l_{roll}} = -AR \sum_{m=1}^{\frac{r}{2}-1} \left(\frac{c_l . c}{b} \right)_m \sigma_{ma} \tag{3.18}$$

$$C_{l_{roll}} = -AR \sum_{m=1}^{r-1} \left(\frac{c_l . c}{b} \right)_m \sigma_m \tag{3.19}$$

An induced angle of attack results in an induced drag, thus a yawing moment is induced on the aircraft, and this is a resultant moment of an asymmetrical distribution:

$$C_{n_i} = \frac{\pi AR}{180} \sum_{m=1}^{r-1} \left(\frac{c_l . c}{b} . \alpha_i \right)_m \sigma_m \tag{3.20}$$

3.2.2. Bending Actuation

Bending actuation is second in priority to twisting actuation as majority of the aerodynamic disturbances result in lateral stability considerations. Dihedral actuation has been highly considered in flapping flight vehicles such as an ornithopter from as early as the work of DeLaurier and Harris (1993), to the works of Taha *et al.,* (2014) focusing their work on flapping flight of a Micro-Air Vehicle (MAV).

3.2.2.1. Actuator Positioning and Deflections

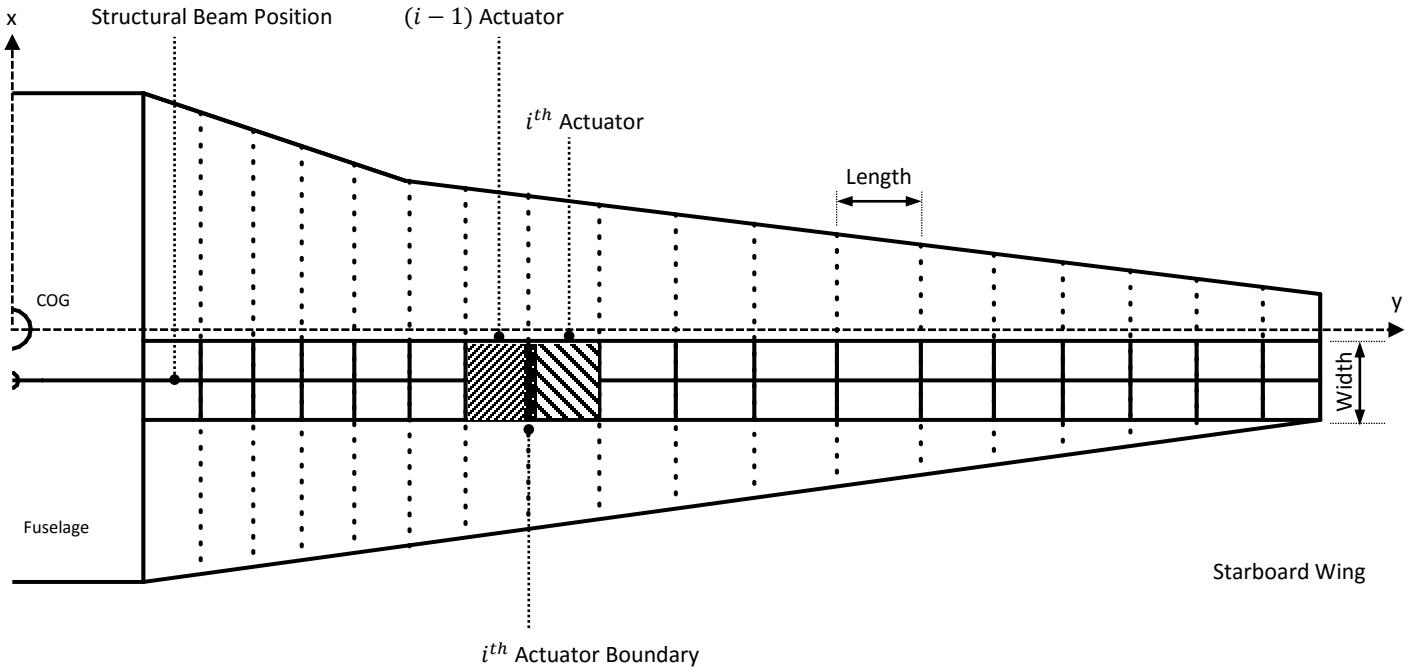

Figure 35: Starboard Wing Planform Showing Actuator Placements for Bending

The bending actuation is brought about by utilising the vertical bending as indicated in Figure 28. The bending does not cause any curvature on the shape of the wing, hence maintaining camber and straight-line configuration of the wing (Assumption 2 and 4). The method in which the actuators are positioned are shown in Figure 35.

Compared to the actuators for twisting, which were placed chordwise, the actuators for bending have been placed spanwise. As it can be seen, the actuators are placed along the structural beam, or in other words, the main spar of the wing. The actuator width is evenly distributed along either side of the structural beam. The length of each actuator varies along the spanwise station as described by the chordwise actuators for twisting actuation (Figure 31).

The boundary of each actuator is the point at which the ith actuator's end connects to actuator $(i-1)$'s leading edge. Thus to scope the geometry of the system, the actuators are placed such that each actuator points to the wing tip, whereas in twisting actuation, the fore actuators point to the leading edge, and the aft actuator to the trailing edge. The reason for this is that each actuator would control the vertical displacement of each mass element in that section of wing, for ease of calculation.

The exact details of these bending actuator placements have not been developed for this research. Through assumption, the actuators are, by design, set to be placed above and below the structural beam, assuring that as the actuators above the beam deflect, so too will the actuators at the bottom.

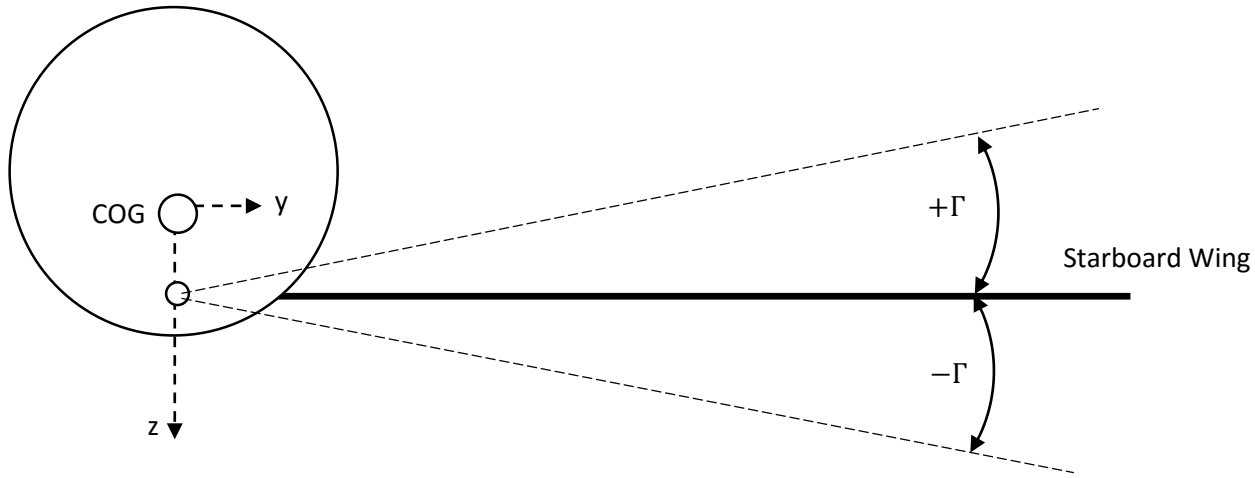

Figure 36: Bending Actuation Deflection on Starboard Wing

Figure 36 details the deflection of the starboard wing in both positive and negative dihedral angle, Γ. It can be noted that no curvature in bending is visible, due to the amount of actuators providing linear vertical displacement at each section. Having this stated, the actuation is more of a change in dihedral through vertical bending of the wing, however the notation of 'bending' is selected for naming purposes.

3.2.2.2. Modes of Bending Actuation

Upon analysis, two modes of bending actuation were selected. These are linear bending and linear bending symmetric. Before each mode is described, the reference frame for this type of actuation must be described. Figure 36 displays the positive and negative directions of the bending actuation, showing magnitudes of the dihedral angle Γ. The starboard wing is taken as the positive section, following the body axis y-direction. All calculations commence with reference to the starboard wing, with the port wing following accordingly, depending on the actuation mode.

Actuation of bending in the Simulink model was once again set as an external input which could be initiated at any time during the simulation. The dashboard items are the same as those in Figure 33.

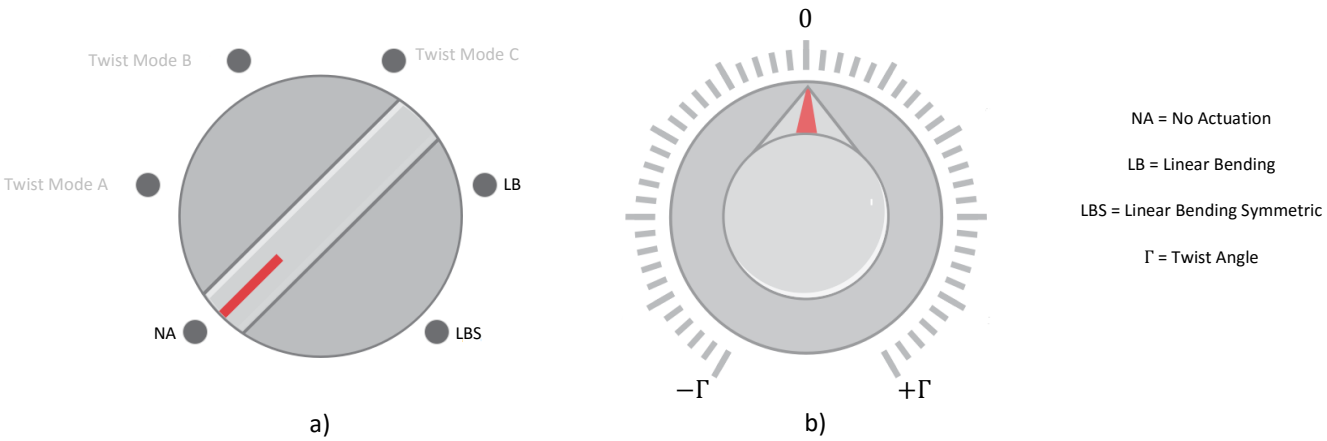

Figure 37: Bending Actuation as an External Input in Simulink. a) Rotary Switch for Actuation Type, b) Knob for Magnitude of Dihedral

As shown in Figure 37, the layout imitates that of twisting actuation, the difference being that the rotary switch is selected for bending actuation, and the knob automatically refers to the amount of dihedral required in magnitude.

Similar to twist, the rotary switch pre-selects the actuation type required, while the knob refers to setting the dihedral angle, Γ, on the starboard wing, with the port wing following in accordance to mode of actuation.

Linear Bending: This mode of bending initiates a setting of Γ on the starboard wing, with the port wing being set to the opposite magnitude. For example, if a dihedral setting of $+\Gamma$ is initiated, the starboard wing is set at $+\Gamma$, while the port wing is set at $-\Gamma$.

Linear Bending Symmetric: This mode of bending initiates a setting of Γ on both the starboard and port wing. For example, if a dihedral setting of $+\Gamma$ is initiated, the starboard wing and port wing will both maintain that dihedral, or anhedral if Γ is a negative.

Table 15 illustrates the modes of bending on the wing with the relative setting of Γ. Upon initial inspection, Linear Bending mode creates an anti-symmetric configuration of the aircraft, while the linear bending symmetric mode maintains the aircraft's nominal structure.

Table 15: Variation of Dihedral Angle Γ through Various Modes of Bending

Bending Type	Dihedral Value	Graphs Showing Γ Magnitude on Aircraft Geometry
LB (Linear Bending)	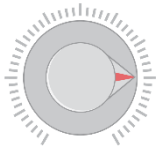	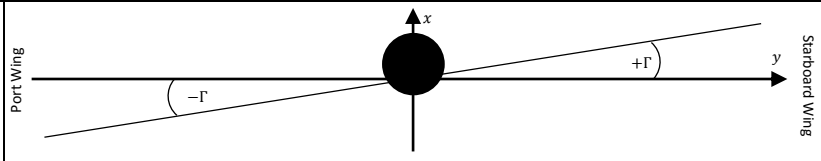
	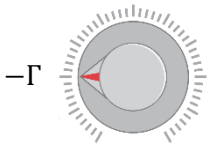	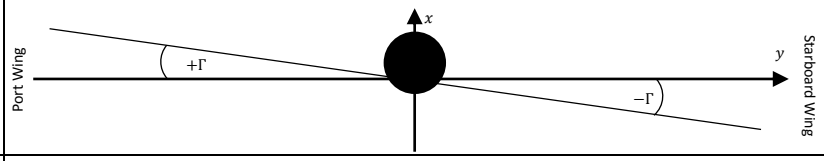
LBS (Linear Bending Symmetric)	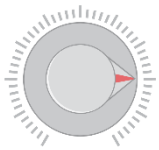	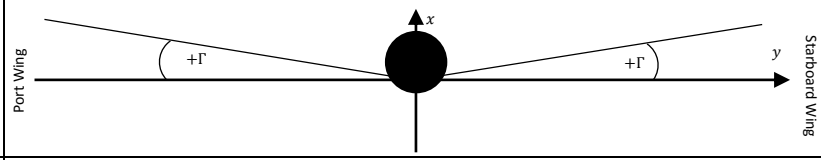
	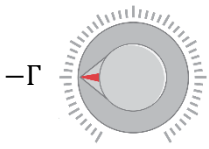	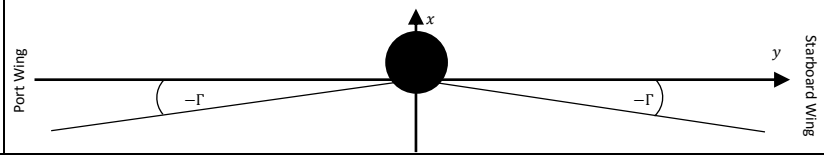

Table 16: Affected Aerodynamic Properties Due to Dihedral Geometry Alterations on the Wing

Variable	Name	Description
C_l	Lift Coefficient	Change of lift across the span of the wing
C_d	Drag Coefficient	Change in drag due to differing geometry
C_{l_p}	Rolling Moment due to Roll Rate P	Rolling moment caused by the roll rate
C_{s_p}	Side Force Coefficient Due to Roll Rate P	Side force caused by an initiated roll rate
C_{n_p}	Yawing Moment due to Roll Rate P	Yawing moment induced by roll rate
$C_{l_{\beta_\Gamma}}$	Roll Stability Derivative	Static stability derivative due to β for the roll coefficient as a function of dihedral
C_{s_Γ}	Side Force Coefficient Due to Dihedral	Side force resulting from Linear Bending mode

3.2.2.3. Aerodynamics Due to Bending

Upon altering between the bending modes described, certain aerodynamic properties are affected. These are shown in Table 16. These aerodynamic coefficients were adapted from work by Quejio and Jaquet (1948) and through the theory provided by Yechout *et al.,* (2003) as well as Maggin and Shanks (1946).

Table 16 shows that most of the aerodynamic properties are directly related to the roll rate P, hence indicating that changes in dihedral come in effect commonly in lateral stability conditions. The effect dihedral has on the aircraft in longitudinal flight mainly results with altercations in drag and lift. As dihedral is increased or decreased, the lift curve slope of the wing changes, resulting in decreased lift, however drag increases, described by Maggin and Shanks (1946):

$$C_{l_{\alpha_\Gamma}} = \left(C_{l_\alpha}\right)_{\Gamma=0^o}.\cos^2(\Gamma) \tag{3.21}$$

Here, $C_{l_{\alpha_\Gamma}}$ is the lift curve slope of the wing as a function of the dihedral angle, Γ, and C_{l_α} the lift curve slope when Γ is set to zero. The authors permit usage of the nominal C_{l_α} as common dihedral angles do not exceed three degrees. It can be noted regardless of Γ being positive or negative, the square on the trigonometric Cos-function will always result in a positive value for $C_{l_{\alpha_\Gamma}}$.

Lift and drag were obtained by simply utilising the change in $C_{l_{\alpha_\Gamma}}$. Drag remains as a function of lift. Despite lift decreasing in the z-axis of the aircraft's body axes, the lift produced perpendicular to the wing still cause drag based on the lift coefficient, and not that due to the altered lift found by $C_{l_{\alpha_\Gamma}}$.

The effect of increasing the dihedral angle increases inherent stability, however this decreases lift and increases drag, simultaneously decreasing the axial roll rate. Queijo and Jaquet (1948) calculated the effects of geometric dihedral on wings in roll. Queijo and Jaquet (1948) concluded the considerable effect dihedral had on the lateral force due to rolling, the damping in the roll in some conditions and the indifference in any effect of yawing moment due to rolling. The authors permit usage of the method for wings with taper ratio to as low as 0.5.

Queijo and Jaquet (1948) utilised strip theory to obtain their results. The integration was performed on only one rolling wing, which was extrapolated to obtain an average in the case of the linear bending mode of this research. The resulting rolling moment due to dihedral angle is:

$$\left(C_{l_p}\right)_\Gamma = \left[1 - 3\left(\frac{z}{b/2}\right).\sin(\Gamma) + 3\left(\frac{z}{b/2}\right)^2.\sin^2(\Gamma)\right].\left(-\frac{1}{6}C_{l_\alpha}.\cos(\Lambda)\right) \tag{3.22}$$

Where z is the vertical distance between the COG and root chord, b the wing span, C_{l_α} is the zero dihedral lift curve slope, or nominal lift curve slope, and Λ is the wing sweep angle. The rate of change of C_{l_p} with respect to dihedral, for intermediate stability analysis is:

$$\frac{\partial C_{l_p}}{\partial \Gamma} = -\frac{3z}{b/2}.\left(-\frac{1}{6}C_{l_\alpha}.\cos(\Lambda)\right) \tag{3.23}$$

The resulting lateral force coefficient is:

$$\left(C_{s_p}\right)_\Gamma = C_l.\frac{AR + \cos(\Lambda)}{AR + 4.\cos(\Lambda)}.\tan(\Lambda) + \left[-C_{l_\alpha}.\cos(\Lambda).\sin(\Gamma).\left(\frac{1}{2} - \frac{z}{b/2}.\sin(\Gamma)\right)\right] \tag{3.24}$$

Here, C_l is the lift coefficient from the altered lift curve slope, $C_{l_{\alpha_\Gamma}}$ and AR is the aspect ratio of the wing. The rate of change of C_{s_p} with respect to dihedral, for intermediate stability analysis is:

$$\frac{\partial C_{s_p}}{\partial \Gamma} = 3\left(-\frac{1}{6}C_{l_\alpha}.\cos(\Lambda)\right) \tag{3.25}$$

As mentioned before, regardless of the effect on yawing moment due to rolling being insignificant, there is still however yawing in rolling, more prominent in the case of the linear bending mode, this is given by:

$$\begin{aligned}\left(C_{n_p}\right)_\Gamma = C_l.\frac{AR + \cos(\Lambda)}{AR + 4.\cos(\Lambda)}.\left[1 + 6\left(1 + \frac{\cos(\Lambda)}{AR}\right).\left(\frac{\bar{x}}{MAC}.\frac{\tan(\Lambda)}{AR} + \frac{\tan^2(\Lambda)}{12}\right)\right]\left(\frac{C_{n_p}}{C_l}\right)_{\Gamma,\Lambda=0^\circ} \\ -\frac{(AR+4).\cos(\Lambda)}{AR + 4.\cos(\Lambda)}.\sin(\Gamma)\left[\frac{\tan(\Lambda)}{4} + \frac{6}{AR}.\frac{\bar{x}}{MAC}.\left(\frac{1}{2} - \frac{z}{b/2}.\sin(\Gamma)\right)\right]\left(C_{l_p}\right)_{\Gamma,\Lambda=0^\circ}\end{aligned} \tag{3.26}$$

$\bar{x}$ is the longitudinal distance rearward from the COG to the mean aerodynamic chord, $\bar{c}$. C_{n_p}, C_l and C_{l_p} are the yawing moment due to roll rate P, lift due to altered lift curve slope $C_{l_{\alpha_\Gamma}}$ and rolling coefficient due to roll rate P respectively. These are shown in brackets with dihedral and sweep angles set to zero. Despite this, the nominal values of these coefficients may be utilised as for this case, the sweep and

dihedral angles for the initial wing settings are relatively low. The rate of change of C_{n_p} with respect to dihedral, for intermediate stability analysis is:

$$\frac{\partial C_{n_p}}{\partial \Gamma} = -\left(\frac{\tan(\Lambda)}{4} + \frac{3.\bar{x}}{AR.MAC}\right).\left(-\frac{1}{6}C_{l_\alpha}.\cos(\Lambda)\right) \tag{3.27}$$

The static roll stability derivative, C_{l_β}, also known as the dihedral effect, is always negative. This entails that the aircraft generates a rolling moment that rolls the aircraft away from the direction of side slip [Yechout *et al.,* (2003)]. The formal equation for C_{l_β} is:

$$C_{l_\beta} = C_{l_{\beta_\Gamma}} + C_{l_{\beta_{body}}} \tag{3.28}$$

$C_{l_{\beta_{body}}}$ was determined as the total C_{l_β} of the aircraft, where $C_{l_{\beta_\Gamma}}$ is added to it. $C_{l_{\beta_\Gamma}}$ is obtained by,

$$C_{l_{\beta_\Gamma}} = -\frac{1}{6}.C_{l_\alpha}.\Gamma.\left(\frac{1+2\lambda}{1+\lambda}\right) \tag{3.29}$$

Here, C_{l_α} is the lift curve slope of the wing, which is not the same as the altered lift curve slope due to dihedral, $C_{l_{\alpha_\Gamma}}$, and λ is the taper ratio of the wing.

A unique addition to the bending actuation is the ability to produce a side force on the aircraft, without inducing a large roll. This is achieved by setting the bending mode to linear bending. As described, the resultant anti-symmetric configuration of the wing tilts the lift vector depending on the dihedral setting, Figure 38.

As the figure shows, when a setting of $+\Gamma$ is initiated, the lift vector tilts in the counter clockwise direction, which breaks down to a force component in the z-axis, and a side force component. When this side force component is multiplied by the distance between the wing root and COG, z, a rolling moment results causing the aircraft to roll in the clockwise direction. This rolling moment can be counteracted by applying the ailerons appropriately. With Lift available, the side force and side force coefficient respectively can be calculated as:

$$S = -L.\sin(\Gamma) \tag{3.30}$$

$$C_{S_\Gamma} = \frac{S}{q.S_{ref}} \tag{3.31}$$

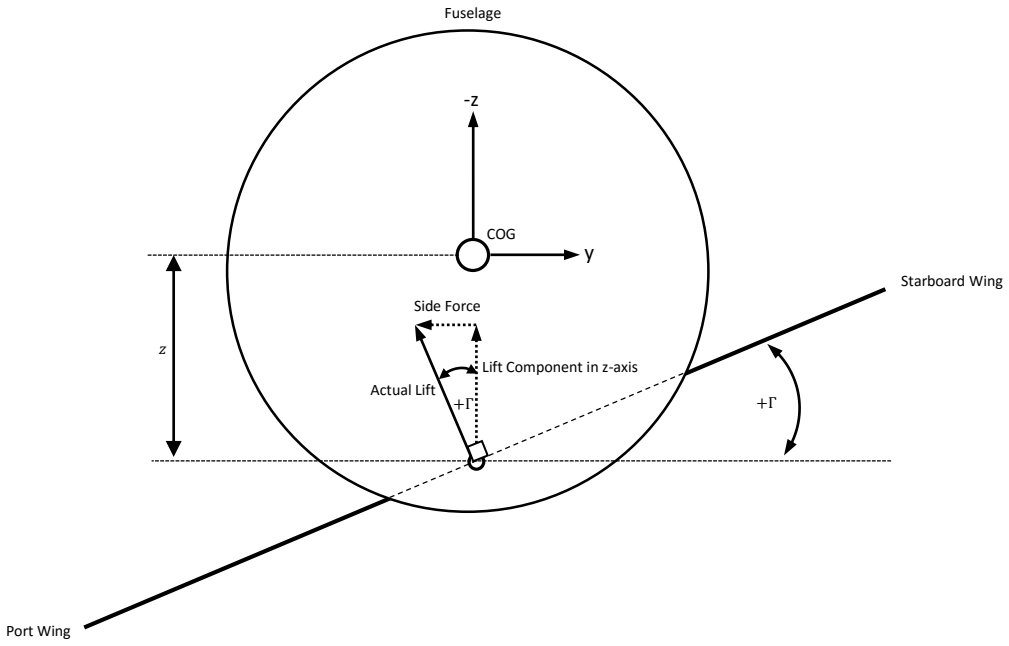

Figure 38: Resulting Side Force on a Linear Bending mode Actuation

where S is the side force, L isthe aircraft lift, q is the dynamic pressure and S_{ref} is the reference area of the wing. C_{S_Γ}, the side force coefficient due to Dihedral, is added to the side force coefficient of the entire aircraft. A negative is added for the side force equation to correct for positive and negative magnitudes of side force on the y-axis. In this scenario for example, as a positive dihedral is applied, the side force falls in the negative y-axis, hence its magnitude would be a negative.

The roll is described by the following:

$$C_{l_{roll_\Gamma}} = \frac{S.z}{q.S_{ref}.b} \tag{3.32}$$

The magnitude of roll would be automatically determined by the sign of the side force.

The addition of this side force due to the linear bending mode on the aerodynamics provides a novel means of altering the aircrafts trajectory without a combination of primary inputs such as the rudder and

aileron. This type of trajectory alteration is advantageous in landing situations when trying to align the aircraft on final approach for landing.

3.3. Piezoelectric Actuator Simulation

Simulation for the piezoelectric actuator simulations were performed independent to the rigid aircraft model. The conditions for the model were set at sea level, with the aircraft experiencing no roll or yaw, and velocity set to 220 m/s. Figure 39 displays the aerodynamic properties of the linear twist mode. It is noted that with a higher degree of twist on the right wing, the higher the lift on the. The lower the twist, the less of a pitching moment there is, and lift is significantly affected.

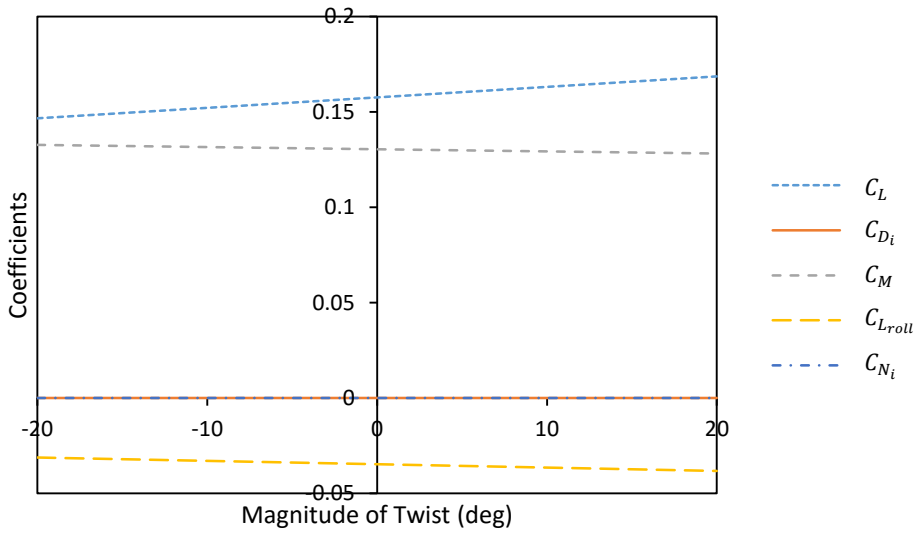

Figure 39: Linear Twist Mode Showing the Various Aerodynamic Coefficients

Figure 40 shows the aerodynamic properties of the inverse linear twist mode. The drop in lift and moment are significantly higher in the negative domain of the graph. This theoretically is correct as the twist angle is lower towards the root as it is towards the wing tips, and this results in a lower angle of attack, and thus a lower lift. Figure 41 depicts the aerodynamic properties of Linear Twist Symmetric Mode.

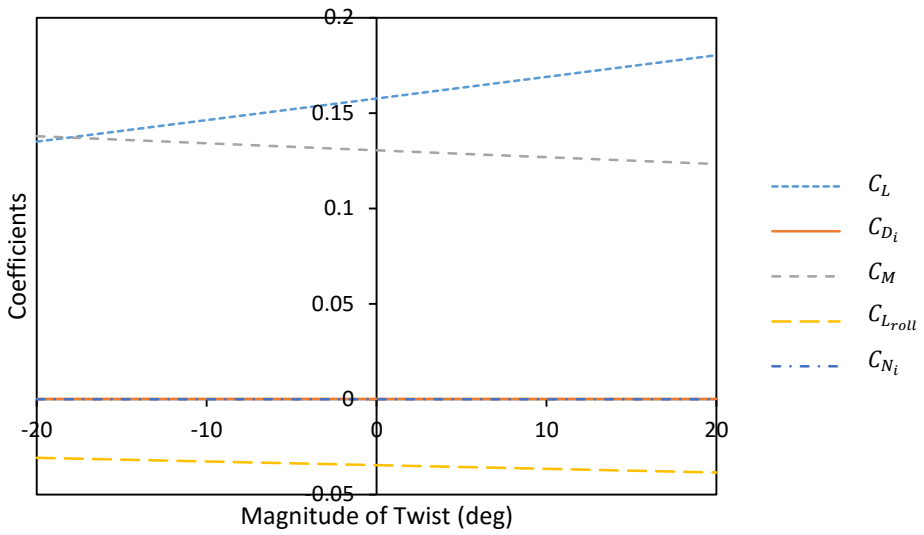

Figure 40: Inverse Linear Twist Mode showing Various Aerodynamic Coefficients

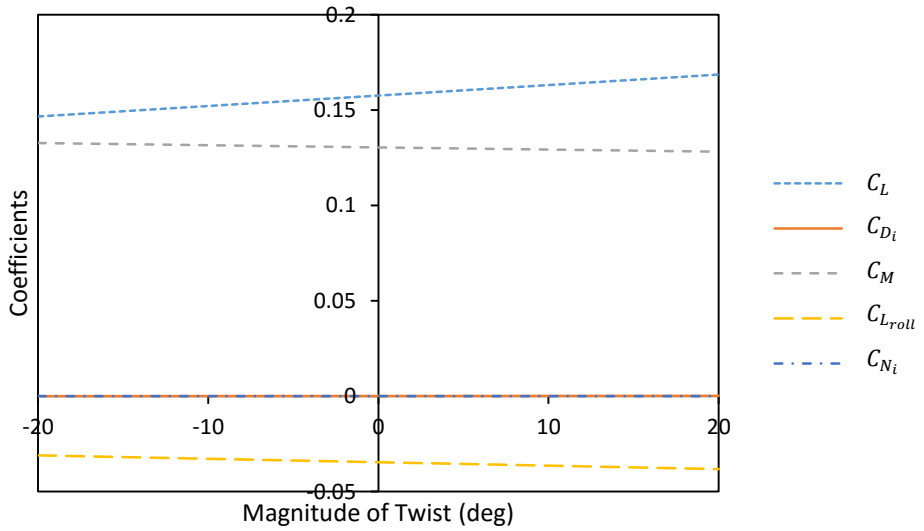

Figure 41: Linear Twist Symmetric Mode Showing Various Aerodynamic Coefficients

Figure 42 and Figure 43 depict the Linear Bending and Linear Bending Symmetric Mode respectively. Note the difference in the side force coefficients between the two modes. Overall, the aerodynamic coefficients

are seen to display adequate changes and respectable magnitudes. These coefficients are incorporated with the rigid flight model, with results discussed at a later stage.

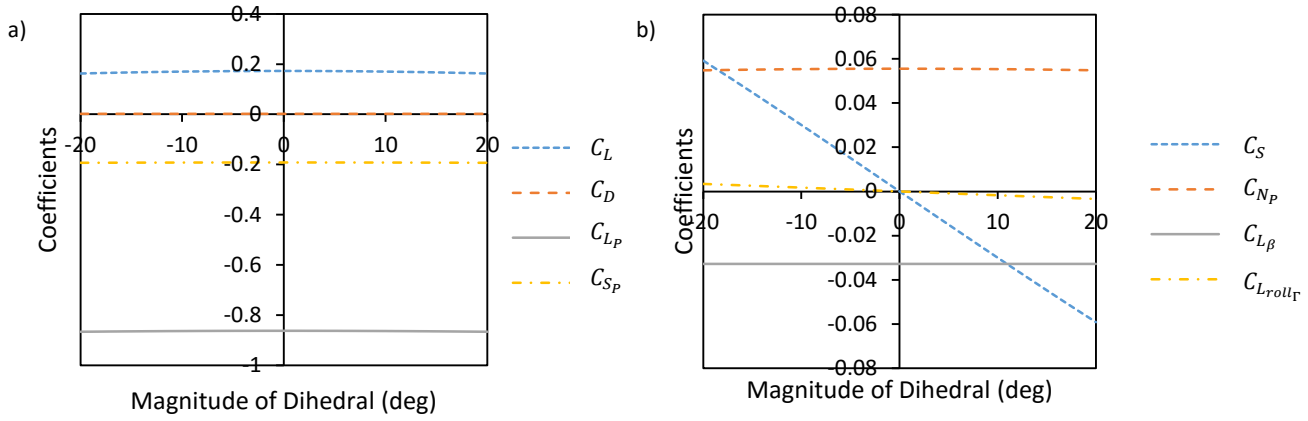

Figure 42: Linear Bending Mode Showing Various Aerodynamic Coefficients

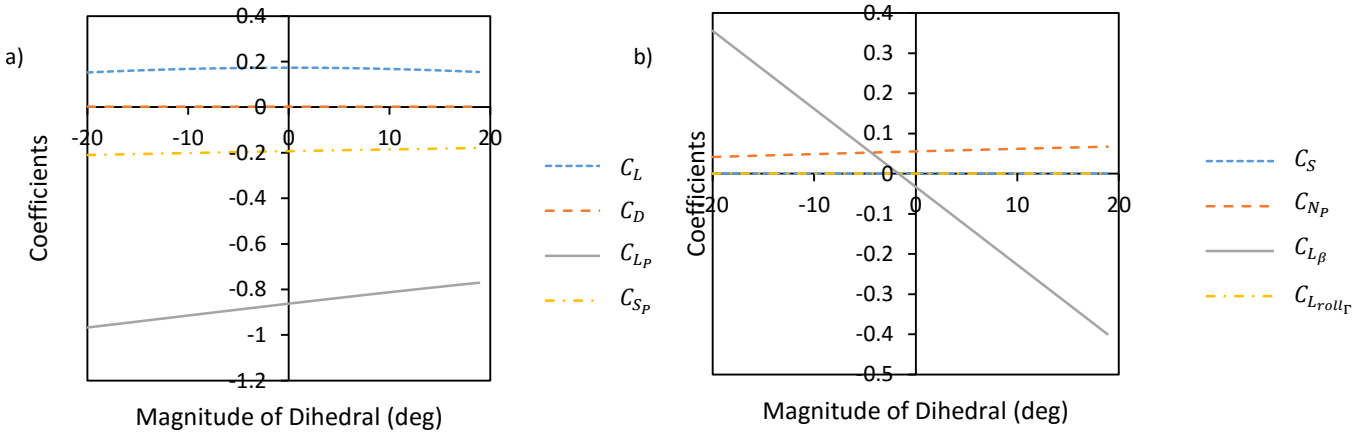

Figure 43: Linear Bending Symmetric Mode Showing Various Aerodynamic Coefficients

4. EFFECTS OF ELASTIC DEFORMATION ON THE AERODYNAMIC FORCES AND MOMENTS

The elastic deformations for this research do not include pure vibrational analysis through FEM as the processing and model setup are a research matter on their own. What has been the key point of the simulation is just how much the dynamics of the rigid body are affected by the elastic motion of the structure [Schmidt (2012)].

To simplify the analysis process, the aircraft structure is broken down to the wing, fuselage, horizontal tail and vertical tail each containing square beams as the frame of those components. The fuselage can be neglected on the assumption that the minute changes do not result in any changed aerodynamic forces. It can also be assumed that the deflections are minute such that they do not affect the other lifting surfaces [Schmidt (2012)].

The vibration of the lifting surfaces are not coupled, and are viewed independently to the vibration modes of the accompanying lifting surfaces.

4.1. Vibration of a Cantilever Beam

The components of the elastic aircraft model are analyzed under free vibration conditions, without damping and an external force (which would be the aerodynamics). This was decided as there is a two-way relationship between the aerodynamics and elasticity of the components. Elasticity affects the aerodynamics, and at the same time, the aerodynamics affect the elasticity. Due to the aim of the research being the effect on the aerodynamics by elastic deformation, free vibration conditions were chosen. A continuous model of a cantilever beam is described by Rao (1995). The free vibration analysis consists of bending and torsional deflections of the cantilever beam.

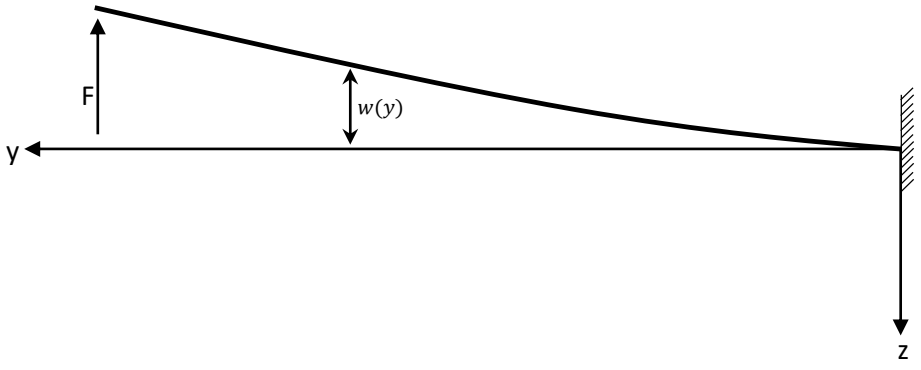

Figure 44: Deflection of a Cantilever Beam Showing Bending with a Point Load of 'F'

Figure 44 shows a cantilever beam with bending deflection due to a point load force of 'F' applied at the free end. The resulting deflection is given by [Rao (1995)]:

$$w(y,t) = \sum_{n=1}^{\infty} W_n(y)(A_n \cos(\omega_n t) + B_n \sin(\omega_n t)) \tag{4.1}$$

Here, A_n and B_n are constants, evaluated at the initial conditions. $W_n(y)$ is the nth normalised bending mode shape of the cantilevered beam. The values are normalised for ease of calculation, after which the constants provide the necessary scale in magnitude of the actual bending deflection. The normalised bending mode shape is [Bismarck-Nasr (1999)]:

$$W_n(y) = \frac{\sin(\zeta y) - \sinh(\zeta y) - \kappa(\cos(\zeta y) - \cosh(\zeta y))}{|\sin(\zeta l) - \sinh(\zeta l) - \kappa(\cos(\zeta l) - \cosh(\zeta l))|} \tag{4.2}$$

and:

$$\kappa = \left(\frac{\sin(\zeta l) + \sinh(\zeta l)}{\cos(\zeta l) + \cosh(\zeta l)}\right) \tag{4.3}$$

y is the span position of the beam, l is the length of the beam and ζl corresponds to the various mode shapes. Four mode shapes were chosen ($n = 4$) for the bending modes, where $\zeta l_1 = 1.875104, \zeta l_2 = 4.694091, \zeta l_3 = 7.854151, \zeta l_4 = 10.995540$.

The natural frequency used in Eq. (4.1), is given by [Rao (1995)]:

$$\omega_n = (\zeta l)^2 \sqrt{\frac{EI}{\rho A l^4}} \tag{4.4}$$

Where EI is the flexural stiffness, ρ the density of the material and A is the cross sectional area of the beam.

Figure 45 shows a cantilever beam with torsion or twist deflection due to a moment 'M' applied at the free end.

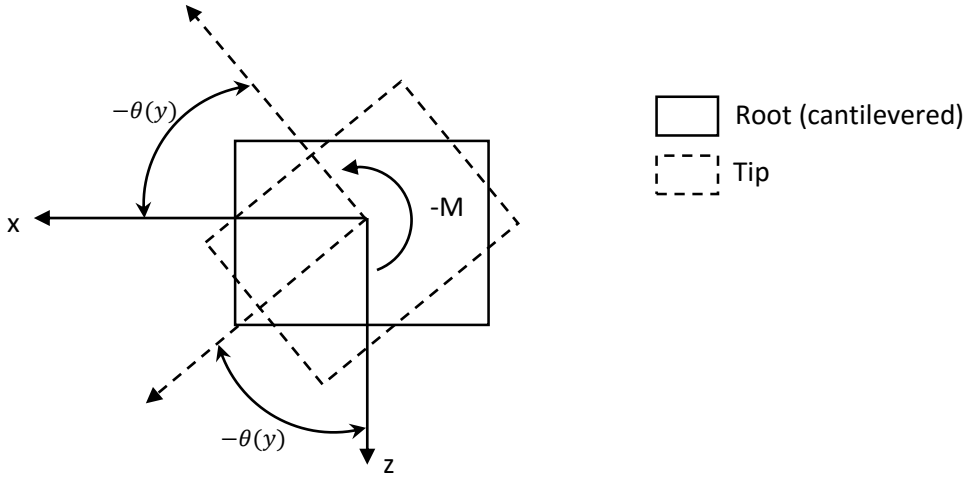

Figure 45: Deflection of a Cantilever beam showing Twist with a Moment 'M'

It must be noted here that regarding the wing, a positive twist depicts the nose of the airfoil to pitch upwards. The resulting deflection is given by [Rao (1995)]:

$$\theta(y,t) = \sum_{n=1}^{\infty} H_n(y)(C_n \cos(\omega_n t) + D_n \sin(\omega_n t)) \tag{4.5}$$

Where $H_n(y)$ is the nth normalised torsion mode, and C_n and D_n are constants, evaluated at the initial conditions. The equation for the first normalised torsion mode is [Bismarck-Nasr (1999)]:

$$H_1(y) = \sin\left(\frac{\pi y}{l}\right) \tag{4.6}$$

To account for higher modes, the equation becomes:

$$H_n(y) = \sin\left(\frac{(2n+1)\pi y}{2l}\right) \tag{4.7}$$

Once again, similar to bending, four torsion modes are chosen for this research ($n = 4$). The natural frequency is given by [Bismarck-Nasr (1999)]:

$$\omega_n = \frac{(2n-1)\pi\gamma}{2l} \tag{4.8}$$

Where:

$$\gamma = \sqrt{\frac{GJ}{I_o}} \tag{4.9}$$

Here GJ is the torsional stiffness with the mass polar moment of inertia:

$$I_o = \frac{I_{xx} + I_{zz}}{l} \tag{4.10}$$

4.1.1. Initial Conditions

The initial conditions are used to determine the constants of the mode shape equations. This is done by taking time derivatives to obtain the velocity of the mode shapes at time zero. In both cases of bending and torsion, the deflections are static in the initial conditions, thus both B_n and D_n are zero [Rao (1995)]. The vibrational analysis considers a load being applied on the cantilever beam at time zero, which creates an initial deflection, after which the load is removed and the structure is left to vibrate freely. The static deflection due to initial loads on the beam are given by [Hibbeler 2000]:

$$w(y) = \frac{F}{EI}\left(-\frac{y^3}{6} + \frac{ly^2}{2}\right) \tag{4.11}$$

For bending deflection, and for torsion deflection:

$$\theta(y) = \frac{My}{GJ} \tag{4.12}$$

Where F and M is the force resulting in the vertical displacement, and the moment resulting in a twist displacement. Both F and $M$are set to 1000N and 1000Nm respectively. Upon considering conditions at time t=0, Eqs. (4.11) and (4.12) are related to Eqs. (4.1) and (4.5), noting that B_n and D_n are zero.

$$\sum_{n=1}^{\infty} W_n(y)\, A_n = \frac{F}{EI}\left(-\frac{y^3}{6} + \frac{ly^2}{2}\right) \tag{4.13}$$

$$\sum_{n=1}^{\infty} H_n(y)\, C_n = \frac{My}{GJ} \tag{4.14}$$

Thus there are n set of equations with n unknowns, with y being n arbitrary points along the length of the beam. The constants A_n can be found by using a formula described by Whitney (1999). The equation takes into account the added force and the structural properties of the beam.

$$A_n = \left[\frac{4Fl}{EI\rho A\zeta_n^4\left(\sin(\zeta_n l)\, e^{\zeta_n l} + e^{2\zeta_n l} - 1\right)}\right] \tag{4.15}$$
$$* \left[3\sin(\zeta_n l)\left(e^{2\zeta_n l}+1\right) - 2(\zeta_n l)^3 e^{\zeta_n l} + \cos(\zeta_n l)\left(3 - (\zeta_n l)^3\left(e^{2\zeta_n l}+1\right) - 3e^{2\zeta_n l}\right)\right]$$

Care must be taken when selecting a sign for F, where a positive indicates an upward direction, or the direction of the positive axis, and negative for the negative axis.

Applying this methodology of vibration for the wing, horizontal tail and vertical tail respectively, the mode shape equations and coordinates were developed. These are shown in Table 17.

Table 17: Mode shape equations of Twist and Bending showing Constants

	n	**Bending Mode Shape (Use 'z' for Vertical Tail)**							**Twist Mode Shape (Use 'z' for Vertical Tail)**							A_n	C_n
		y^6	y^5	y^4	y^3	y^2	y	y^0	y^6	y^5	y^4	y^3	y^2	y	y^0		
Wing	1					-9E-06	0.0002	- 1E-05					-9E-06	0.0002	- 1E-05	0.0641	0.000783
	2				-1E-06	2E-05	- 7E-05	6E-06				-1E-06	2E-05	-7E-05	6E-06	-0.00143	-7.14E-05
	3		-4E-08	6E-07	- 2E-06	- 3E-06	2E-05	- 4E-07		-4E-0	6E-07	- 2E-06	- 3E-06	2E-05	- 4E-07	1.662E-04	1.694E-05
	4	-7E-08	2E-06	- 2E-05	7E-05	- 0.0001	2E-05	- 6E-07	-7E-09	2E-07	- 1E-06	3E-06	3E-07	- 7E-06	1E-07	-4.799E-05	-4.36E-06
Horizontal Tail	1					0.0004	0.0008	- 0.0002					0.0006	0.0043	- 0.0002	0.00612	0.00733
	2			-1E-05	1E-04	0.0002	2E-06	2E-07			-6E-05	0.0002	0.0003	- 0.0011	1E-05	-0.00014	-6.40E-4
	3		-4E-06	3E-05	- 9E-05	8E-05	6E-06	1E-07		-4E-05	0.0002	- 0.0003	- 0.0002	0.0004	- 5E-06	1.59E-05	1.39E-04
	4	-2E-06	2E-05	- 8E-05	0.0001	- 7E-05	7E-06	- 6E-08	-2E-05	0.0001	- 0.0004	0.0003	9E-05	- 0.0002	1E-06	-4.58E-06	-3.18E-05
Vertical Tail	1					8E-05	0.0001	- 3E-05					-0.0002	0.0016	- 5E-05	0.00102	0.00243
	2			-4E-06	2E-05	- 3E-05	4E-07	3E-08				-8E-05	0.0005	- 0.0007	3E-05	-2.28E-05	-2.26E-04
	3		-1E-06	9E-06	- 2E-05	2E-05	- 1E-06	1E-08		-3E-05	0.0001	- 0.0002	- 0.0001	0.0002	- 2E-06	2.64E-06	5.59E-05
	4	-7E-07	6E-06	- 2E-05	3E-05	1E-05	1E-06	- 7E-09	-2E-05	0.0001	- 0.0003	0.0002	6E-05	- 8E-05	6E-07	-7.63E-07	-1.561E-05

4.2. Elastic Effects on the Aircraft Aerodynamics

In this section, the elastic effects on the aircraft aerodynamics will be identified. Once again, each component is analyzed independently of the next, and no external effects on the flexible structure is considered.

The equations have been adopted from Schmidt (2012), which include resultant effects on the aircraft aerodynamics in the stability axes through forces in the XYZ domain, and the moments, LMN, which are then added to the rigid aircraft model in the same domains.

$$\begin{aligned} F_{A_{X_E}} &= \sum_{i=1}^{n}\left(\frac{\partial F_{A_X}}{\partial \eta_i}\eta_i + \frac{\partial F_{A_X}}{\partial \dot{\eta}_i}\dot{\eta}_i\right) \\ F_{A_{Y_E}} &= \sum_{i=1}^{n}\left(\frac{\partial F_{A_Y}}{\partial \eta_i}\eta_i + \frac{\partial F_{A_Y}}{\partial \dot{\eta}_i}\dot{\eta}_i\right) \\ F_{A_{Z_E}} &= \sum_{i=1}^{n}\left(\frac{\partial F_{A_Z}}{\partial \eta_i}\eta_i + \frac{\partial F_{A_Z}}{\partial \dot{\eta}_i}\dot{\eta}_i\right) \end{aligned} \tag{4.16}$$

$$\begin{aligned} L_{roll_{A_E}} &= \sum_{i=1}^{n}\left(\frac{\partial L_{roll}}{\partial \eta_i}\eta_i + \frac{\partial L_{roll}}{\partial \dot{\eta}_i}\dot{\eta}_i\right) \\ M_{A_E} &= \sum_{i=1}^{n}\left(\frac{\partial M}{\partial \eta_i}\eta_i + \frac{\partial M}{\partial \dot{\eta}_i}\dot{\eta}_i\right) \\ N_{A_E} &= \sum_{i=1}^{n}\left(\frac{\partial N}{\partial \eta_i}\eta_i + \frac{\partial N}{\partial \dot{\eta}_i}\dot{\eta}_i\right) \end{aligned} \tag{4.17}$$

The method described by Schmidt (2012) on the elastic aerodynamics considers the mode shapes in both twisting and bending, and the resultant aerodynamic force thereafter. The results are given in both the modal displacement η_i, and modal velocity $\dot{\eta}_i$, and the sum is taken of the two components, as shown by Eqs. (4.16) and (4.17).

The forces in the XYZ direction are obtained by lift, side force and drag components, given by:

$$\begin{aligned} F_{A_X} &= -D\,cos(\alpha)\,cos(\beta) - S\,cos(\alpha)\,sin(\beta) + L\,sin(\alpha) \\ F_{A_Y} &= -D\,sin(\beta) + S\,cos(\beta) \\ F_{A_Z} &= -D\,sin(\alpha)\,cos(\beta) - S\,sin(\alpha)\,sin(\beta) - L\,cos(\alpha) \end{aligned} \tag{4.18}$$

Drag has an insignificant effect on the results, thus it is ignored. The components described by Eqs.(4.16) and (4.17) are given below.

4.2.1. Lift

The lift comprises of components from the wing and the horizontal tail. The twisting motion of the beam as well as vertical displacements through bending create fluctuations in lift. The equations described utilize strip theory, where an integral from naught to the beam length, or in this case, half wing span are stated as limits. The reason the entire wing span is not chosen for integration is because of the symmetry of vibrations on the beams. In this research with independent analysis of the lifting surfaces, there is no coupling, and thus no anti-symmetric modes being developed. Therefore, the equations are multiplied by two to account for the other half of the lifting surface (only for wing and horizontal tail). The modal displacement equations for lift of the wing plus the horizontal tail are:

$$\frac{\partial L}{\partial \eta_i} \triangleq C_{L_{\eta_i}} q_\infty S_w = \frac{\partial L_{E_W}}{\partial \eta_i} + \frac{\partial L_{E_H}}{\partial \eta_i}$$

$$\frac{\partial L_{E_W}}{\partial \eta_i} = 2q_\infty \int_0^{b_{w/2}} c_{l_{\alpha_W}}(y)\, v'_{z_{i_w}}(y)\, c_W(y)\, dy \tag{4.19}$$

$$\frac{\partial L_{E_H}}{\partial \eta_i} = 2q_H \int_0^{b_{H/2}} c_{l_{\alpha_H}}(y) \left(v'_{z_{i_H}}(y) - \frac{d\epsilon_H}{d\alpha_W} v'_{z_{i_w}}(y) \right) c_H(y) dy$$

Here, q_∞ is the dynamic pressure. q_H is the dynamic pressure at the tail, set to 0.9 of q_∞. S_w, $c_{l_{\alpha_{component}}}$, $c_{component}$ are the wing reference area, lift curve slope and chord of the component under consideration (W = wing, H = horizontal tail and V = vertical tail). $\frac{d\epsilon_H}{d\alpha_W}$ is the downwash at the tail.

$v'_{z_{i_{component}}}$ is the twist mode shape equation, given in Table 17 for $i = 1,2,3,4$. An addition to the elastic analysis of lift is the modal displacement lift effectiveness $C_{L_{\eta_i}}$. This coefficient is helpful in analyzing the magnitude of the elastic effect on lift.

The modal velocity of lift is given by:

$$\frac{\partial L}{\partial \dot{\eta}_i} \triangleq C_{L_{\dot{\eta}_i}} q_\infty S_w = \frac{\partial L_{E_W}}{\partial \dot{\eta}_i} + \frac{\partial L_{E_H}}{\partial \dot{\eta}_i} \tag{4.20}$$

$$\frac{\partial L_{E_W}}{\partial \dot{\eta}_i} = \frac{2q_\infty}{V_\infty} \int_0^{b_{w/2}} c_{l_{\alpha_W}}(y)\, v_{Z_{i_W}}(y)\, c_W(y)\, dy$$

$$\frac{\partial L_{E_H}}{\partial \dot{\eta}_i} = \frac{2q_H}{V_\infty} \int_0^{b_{H/2}} c_{l_{\alpha_H}}(y) \left(v_{Z_{i_H}}(y) - \frac{d\epsilon_H}{d\alpha_W} v_{Z_{i_W}}(y) \right) c_H(y) dy$$

Here, V_∞ is the speed of the aircraft model, with $\dot{\eta}_i$ being the velocity of the modal coordinate (time derivative of the modal coordinate η_i). $v_{Z_{i_{component}}}$ is the vertical displacement mode shape equation given in Table 17.

4.2.2. Side Force

The modal displacement of side force is given by:

$$\frac{\partial S_{e_v}}{\partial \eta_i} \triangleq C_{S_{\eta_i}} q_\infty S_w$$
$$\frac{\partial S_{e_v}}{\partial \eta_i} = 2q_H \int_0^{b_v} c_{l_{\alpha_V}}(z)\, v'_{Y_{i_V}}(z)\, c_V(z)\, dz \tag{4.21}$$

The integrand is a function of z as it is the vertical component on the body axes of the aircraft. This should not be confused with the coordinates given as y in Table 17 for the vertical tail. They are interchangeable only for the vertical tail.

The modal velocity of side force is given by:

$$\frac{\partial S_{e_v}}{\partial \dot{\eta}_i} \triangleq C_{S_{\dot{\eta}_i}} q_\infty S_w$$
$$\frac{\partial S_{e_v}}{\partial \dot{\eta}_i} = -\frac{q_H}{V_\infty} \int_0^{b_v} c_{l_{\alpha_V}}(z)\, v_{Y_{i_V}}(z)\, c_V(z)\, dz \tag{4.22}$$

4.2.3. Pitching Moment

The modal displacement for pitching moment is gen by:

$$\frac{\partial M}{\partial \eta_i} \triangleq C_{M_{\eta_i}} q_\infty S_w \bar{c}_w = \frac{\partial M_{E_W}}{\partial \eta_i} + \frac{\partial M_{E_H}}{\partial \eta_i}$$

$$\frac{\partial M_{E_W}}{\partial \eta_i} = 2q_\infty \int_0^{b_{w/2}} c_{l_{\alpha_W}}(y)\, v'_{z_{i_w}}(y) \left(x_{AC_W}(y) - X_{ref}\right) c_W(y)\, dy \tag{4.23}$$

$$\frac{\partial M_{E_H}}{\partial \eta_i} = -2q_H \int_0^{\frac{b_H}{2}} c_{l_{\alpha_H}}(y) \left(v'_{z_{i_H}}(y) - \frac{d\epsilon_H}{d\alpha_W} v'_{z_{i_w}}(y) \right) \left(X_{ref} - x_{AC_H}(y)\right) c_H(y) dy$$

Where $\bar{c}_w$ is the mean aerodynamic chord of the wing, also written as MAC. $\left(x_{AC_W}(y) - X_{ref}\right)$ is the distance between the COG and the locus of aerodynamic centers of the wing, shown in Figure 46 [Schmidt (2012)]. Similarly, $\left(X_{ref} - x_{AC_H}(y)\right)$ is the distance between COG and the locus of aerodynamic centers of the horizontal tail.

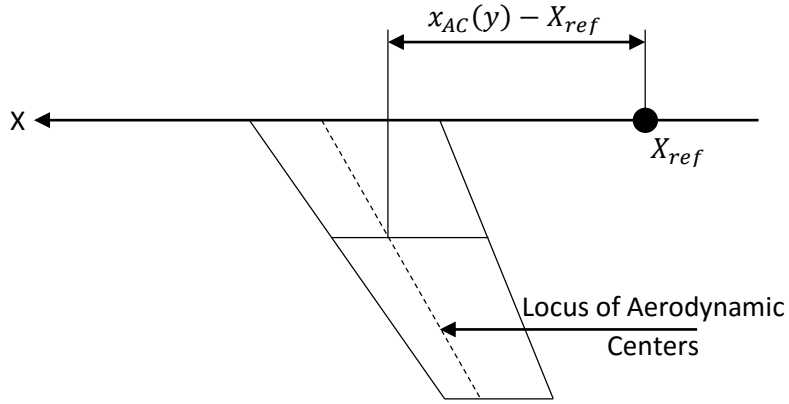

Figure 46: Description of Distance between Locus of Aerodynamic Centers and COG of the Wing

The modal velocity of the pitching moment is given by:

$$\frac{\partial M}{\partial \dot{\eta}_i} \triangleq C_{M_{\dot{\eta}_i}} q_\infty S_w \bar{c}_w = \frac{\partial M_{E_W}}{\partial \dot{\eta}_i} + \frac{\partial M_{E_H}}{\partial \dot{\eta}_i}$$

$$\frac{\partial M_{E_W}}{\partial \dot{\eta}_i} = \frac{2q_\infty}{V_\infty} \int_0^{b_{w/2}} c_{l_{\alpha_W}}(y)\, v_{Z_{i_W}}(y) \left(x_{AC_W}(y) - X_{ref}\right) c_W(y)\, dy \tag{4.24}$$

$$\frac{\partial M_{E_H}}{\partial \dot{\eta}_i} = -\frac{2q_H}{V_\infty}\int_0^{\frac{b_H}{2}} c_{l_{\alpha_H}}(y)\left(v_{Z_{i_H}}(y) - \frac{d\epsilon_H}{d\alpha_W}v_{Z_{i_W}}(y)\right)\left(X_{ref} - x_{AC_H}(y)\right)c_H(y)dy$$

4.2.4. Rolling Moment

The rolling moment modal displacement requires finding the height, $z_{AC}(z)$, above the vehicle fixed axis X. The equation is given by:

$$z_{AC}(z) = (z + z_{root})\cos(\alpha_0) - \left(X_{ref} - x_{AC}(z)\right)\sin(\alpha_0) \tag{4.25}$$

Where z_{root} is the distance between the root of the vertical tail and the reference axis X, and α_0 being the angle of attack. Whilst $\left(X_{ref} - x_{AC}(z)\right)$ being the distance between the locus of aerodynamic centers of the vertical tail and the COG, shown in Figure 47.

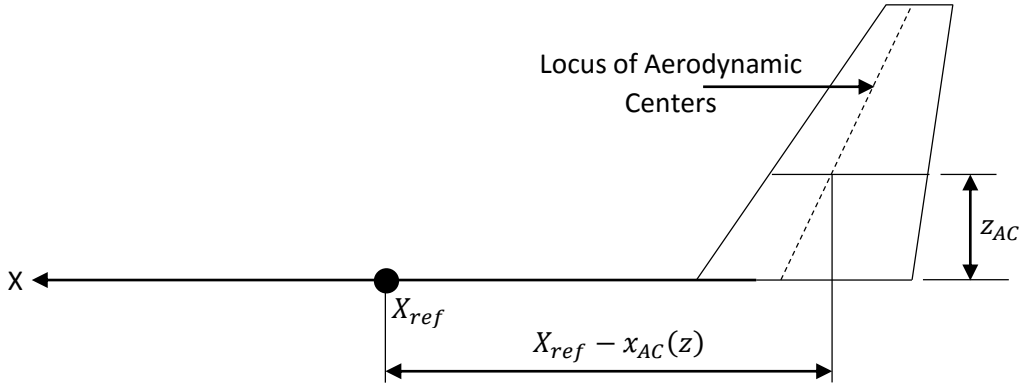

Figure 47: Description of Distance between Locus of Aerodynamic Centers and COG of the Vertical Tail

The modal displacement for roll is given by:

$$\frac{\partial L_{roll}}{\partial \eta_i} \triangleq C_{L_{roll_{\eta_i}}} q_\infty S_w b_W = \frac{\partial L_{roll_{E_W}}}{\partial \eta_i} + \frac{\partial L_{roll_{E_H}}}{\partial \eta_i} + \frac{\partial L_{roll_{E_V}}}{\partial \eta_i}$$

$$\frac{\partial L_{roll_{E_W}}}{\partial \eta_i} = -q_\infty \int_{-b_{w/2}}^{b_{w/2}} c_{l_{\alpha_W}}(y)\, v'_{z_{i_w}}(y)\, c_W(y)\, dy \tag{4.26}$$

$$\frac{\partial L_{roll_{E_H}}}{\partial \eta_i} = -q_H \int_{-b_{H/2}}^{b_{H/2}} c_{l_{\alpha_H}}(y)\left(v'_{z_{i_H}}(y) - \frac{d\epsilon_H}{d\alpha_W} v'_{z_{i_W}}(y)\right) c_H(y)dy$$

$$\frac{\partial L_{roll_{E_V}}}{\partial \eta_i} = -q_H \int_0^{b_V} c_{l_{\alpha_V}}(z)\, v'_{Y_{i_V}}(z)\, z_{AC}(z)\, c_V(z)\, dz$$

And the modal velocity for roll by Eq. (4.27). Where b_W is the wing span. The integration limits are from end to end of the wing and horizontal tail, considering the entire span of these lifting surfaces. In the analysis presented here, as there are no anti-symmetric modes (which are necessary for roll resultant moments), the values of $L_{roll_{E_W}}$ and $L_{roll_{E_H}}$ are zero.

$$\frac{\partial L_{roll}}{\partial \dot{\eta}_i} \triangleq C_{L_{roll_{\dot{\eta}_i}}} q_\infty S_w b_W = \frac{\partial L_{roll_{E_W}}}{\partial \dot{\eta}_i} + \frac{\partial L_{roll_{E_H}}}{\partial \dot{\eta}_i} + \frac{\partial L_{roll_{E_V}}}{\partial \dot{\eta}_i}$$

$$\frac{\partial L_{roll_{E_W}}}{\partial \dot{\eta}_i} = -\frac{q_\infty}{V_\infty} \int_{-b_{w/2}}^{b_{w/2}} c_{l_{\alpha_W}}(y)\, v_{Z_{i_W}}(y)\, c_W(y)\, dy$$

$$\frac{\partial L_{roll_{E_H}}}{\partial \dot{\eta}_i} = -\frac{q_H}{V_\infty} \int_{-b_{H/2}}^{b_{H/2}} c_{l_{\alpha_H}}(y)\left(v_{Z_{i_H}}(y) - \frac{d\epsilon_H}{d\alpha_W} v_{Z_{i_W}}(y)\right) c_H(y)dy \quad (4.27)$$

$$\frac{\partial L_{roll_{E_V}}}{\partial \dot{\eta}_i} = -\frac{q_H}{V_\infty} \int_0^{b_V} c_{l_{\alpha_V}}(z)\, v_{Y_{i_V}}(z)\, z_{AC}(z)\, c_V(z)\, dz$$

4.2.5. Yawing Moment

The modal displacement yawing moment is given by:

$$\frac{\partial N_e}{\partial \eta_i} \triangleq C_{N_{\eta_i}} q_\infty S_w b_W$$

$$\frac{\partial N_e}{\partial \eta_i} = -q_H \int_0^{b_v} c_{l_{\alpha_V}}(z)\, v'_{Y_{i_V}}(z)\left(X_{ref} - x_{AC_v}(z)\right) c_V(z)\, dz \quad (4.28)$$

And the modal velocity for yaw by:

$$\frac{\partial N_e}{\partial \dot{\eta}_i} \triangleq C_{N_{\dot{\eta}_i}} q_\infty S_w b_W$$

$$\frac{\partial N_e}{\partial \dot{\eta}_i} = \frac{1}{V_\infty} \int_0^{b_v} c_{l_{\alpha_V}}(z)\, v_{Y_{i_V}}(z) \left(X_{ref} - x_{AC_v}(z)\right) q_H(z)\, c_V(z)\, dz \tag{4.29}$$

Here, the dynamic pressure at the tail, q_H is a function of the span of the vertical tail. It can be set as a constant, as 0.9 of the dynamic pressure q_∞.

4.3. Simulation of Deformation Effects

The elastic aerodynamics were performed independent to the rigid aircraft model. Here the velocity was set to 220 m/s, with sea level conditions for analysis purposes. Figure 49 to Figure 52 show the lift, drag, rolling moment, pitching moment and yawing moment.

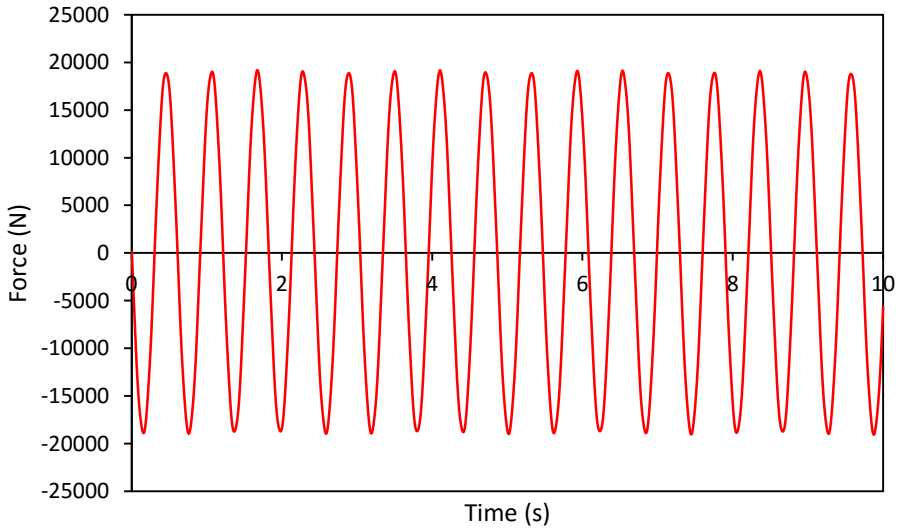

Figure 48: Summation of the Lift Force from all Four Vibration Modes in Bending and Twisting

The lift is seen to fluctuate and causes a significant change in the aircraft's flying capabilities. The drag however has minimal effect, as stated earlier by Schmidt (2012).

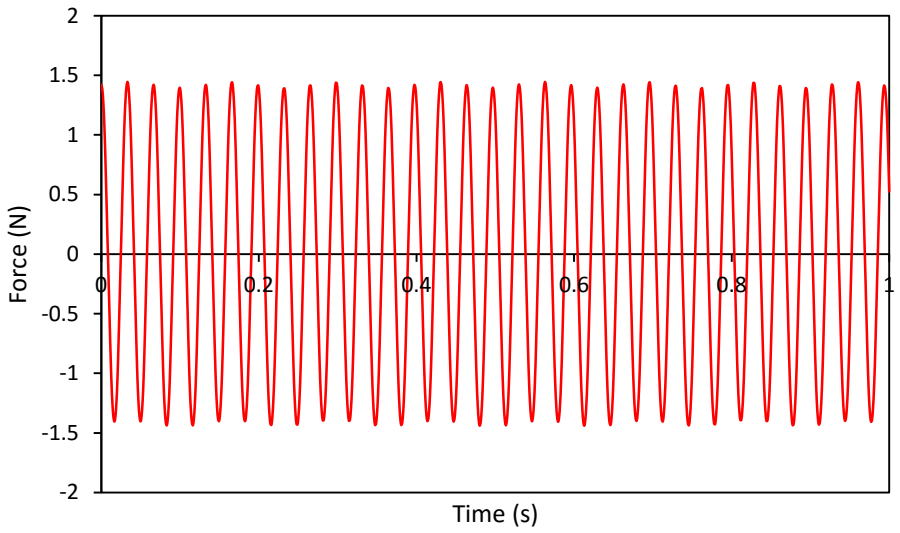

Figure 49: Summation of the Side Force from all Four Vibration Modes in Bending and Twisting. Period of One Second Shown

The rolling moment and yawing moment are presented at a time scale of one second. It was displayed such to show the frequency of the moments, which in this was extremely high, hence the one second time frame. Given that such high frequencies are pointless to consider, it will be considered for this context to provide a holistic approach to the final model. The effects of the rolling and yawing moments will not cause erroneous disturbances to the final model.

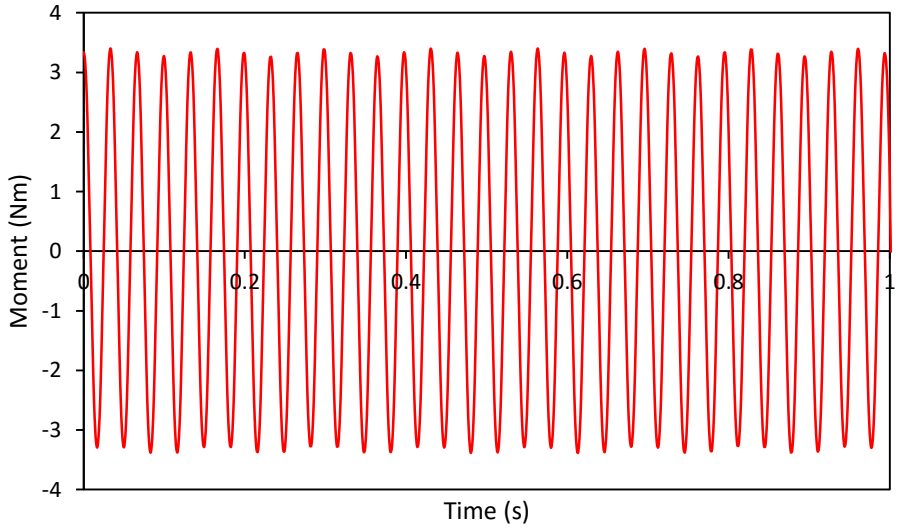

Figure 50: Summation of the Rolling Moment from all Four Vibration Modes in Bending and Twisting. Period of One Second Shown

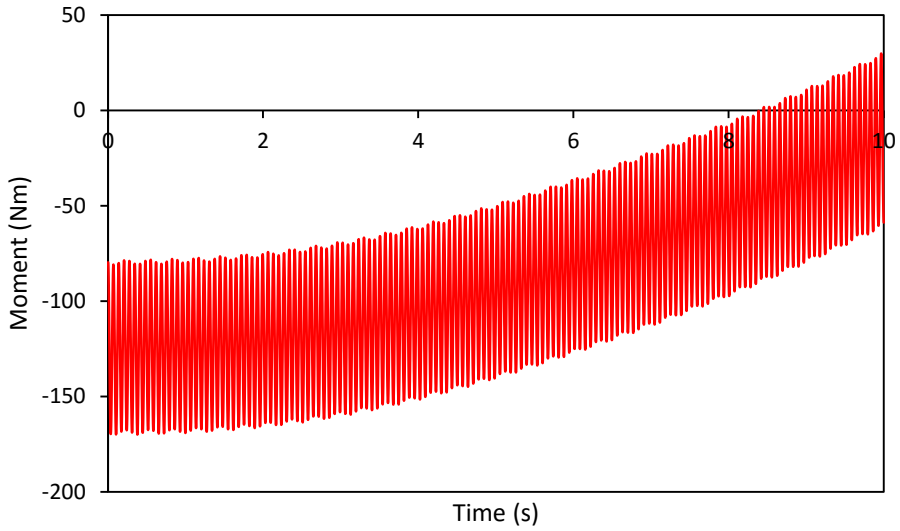

Figure 51: Summation of the Pitching Moment from all Four Vibration Modes in Bending and Twisting

Figure 51 shows the frequency of the pitching moment. The pitching moment is seen to decrease, and can cause a somewhat significant effect on the aircraft.

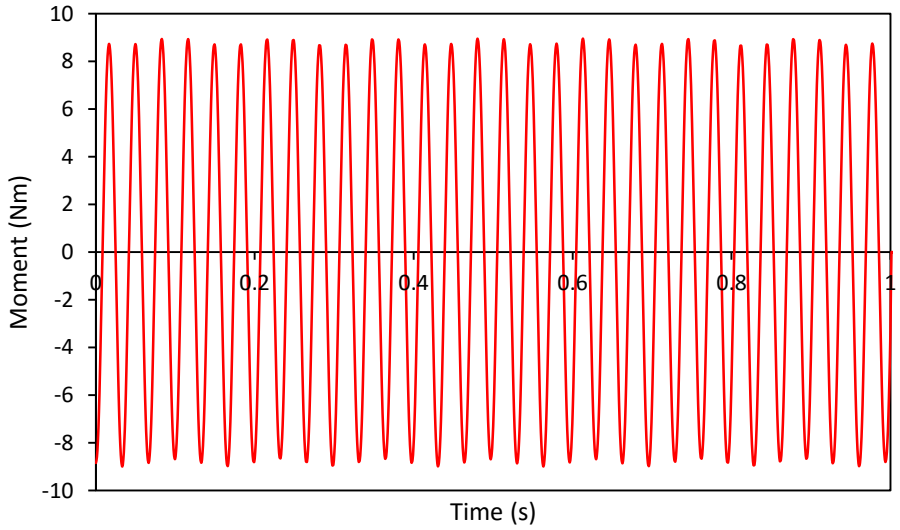

Figure 52: Summation of the Yawing Moment from all Four Vibration Modes in Bending and Twisting

5. RESULTS

The following graphs illustrate results from the models described above. The actuation has been provided by a step change at 5 seconds into the simulation. Due to the large amount of visual data, results have been limited to the following:

- Conventional Actuation
  - Elevator deflection of +5° and -5°
- Rigid aircraft model + piezoelectric actuation and rigid aircraft model + piezoelectric actuation + effects of elastic aerodynamics
  - +5° for both twist and bending modes

5.1. Conventional Actuation

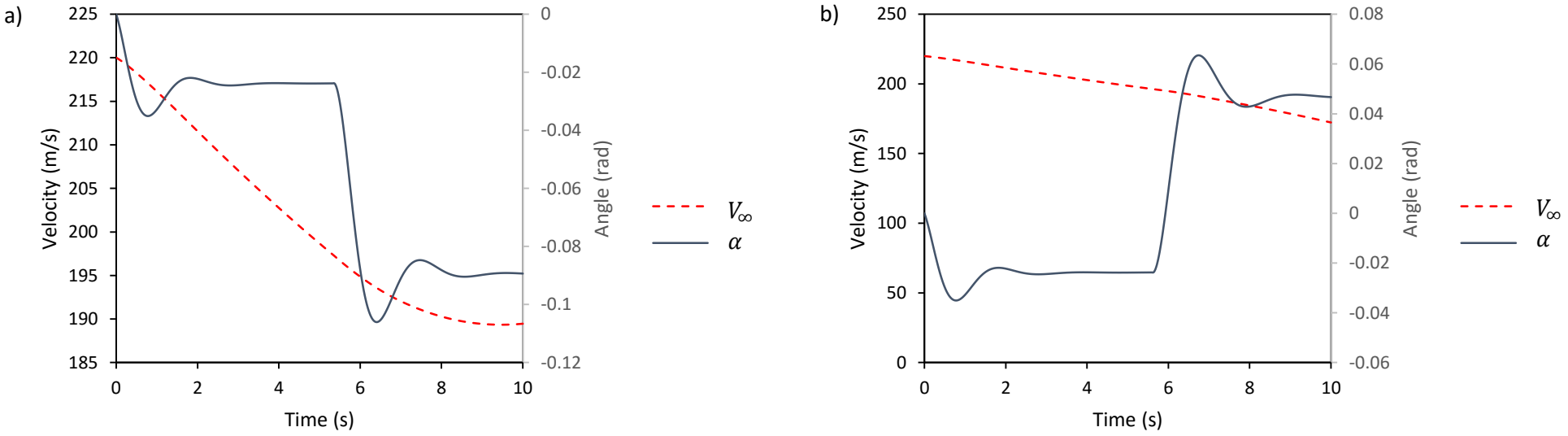

Figure 53: Graph Showing Velocity and Angle of Attack with Step Input at five seconds with Elevator at, a) +5° and b) -5°

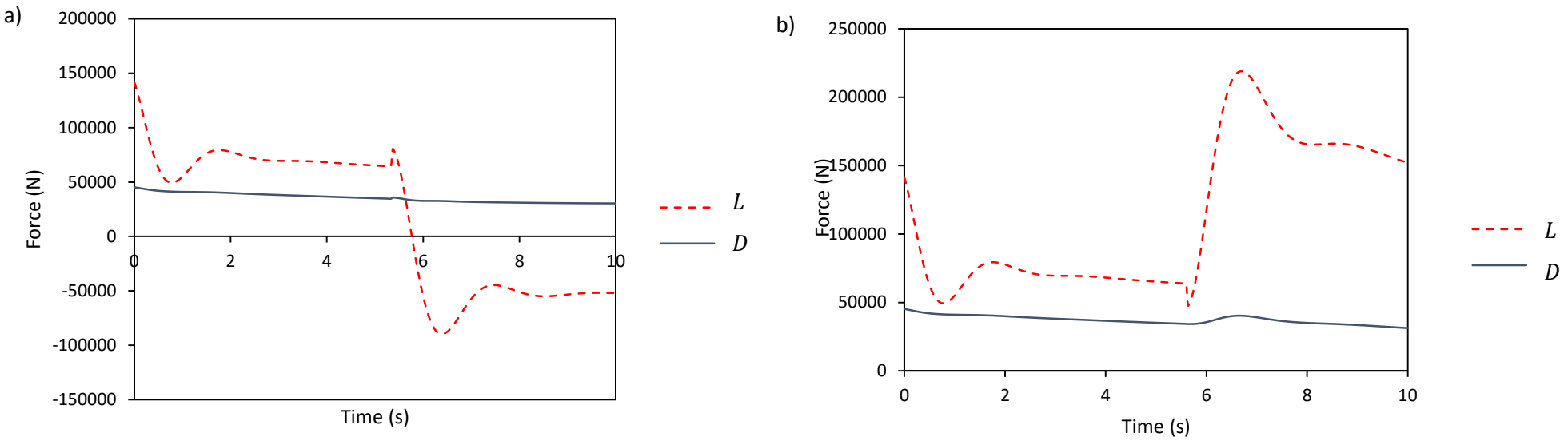

Figure 54: Graph Showing Lift and Drag with Step Input at five seconds with Elevator at, a) +5° and b) -5°

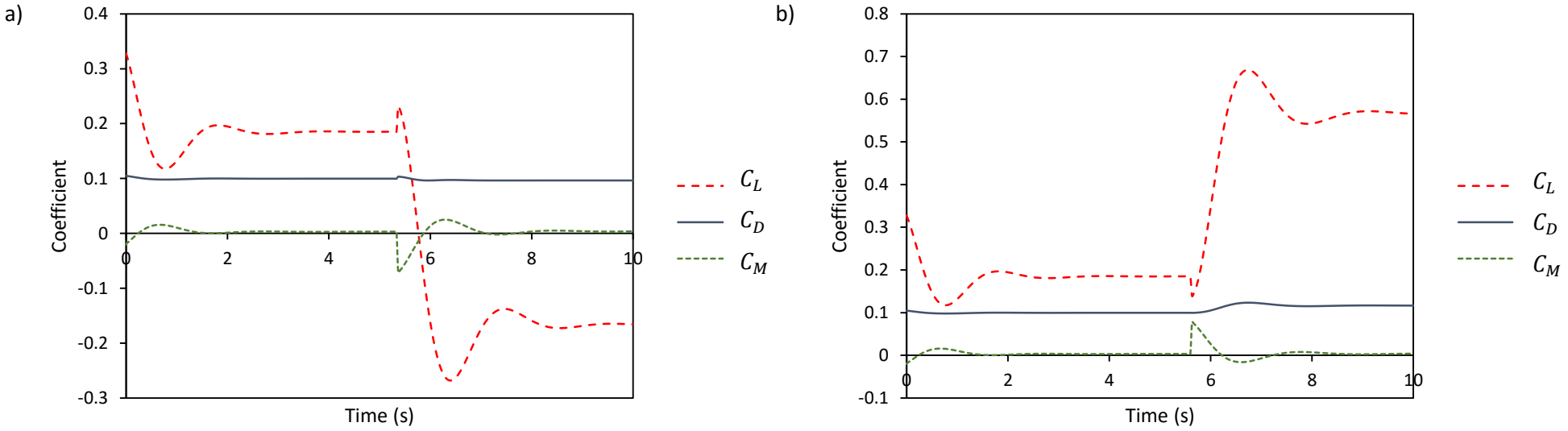

Figure 55: Graph Showing Lift, Drag and Pitching Moment Coefficient with Step Input at five seconds with Elevator at, a) +5° and b) -5°

Figure 53 to Figure 55 show aerodynamics of the rigid aircraft model with elevator step input of 5° at just over 5 seconds into the simulation. It is seen that the aircraft shows dynamic stability behavior. This is evident through the stabilization of the pitching moment coefficient, as well as velocity and coefficient of lift. Through longer time periods of simulation, the aircraft does not experience phugoid oscillation, and maintains its flight path.

5.2. Rigid Aircraft Model + Piezoelectric Actuation

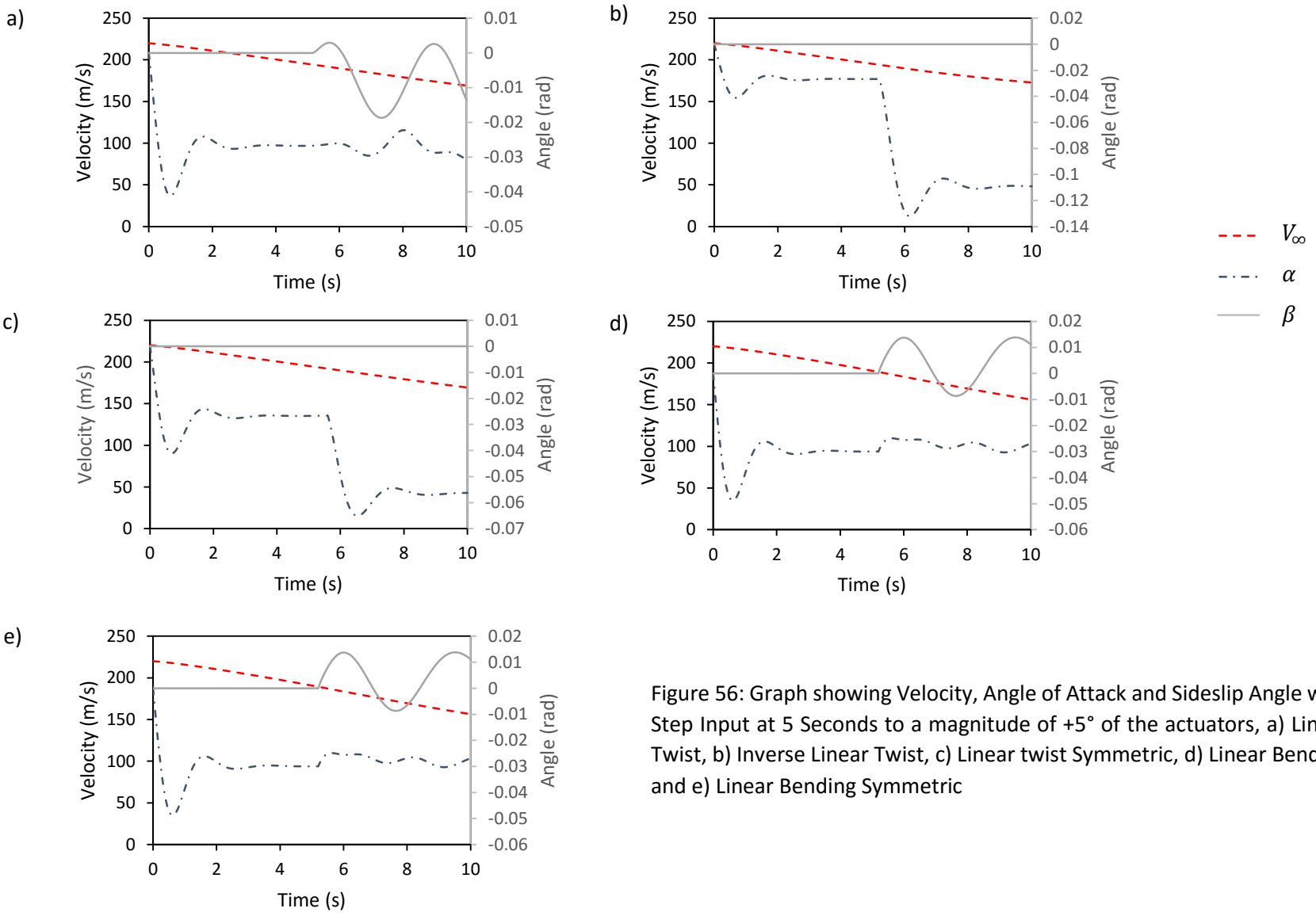

Figure 56: Graph showing Velocity, Angle of Attack and Sideslip Angle with Step Input at 5 Seconds to a magnitude of +5° of the actuators, a) Linear Twist, b) Inverse Linear Twist, c) Linear twist Symmetric, d) Linear Bending and e) Linear Bending Symmetric

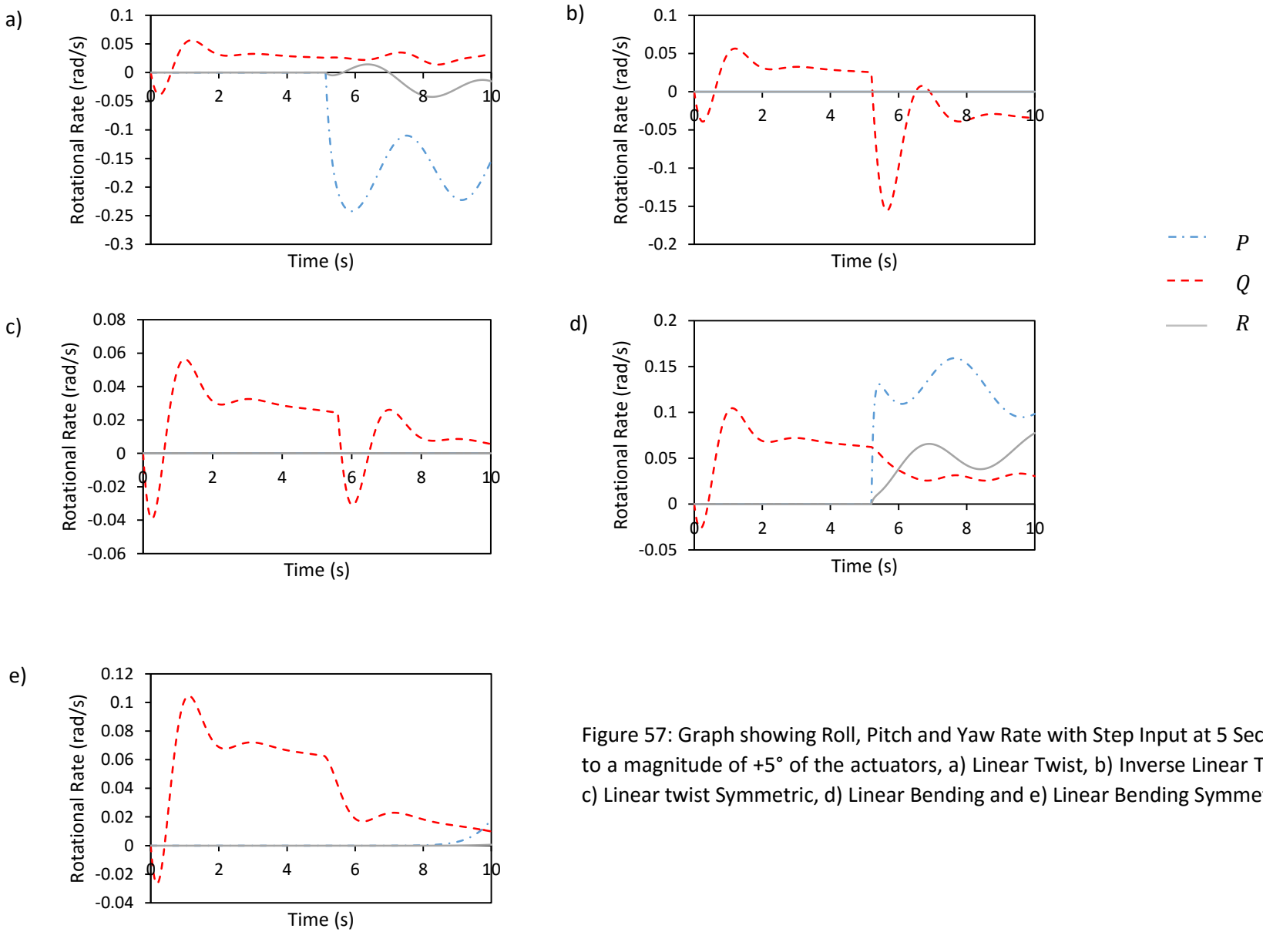

Figure 57: Graph showing Roll, Pitch and Yaw Rate with Step Input at 5 Seconds to a magnitude of +5° of the actuators, a) Linear Twist, b) Inverse Linear Twist, c) Linear twist Symmetric, d) Linear Bending and e) Linear Bending Symmetric

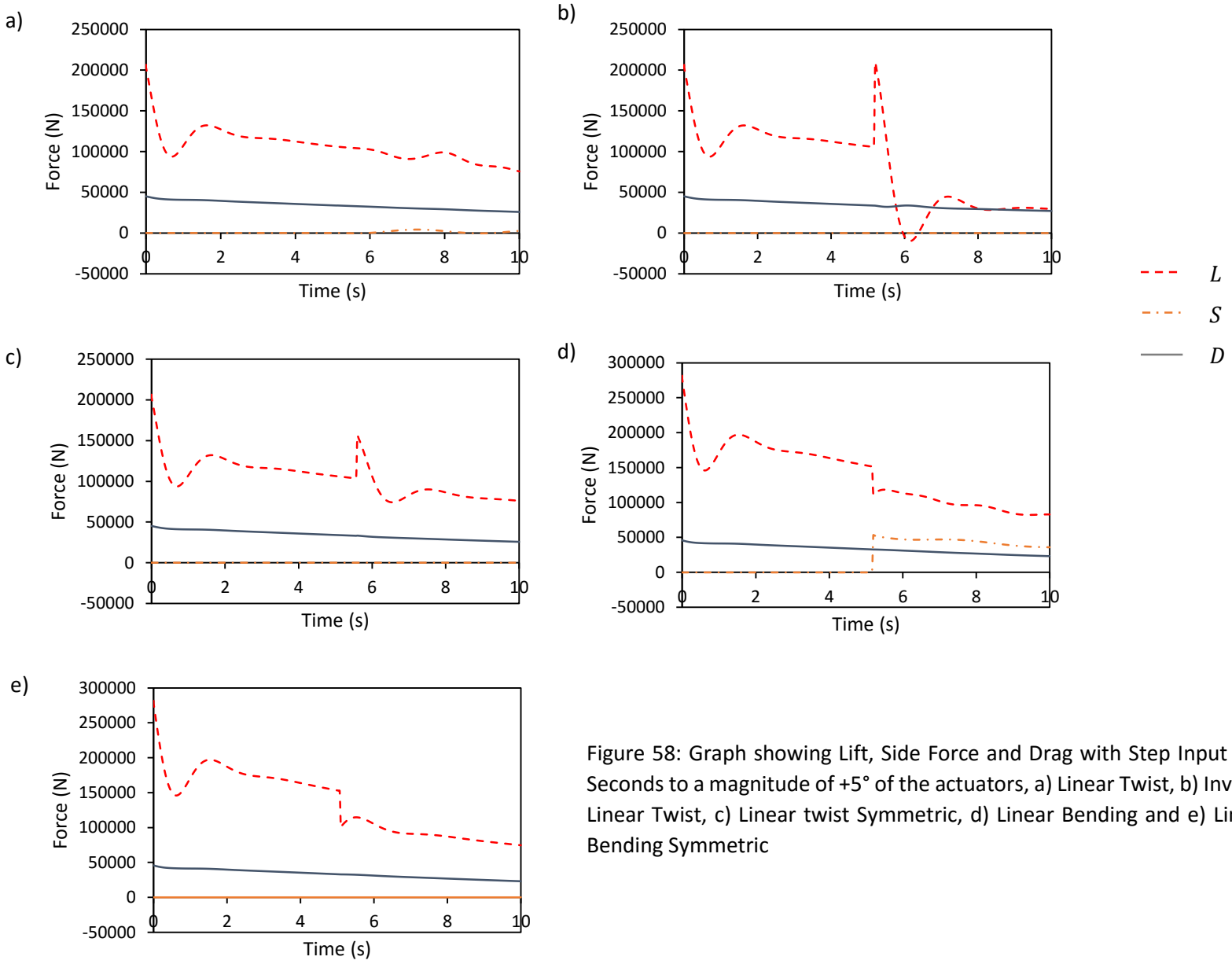

Figure 58: Graph showing Lift, Side Force and Drag with Step Input at 5 Seconds to a magnitude of +5° of the actuators, a) Linear Twist, b) Inverse Linear Twist, c) Linear twist Symmetric, d) Linear Bending and e) Linear Bending Symmetric

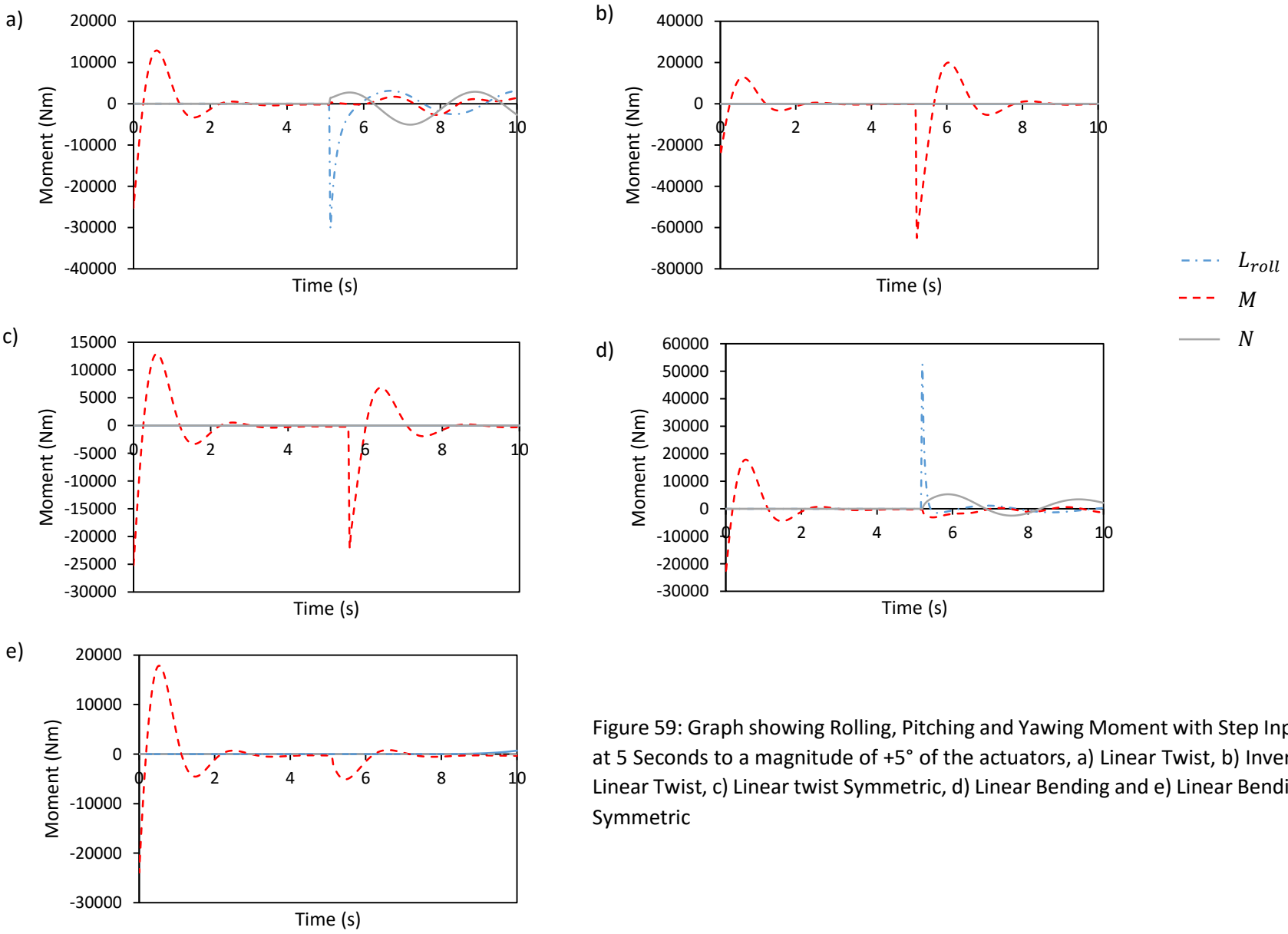

Figure 59: Graph showing Rolling, Pitching and Yawing Moment with Step Input at 5 Seconds to a magnitude of +5° of the actuators, a) Linear Twist, b) Inverse Linear Twist, c) Linear twist Symmetric, d) Linear Bending and e) Linear Bending Symmetric

Figure 56 through Figure 59 display various aerodynamic properties of the rigid aircraft model undergoing piezoelectric actuation to magnitude of 5° for both actuation modes of twist and bending. The magnitude of 5° relates to altering the twist (for twist mode) and dihedral (bending mode) of the right wing, with the left wing following in the appropriate manner.

The effect of the linear twist mode increases lift on one wing, and decreases it on the other. Thus creating an imbalance and resulting in rolling and side slipping. The oscillation of the side slip angle and angle of attack shows that there is a hint of Dutch roll that exists in the model. The roll rate authority also increases, performing a similar function to the ailerons. The lift is slightly optimized in comparison to the lift from the rigid model, however lift cannot be measured in this case as the majority of the aerodynamics are lateral. Linear twist would be a viable mode in terms of coordinated turns, requiring less elevator input, but with slight rudder input.

A good situation to utilize linear twist would be in cases of engine failure. If the engine on the right wing fails, drag is increased on that wing accompanied by clockwise yawing moment, and thus reduced lift. Applying twist on the right wing could counteract these changes in the aerodynamics, requiring the pilot to utilize less rudder and aileron input (side-slipping).

The effect of inverse linear twist increases or decreases lift closer to the root of the wing. This type of scenario is useful in improving angle of attack of the aircraft. Compared to that of the linear twist mode, the angle of attack sits much lower with inverse linear twist, and a greater drop in lift is seen. Ideally in flight, lift is preferred at the tip than it is at the root of the wing, but this is purely for stall conditions. This type of actuation is useful in landing scenarios, when a lower lift is required at the root of the wing.

The effect of linear twist symmetric increases or decreases lift on the tip of the wing. This is a favorable item to have, as this increases roll authority, as well as pitch authority of the aircraft. The angle of attack of the aircraft also decreases, whilst not causing a major decrease on the aircraft lift. This, compared to inverse linear twist is advantageous when considering aircraft approach and take-off angles, increasing visibility and less need for elevator input.

The increase in lift for this twist mode as shown in the Figures in the cruise phase increases the aircrafts glide ratio, and thus creating efficiency in flight, compared to that of the rigid aircraft model. The effect of linear bending changes dihedral of the wing creating an anti-symmetric wing configuration. This causes an imbalance in lift and alleviates roll and yaw efficiency. A unique addition to this bending mode is that of the side force, as shown by side force in the Figures above. Instead of an aircraft having to alter its line

of flight through a combination of rudder and elevator (creating side-slip angle), a side force is created which will move the aircraft in its Y-direction. This is another useful aspect when considering one engine inoperative conditions.

Linear bending symmetric increases or decreases dihedral on both wings equally. Dihedral is extremely significant in cases of side slip and rolling, thus having the ability to change aircraft dihedral will enhance roll authority and prevent aircraft spiral dives. The results also show an increase in pitch rate, and a slight addition of yaw as well.

5.3. Rigid Aircraft Model + Piezoelectric Actuation + Effects on Aerodynamics due to Elastic Deformation

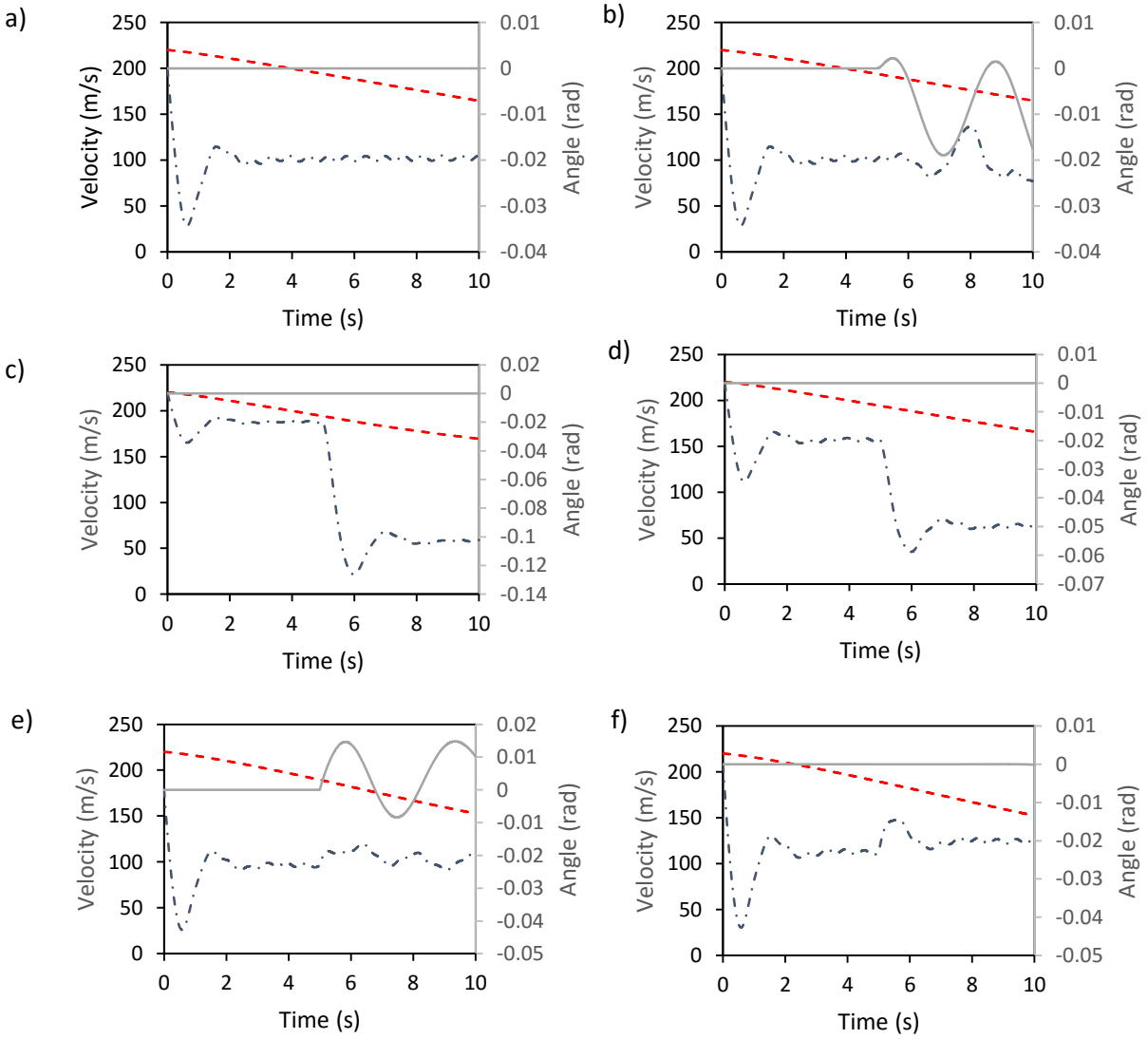

Figure 60: Graph Showing Velocity, Angle of Attack and Side Slip Angle with a Step Input at 5 Seconds to a Magnitude of +5°, a) No actuation, b) Linear Twist, c) Inverse Linear Twist, d) Linear Twist Symmetric, e) Linear Bending and f) Linear Bending Symmetric

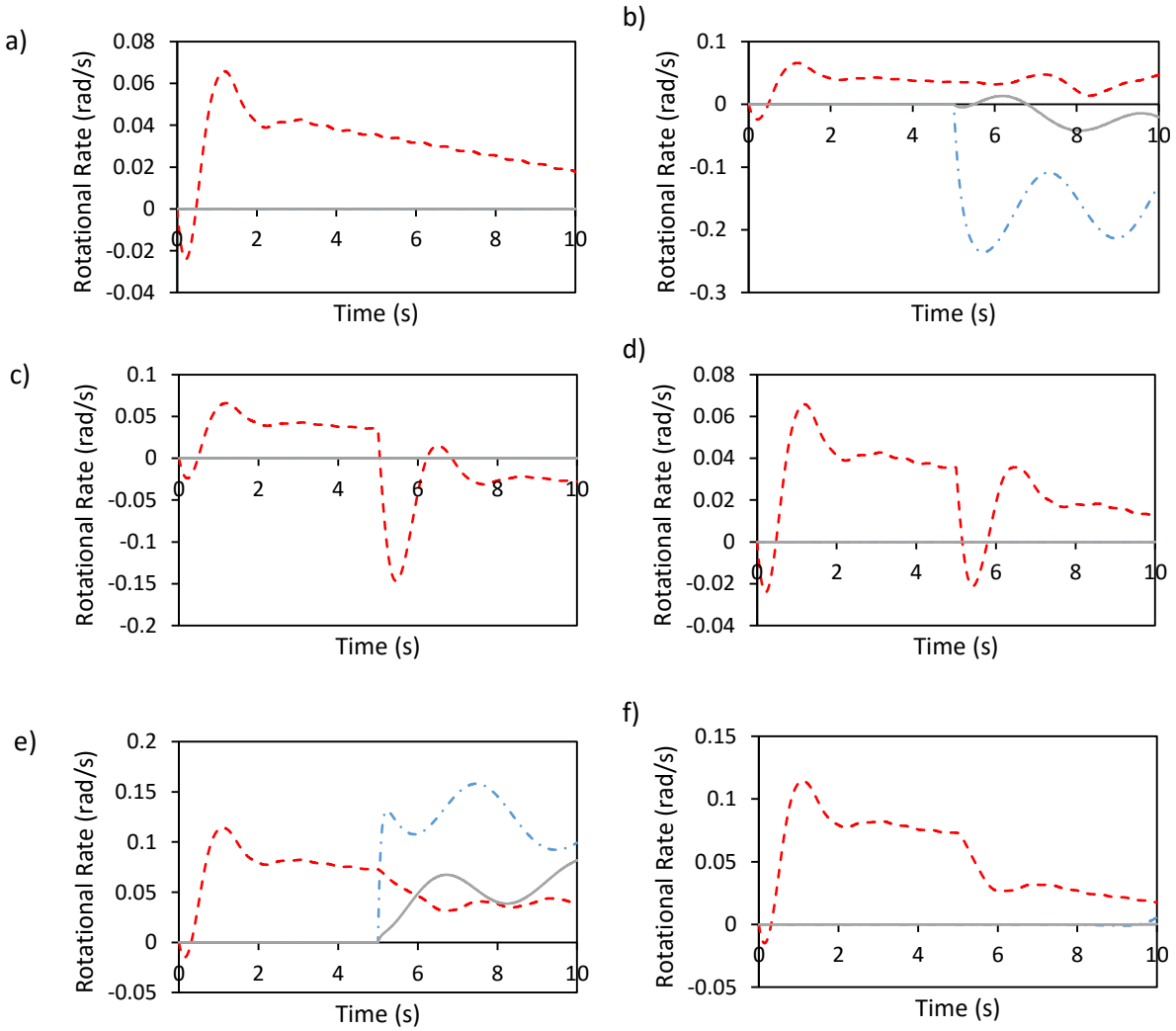

Figure 61: Graph Showing Roll, Pitch and Yaw Rate with a Step Input at 5 Seconds to a Magnitude of +5°, a) No actuation, b) Linear Twist, c) Inverse Linear Twist, d) Linear Twist Symmetric, e) Linear Bending and f) Linear Bending Symmetric

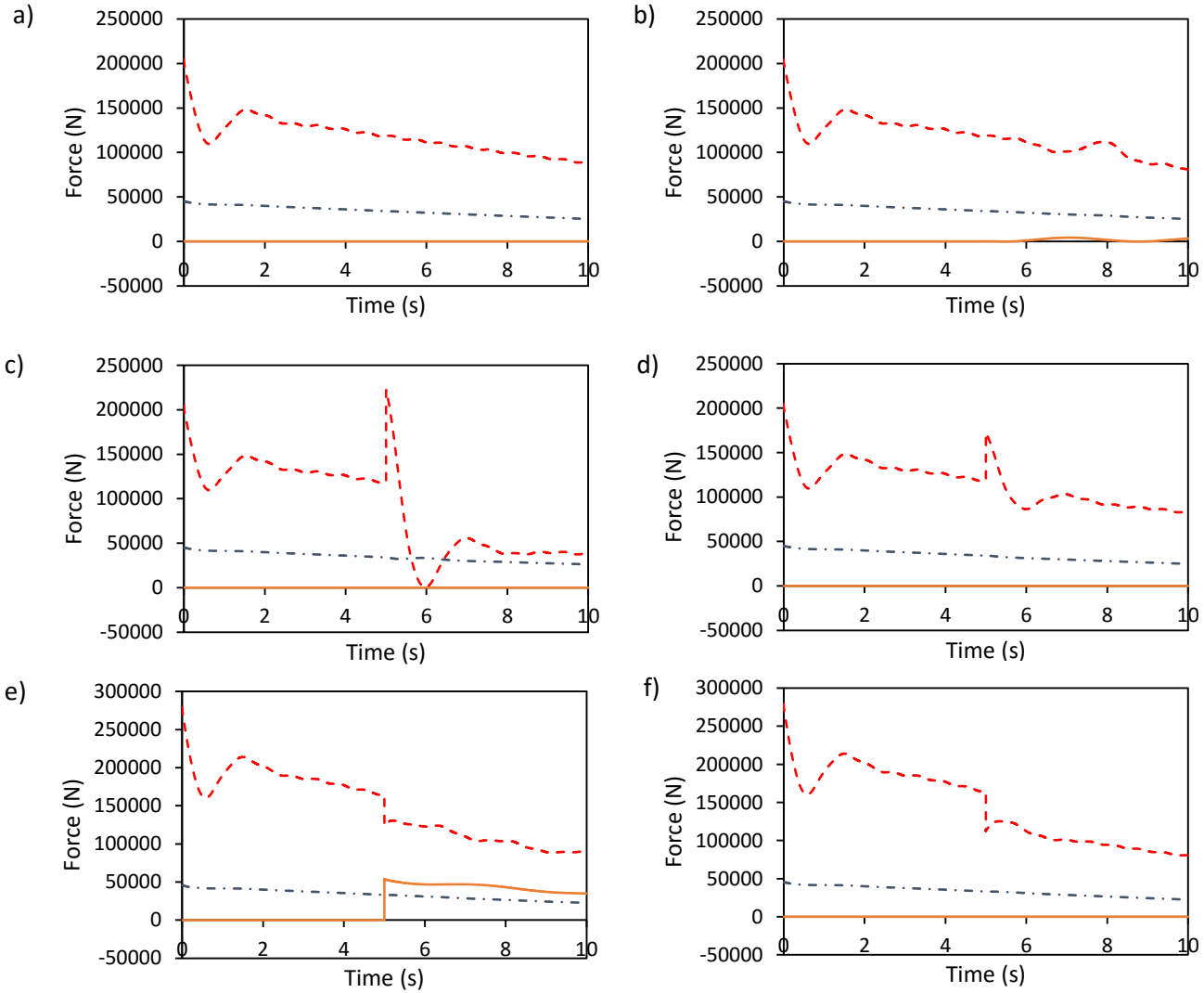

Figure 62: Graph Showing Lift, Side Force and Drag with a Step Input at 5 Seconds to a Magnitude of +5°, a) No actuation, b) Linear Twist, c) Inverse Linear Twist, d) Linear Twist Symmetric, e) Linear Bending and f) Linear Bending Symmetric

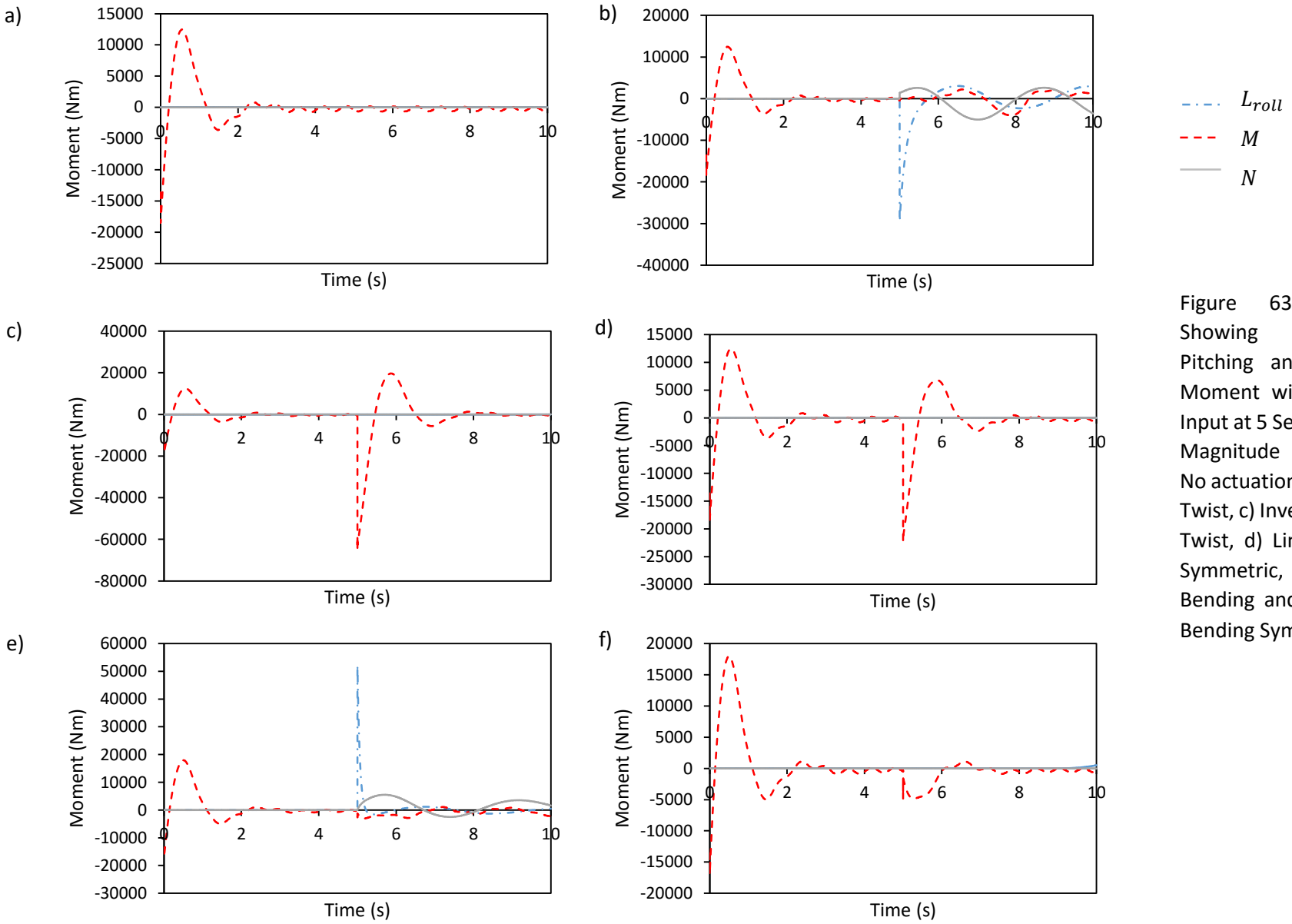

Figure 63: Graph Showing Rolling, Pitching and Yawing Moment with a Step Input at 5 Seconds to a Magnitude of +5°, a) No actuation, b) Linear Twist, c) Inverse Linear Twist, d) Linear Twist Symmetric, e) Linear Bending and f) Linear Bending Symmetric

Figure 60 through Figure 63 show the various aerodynamic characteristics of the same procedure as that with rigid model + piezoelectric actuation model, but with elastic effects incorporated.

The analysis of elastic aerodynamic effects in this case was broken down to the wing, vertical tail and horizontal tail. The results very much replicate those of the rigid model + piezoelectric actuation. The equations developed for the vibrational analysis did not include damping, and thus oscillations are seen to be continuous, however not significant. However, a vibrational analysis on the entire aircraft would provide much more accurate results. The vibration frequencies determined were too high and pointless to integrate into the system.

Through individual analysis, the major significance of vibration was seen to be from lift, which is aptly described in the Figures, compared to those of the other two simulation models.

6. CONCLUSIONS

The intention of this project was to apply the piezoelectric actuators such that they perform the same function as rolling, pitching and yawing, whilst simultaneously improving the aerodynamic efficiency of the wing (lift to drag ratio).

The methodology was to develop a rigid aircraft as the base model, and append the models of piezoelectric actuation and conclusively the elastic aerodynamic effects. The chosen aircraft was the Cessna Citation V. The reason this aircraft was chosen was that much of the research of piezoelectric analysis on aircraft was conducted on this model, thus maintaining a standard and provision of data for future work.

The cruise flight condition was set out, with a cruise speed of 220 m/s at an altitude of 8000 m. The majority of the analysis considers longitudinal aircraft dynamics, with a look at lateral dynamics as well.

Following the flight condition, the rigid aircraft flight dynamic model was developed. The aerodynamic derivatives were formulated by a DATCOM model. The model did not take into account effects of rudder and a few other coefficients. These were completed by following a method described by Roskam (2001).

The piezoelectric actuation model was developed by considering the modes of vibration of a cantilevered beam, and utilizing those deflections as a means of geometry change for the wing. It was stated that the wing will not go through camber changes, and thus maintaining the shape of the aerofoil throughout various deflections.

The elastic aerodynamics were finally described stating that vibrational analysis on each lifting body (wing, horizontal tail and vertical tail).

All three models were developed in MATLAB's Simulink R2015a.

6.1. Conclusions

The rigid aircraft model was seen to be self-regulating and maintained a dynamically stable flight characteristic. The inputs from the elevator altered the longitudinal dynamics of the aircraft as desired. The validation process of the rigid aerodynamics and flight dynamics was done by utilizing the formulation of equations by Roskam (2001), and comparing them to those of the DATCOM model. The differences were quite large, and in instances most of the equations formulated by Roskam (2001) did not take into

account boundary conditions of the angle of attack and other outlying aerodynamic factors. Implementing both sets of aerodynamic properties into the Simulink model, it was found that the DATCOM model provided the most accurate flight characteristics, accounting for high angle of attacks and stall situations.

The elastic aerodynamics, due to the individual vibrational analysis of the components yielded results which were significant only by lift, and slight undulations by the pitching moment. Not having a detrimental effect on the overall aircraft dynamics, the elastic aerodynamics provided results closely matching those of the rigid model + piezoelectric actuation. Due to the high vibration modes of the horizontal and vertical tail, the effects of these components in vibration were insignificant.

The piezoelectric actuation was seen to be well received by the rigid model, and the aerodynamics proved the viable usage of this type of actuation over the conventional methods (elevator, aileron and rudder). This was found by increases in lift, pitch, roll and yaw authority. Table 18 shows the conclusion of the actuation type and their uses over the conventional methods. As shown by the table, piezoelectric actuation can be easily utilized as both a primary and secondary actuation method, with one for flight trajectory alterations and the other for trim conditions, which is evident from the aerodynamic and flight dynamic analysis conducted.

6.2. Recommendations for Future Work

Much of the work presented in this research had taken assumptions into considerations to simplify and provide base work for future considerations. Many of these assumptions need to be addressed to clearly advance the scope of practice of the piezoelectric actuators as actuating mechanisms on aircraft. An assumption was made that the actuators do not cause changes in camber. In reality, this is of course not the case. An inherent solution which will take into consideration the changes in camber of the airfoil must be investigated to further add to the actuation model, and be provided with the relevant aerodynamics and flight dynamics to be compared to those given in this report.

It was also assumed that the piezoelectric actuators are of single size, and actuation does not take into account control factors of the model. This needs further investigation as in effect the actuators are currently manufactured for small scale applications. Adapting them towards larger applications like this will require a thorough analysis in the structural domain of both the aircraft and the actuator. The control aspect needs to be further developed. Whilst in this research no control theories were applied, and effects

such as hysteresis residuals and have not been incorporated into the models, further development of this is required.

Table 18: Concluding uses for Piezoelectric Actuation above conventional Methods

Actuation Type	Dynamic Effects	Uses
Linear twist	Roll authority, sideslip	One engine inoperative conditions. Increase roll authority without the use of elevator simultaneous with ailerons
Inverse Linear Twist	Increase or decrease wing root lift	Stalling the root to increase tip lift and thus roll authority
Linear Twist symmetric	Increase or decrease wing tip lift	Provides shallower approach angles for landing. Increases roll authority. Increase glide ratio and improves cruise phase flight. Enhance deep stall by decreasing the twist at the wing tips
Linear Bending	Increase roll and side slip with a slight yaw	Performing lateral movements without the use of rudder and aileron
Linear Bending Symmetric	Angle of attack in coordinated turns increases	Prevents spiral dives and more control in roll and side slip

The vibrational analysis conducted in this research does not consider vibration of the entire aircraft. Thus investigation of the entire aircraft through FEM/FEA is required, especially with the addition of actuators in the wing of the aircraft.

The analysis of piezoelectric actuation in this research only considers application on the wing. A good recommendation for future work would be to apply these actuators on the entire aircraft, especially the vertical tail and horizontal tail. In essence, piezoelectric actuators can be utilized above conventional actuation methods, as well as structural strengthening components (in vibration), and also sensing elements.

REFERENCES

Addington, M. and Schodek, D. (2005). “Smart Materials and New Technologies”, *Architectural Press*, Oxford, London, 2005.

Akhras, G. (2000). “Smart Materials and Smart Systems for the Future”, *Canadian Military Journal*, Vol. 1, Issue 3, pp. 25-32.

Andrews, S. P. (2011). “Modelling and Simulation of Flexible Aircraft: Handling Qualities with Active Load Control”. *PhD Thesis.* Cranfield University, 2011.

Anonymous (1955). “Standard Atmosphere – Tables and data for Altitudes to 65800 feet”, *Technical Report*, NASA – TR – 1235, National Aeronautics and Space Administration. 1955.

Bilgen, O., Butt, L.M., Day, S.R., Sossi, C.A., Weaver, J.P., Wolek, A., Mason, W.H. and Inman, D.J. (2013). “A Novel Unmanned Aircraft With Solid-State Control Surfaces: Analysis and Flight Demonstration”, *Journal of Intelligent Material Systems and Structures*, Vol. 24, Issue 2, pp. 147-167.

Bismarck-Nasr, M. N. (1999). “Structural Dynamics in Aeronautical Engineering”, *AIAA Education Series,* ISBN 1-56347-323-2, 1999.

Boeing (2013). “Statistical Summary of Commercial Jet Airplane Accidents”, *Aviation Safety,* Boeing Commercial Airplanes, August 2013.

Chattot, J. J. and Hafez, M. M. (2015). “Theoretical and Applied Aerodynamics”, *Springer Science + Business Media Dordrecht,* New York, Springer, 2015.

Chen, Y., Ulker, F.D., Nalbantoglu, V., Wickramasinghe, V., Zimcik, D. and Yaman, Y. (2009). “Active Control of Smart Fin Model for Aircraft Buffeting Load Alleviation Applications”, *Journal of Aircraft*, Vol. 46, Issue 6, pp. 1965-1972.

Cochoy, O., Hanke, S. and Carl, U.B. (2007). “Concepts for Position and Load Control for Hybrid Actuation in Primary Flight Controls”, *Aerospace Science and Technology*, Vol. 11, Issues 2-3, pp. 194-201.

Collinson, R.P.G. (1999). “Fly-by-wire flight Control”, *Computing and Control Engineering Journal*, Vol. 10, Issue 4, pp. 141-152.

DeLaurier, J.D. and Harris, J.M. (1993). “A Study of Mechanical Flapping-Wing Flight”. *Aeronautical Journal,* Vol. 97, pp. 277-286.

Duquette, S.M. and Fu-Shang, W. (2007). "Development of Piezoelectric Servo Flap Actuator", *Proceedings of the 45th Aerospace Sciences Meeting and Exhibit (AIAA'07),* Vol. 21, pp. 15054-15063.

Etkin, B. (1959). "Dynamics of Flight", *John Wiley & Sons, Inc.*, New York.

Flick, P.M., Love, M.H. and Zink, P.S. (1999). "The Impact of Active Aeroelastic Wing Technology on Conceptual Aircraft Design", *RTO AVT Specialists' Meeting on "Structural Aspects of Aircraft Control",* Ottawa, Canada, 18-20 October 1999.

Gandhi, M.V. and Thompson, B.D. (1992). "Smart Materials and Structures", *Kluwer Academic Publishers,* London, Edition 92.

Gibson, T.E., Annaswamy, A.M. and Lavretsky, E. (2011). "Modelling for Control of Very Flexible Aircraft", *AIAA Guidance, Navigation and Control Conference,* AIAA Paper, 2011-6202, Oregon, August 2011.

Hibbeler, R. (2000). "Mechanics of Materials", *Fourth Edition,* Prentice Hall, United States of America.

Hodges, D.H. and Pierce, G.A. (2014). "Introduction to Structural Dynamics and Aeroelasticity", *2nd Edition,* Cambridge University Press, Cambridge.

Hu, H., Kumar, A.G., Abate, G. and Albertani, R. (2010). "An Experimental Investigation on the Aerodynamic Performances of Flexible Membrane Wings in Flapping Flight", Aerospace Science and Technology, Vol. 14, Issue 8, pp. 575-586.

Huang, S.N. and Tan, K.K. (2011). "Modelling and Control of Piezoelectric Actuator Systems", in *Piezoelectric Actuators*, in a book edited by Joshua E. Segel, Nova Science Pub Inc., United States of America, pp. 117-138.

Ifju, P.G., Jenkins, D.A., Ettinger, S., Lian, Y. and Shyy, W. (2002). "Flexible-Wing-Based Micro Air Vehicles", *Proceedings of the 40th AIAA Aerospace Sciences and Meeting Exhibit (AIAA'02),* 2002-0705, Reno, Nevada.

Jänker, P., Claeyssen, F., Grohmann, B., Christmann, M., Loskowski, T., LeLetty, R., Sosniki, O. and Pages, A. (2008). "New Actuators for Aircraft and Space Applications", *Proceedings of the 11th International Conference on New Actuators,* Germany, June 2008, pp. 346-354.

Li, M., Chen, W. and Guan, D. (2004). "Improvement of Aircraft Rolling Power by Use of Piezoelectric Actuators", *Chinese Journal of Aeronautics,* Volume 17, Issue 2, pp. 87-92.

Li, M., JunXian, Y.J., De, G. and WeiMin, C. (2011). “Application of Piezoelectric Fiber Composite Actuator to Aircraft Wing for Aerodynamic Performance Improvement”, *Science China Technological Sciences*, Vol. 54, Issue 2, pp. 395-402.

Li, N. X. (2010). “Modeling of Flexible Aircraft for 3D Motion-Based Flight Simulators”, *MSc Dissertation,* University of Toronto, 2010.

Lightman, A., Sarewitz, D. and Desser, C. (2003). “Living with the Genie: Essays on Technology and the Quest for Human Mastery”, *Island Press*, Washington, vol. 100, Issue 7.

Maggin, B. and Shanks, R.E. (1946). “The Effect of Geometric Dihedral on the Aerodynamic Characteristics of a 40° Swept-back wing of Aspect ratio 3”. *National Advisory Committee for Aeronautics,* Langley Research Center.

Martindale, T. (2011). “A First-Order Model of a Variable Camber Wing for a Civil Passenger Aircraft”, *MSc Dissertation*, University of the Witwatersrand, December 2011.

Mehrabian, A.R. and Yousefi-Koma, A. (2007). “Optimal Positioning of Piezoelectric Actuators on a Smart Fin Using Bio-Inspired Algorithms”, *Aerospace Science and Technology*, Vol. 11, pp. 174-182.

Meirovitch, L. and Tuzcu, I. (2006). “Integrated Approach to the Dynamics and Control of Manoeuvring Flexible Aircraft”, *NASA Paper,* Virginia Polytechnic Institute and State University, Blacksburg, Virginia, June 2003, NASA/CR-2003-211748.

Moses, R.W., Pototzky, A.S., Henderson, D.A., Galea, S.C., Manokaran, D.S., Zimcik, D.G., Wickramasinghe, V., Pitt, D.M. and Gamble, M.A. (2005). “Controlling Buffet Loads by Rudder and Piezo-Actuation”, *Forum on Aeroelasticity and Structural Dynamics* (2005).

Multhopp, H. (1950). “Methods for Calculating the Lift Distribution of Wings (Subsonic Lifting-Surface Theory)”. *Aeronautical Research Council Reports and Memoranda,* London, Reports and Memoranda No. 2884, January 1950.

Nguyen, N. and Tuzcu, I. (2009). “Flight Dynamics of Flexible Aircraft with Aeroelastic and inertial Force Interactions”, *AIAA Atmospheric Flight Mechanics Conference,* AIAA Paper, 2009-6045, Chicago, August 2009.

Nir, A. and Abramovich H. (2010). “Design, Analysis and Testing of a Smart Fin”, *Composite Structures*, Vol. 92, Issue 4, pp. 863-867.

Otiefy, R.A.H. and Negm, H.M. (2011). “Wing Box Transonic-Flutter Using Piezoelectric Self-Sensing Diagonal-Link Actuators”, *International Journal of Solids and Structures*, Vol. 48, Issue 1, pp. 31-43.

Park, J. and Kim, J. (2005). “Analytical Development of Single Crystal Macro Fiber Composite Actuators for Active Twist Rotor Blades”, *Smart Materials and Structures*, Vol. 14, Issue 4, pp. 745-753.

PI, *Piezo Mechanisms: Servo control & Different Designs,* Company: PI, USA, Available from <www.piezo.ws>. [21/01/2015].

Prechtl, E.F. (1994). “Development of a Piezoelectric Servo-Flap Actuator for Helicopter Rotor Control”, *MSc Dissertation*, Massachusetts Institute of Technology, May 1994.

Queijo, M.J. and Jaquet, B.M. (1948). “Calculated Effects of Geometric Dihedral on the Low-speed Rolling Derivatives of Swept Wings”. *National Advisory Committee for Aeronautics*, Langley Aeronautical Laboratory, Langley Field, Va, Technical Note No. 1732.

Rabinovitch, O. and Vinson, J.R. (2003). “Smart Fins: Analytical Modelling and Basic Design Concepts”, *Mechanics of Advanced Materials and Structures*, Vol. 10, Issue 3, pp. 249-269.

Rao, S. (1995). “Mechanical Vibrations”, *Third Edition*, Addison-Wesley, Reading, Massachusetts.

Roskam, J. (2001). “Airplane Flight Dynamics and Automatic Flight Controls”, *Part 1,* DARcorporation, United States of America, Third Printing, 2001.

Schmidt, D.K. (2012). “Modern Flight Dynamics”. *International Edition,* McGraw-Hill, New York.

Sivells, J.C. and Neely, R.H. (1947). “Method for Calculating Wing Characteristics by Lifting-Line Theory using Nonlinear Section Lift Data”. *National Advisory Committee For Aeronautics,* Langley Memorial Aeronautical Laboratory, Langley Field, VA, Report No. 865.

Sohn, J.W., Choi, S.B. and Kim, H.S. (2011). “Vibration Control of Smart Hull Structure with Optimally Placed Piezoelectric Composite Actuators”, *International Journal of Mechanical Sciences*, Vol. 53, Issue 8, pp. 647-659.

Sosnicki, O., Lhermet, N. and Claeyssen, F. (2006). “Vibration Energy Harvesting in Aircraft using Piezoelectric Actuators”, *10th International Conference on New Actuators,* Bremen, Germany, pp. 968-971.

Suleman, A. and Costa, A.P. (2004). “Adaptive Control of an Aeroelastic Flight Vehicle Using Piezoelectric Actuators”, *Computers and Structures*, Vol. 82, Issue 17-19, pp. 1303-1314.

Taha, H.E., Hajj, M.R. and Beran, P.S. (2014). “State-space representation of the Unsteady Aerodynamics of Flapping flight”. *Aerospace Science and Technology.* Vol. 34, pp. 1-11, April 2014.

Tuzcu, I. and Meirovitch, L. (2006). “Control of Flying Flexible Aircraft Using Control Surfaces and Dispersed Piezoelectric Actuators”, *Smart Materials and Structures*, Vol. 15, Issue 4, pp. 893-903.

Ulker, F.D., Nalbantoglu, V., Chen, Y., Zimcik, D. and Yaman, Y. (2009). “Active Vibration Control of a Smart Fin”, *Proceedings of the 50th Structural Dynamics and Materials Conference (AIAA ‘09),* 2009-2663, Palm Springs, California.

Waszak, M. R., Davidson, K. B. and Schmidt, D. K. (1987). “A Simulation Study of the Flight Dynamics of Elastic Aircraft: Volume One – Experiment, Results and Analysis”, *NASA contractor Report 4102*, Langley Research Center, 1987.

Whitney, S. (1999). “Vibrations of Cantilever Beams: deflection, Frequency, and Research Uses”, April 23, 1999. Aeronautical Laboratory, Langley Field, Va., Technical Note No. 1169.

Yechout, T.R., Morris, S.L., Bossert, D.E. and Hallgreen, W.F. (2003). “Introduction to Aircraft Flight Mechanics: Performance, Static Stability, Dynamic Stability, and Classical Feedback control”. *American Institute of Aeronautics and Astronautics Education,* Reston, Virginia.

Zareie, S. and Zabihollah, A. (2011). “A Failure Control Method for Smart Composite Morphing Airfoil by Piezoelectric Actuator”, *Transactions of the Canadian Society of Mechanical Engineering*, Vol. 35, Issue 3, pp. 369-381.

APPENDIX A – Aircraft Properties

Table 19: Aircraft Data

	Item	No.	Unit
	Mass	7212.081	kg
	CG Behind MAC Quarter Chord	0.609	m
Wing NACA 23012	Wing Reference Area	32.440	m²
	Wingspan	16.002	m
	Wing Sweep Quarter Chord	28.3˚	
	Root Chord	3.517	m
	Tip Chord	0.945	m
	Taper Ratio	0.269	
	Mean Aerodynamic Chord	2.030	m
	Aspect Ratio	7.893	
	Dihedral	4˚	
	Incidence	3˚	
	Wing Lift Curve Slope	0.097	Per ˚
	Moment Curve Slope	-0.001	Per ˚
Horizontal Tail NACA 0010	Reference Area	8.050	m²
	Tail Span	6.614	m
	Tail Sweep Quarter Chord	23.58˚	
	Root Chord	1.623	m
	Tip Chord	0.811	m
	Taper Ratio	0.499	
	Mean Aerodynamic Chord	1.216	m
	Aspect Ratio	5.434	
	Aerodynamic Centre Aft Of CG	5.523	m
	Tail MAC And Wing MAC	5.584	m
	Incidence	0.002	Rad
	Lift Curve Slop	0.101	Per ˚
	Moment Curve Slope	-0.001	Per ˚
Fin NACA 0012	Reference Area	5.091	M²
	Vertical Sweep Quarter Chord	38.68˚	
	Aerodynamic Centre Aft Of CG	5.142	m
	Lift Curve Slope	0.088	Per ˚
	Moment Curve Slope	-0.001	Per ˚

APPENDIX B – Aircraft Mass Data

	x (m)	Y (m)	Z (m)	Mass (kg)
WING LEFT	0.272415	-0.44044	0.973912	170.3150342
	0.136004	-1.05258	0.956716	72.57498936
	-0.05596	-1.41732	0.968121	117.687431
	0.107452	-1.73863	1.014476	62.26848199
	0.020428	-2.05105	0.997153	75.51663833
	0.0703	-2.41579	1.000277	42.08490507
	-0.01555	-2.77393	0.996112	30.16800593
	-0.14858	-3.13893	0.998017	43.24438715
	-0.02769	-3.59613	0.993648	30.94099398
	-0.01334	-4.05613	0.998499	33.28143003
	0.066746	-4.58902	0.99314	31.7998696
	-0.01352	-5.07975	0.995959	32.29372307
	0.04572	-5.66725	0.991057	24.60678633
	0.081501	-6.16915	0.989305	17.71430953
	0.129781	-6.61746	0.99154	15.03032324
	0.102479	-7.06247	0.987069	13.48434713
	0.130211	-7.49833	0.983107	10.11326035
	0.228778	-7.92404	0.976198	7.171611374
	0.127711	-8.35304	0.983793	6.162432528
WING RIGHT	0.272415	0.440436	0.973912	170.3150342
	0.136004	1.052576	0.956716	72.57498936
	-0.05596	1.41732	0.968121	117.687431
	0.107452	1.73863	1.014476	62.26848199
	0.020428	2.05105	0.997153	75.51663833
	0.0703	2.415794	1.000277	42.08490507
	-0.01555	2.773934	0.996112	30.16800593

	-0.14858	3.138932	0.998017	43.24438715
	-0.02769	3.596132	0.993648	30.94099398
	-0.01334	4.056126	0.998499	33.28143003
	0.066746	4.589018	0.99314	31.7998696
	-0.01352	5.079746	0.995959	32.29372307
	0.04572	5.667248	0.991057	24.60678633
	0.081501	6.169152	0.989305	17.71430953
	0.129781	6.617462	0.99154	15.03032324
	0.102479	7.06247	0.987069	13.48434713
	0.130211	7.498334	0.983107	10.11326035
	0.228778	7.924038	0.976198	7.171611374
	0.127711	8.353044	0.983793	6.162432528
HORIZONTAL TAIL LEFT	-6.19176	-0.08887	-0.96617	27.87051366
	-6.34848	-0.36325	-1.11366	13.26962823
	-6.43534	-0.81295	-1.12283	13.41993146
	-6.40131	-1.27843	-1.11384	12.32486506
	-6.43941	-1.66467	-1.11189	5.861826063
	-6.41274	-1.93538	-1.10272	3.714637029
	-6.45414	-2.22949	-1.10962	7.472217839
	-6.47751	-2.65836	-1.10741	5.561219599
	-6.53212	-3.06629	-1.11011	4.272906178
	-6.40969	-3.25907	-1.08798	2.898705196
HORIZONTAL TAIL RIGHT	-6.19176	0.088872	-0.96617	27.87051366
	-6.34848	0.363245	-1.11366	13.26962823
	-6.43534	0.812952	-1.12283	13.41993146
	-6.40131	1.278433	-1.11384	12.32486506
	-6.43941	1.664665	-1.11189	5.861826063
	-6.41274	1.935378	-1.10272	3.714637029
	-6.45414	2.229485	-1.10962	7.472217839
	-6.47751	2.658364	-1.10741	5.561219599
	-6.53212	3.066288	-1.11011	4.272906178

	-6.40969	3.259074	-1.08798	2.898705196
VERTICAL TAIL	-6.03301	0	-0.4956	18.61612893
	-6.28167	0	-0.77438	8.996722053
	-6.46938	0	-1.08414	7.450745949
	-6.65658	0	-1.36291	6.398623322
	-6.67258	0	-1.70364	15.91067074
	-7.1722	0	-2.01339	3.7790527
	-7.31495	0	-2.32315	1.331257201
	-7.33552	0	-2.6329	3.220783551
	-7.4709	0	-2.6329	1.395672872
	-7.48843	0	-3.25241	11.22979865
FORE FUSELAGE	0.188214	0	0.13208	155.3920704
	0.628396	0	0.050292	44.98361027
	0.98933	0	-0.03912	64.71627749
	1.231646	0	0.08255	162.2845472
	1.399032	0	0.21844	76.33257017
	1.774952	0	0.200152	119.4266541
	2.145538	0	0.185928	68.00147671
	2.57302	0	0.134366	151.4412426
	2.82194	0	0.13716	33.19554247
	3.293618	0	0.041148	220.9242797
	4.069842	0	0.16764	271.9200193
	4.810252	0	-0.00762	218.3691248
	5.19049	0	0.050292	231.6602249
	5.684774	0	0.029464	225.3904329
	6.037834	0	0.16637	53.59383829
	6.38302	0	0.166878	155.3276547
	6.7691	0	0.356108	100.9608284
	7.149338	0	0.449834	21.02098064
	7.418832	0	0.448564	13.74200982
AFT FUS	-0.04242	0	0.020574	30.79069075

	-0.27076	0	0.450088	131.9877099
	-0.56337	0	0.4826	306.6615379
	-1.02641	0	0.0508	25.40124627
	-1.18923	0	0.204216	124.7087391
	-1.67919	0	0.241554	53.8085572
	-2.127	0	0.213106	168.404036
	-2.49453	0	0.098298	124.9878737
	-2.9845	0	-0.21158	126.0399963
	-3.62255	0	-0.16383	129.8619928
	-3.96951	0	-0.27356	106.1784977
	-4.39979	0	-0.28042	25.01475225
	-4.8072	0	-0.3109	45.75659832
	-5.16661	0	-0.17323	26.19570622
	-5.54507	0	-0.49936	18.8952635
	-6.05282	0	-0.25832	12.56105585
	-6.43026	0	-0.37948	12.4536964
	-7.06425	0	-0.44069	2.104245254
Engine Left	-2.60198	-1.62687	-0.48641	646.6259777
	-2.75895	-0.9398	-0.35458	56.83609374
Engine Right	-2.60198	1.62687	-0.48641	646.6259777
	-2.75895	0.9398	-0.35458	56.83609374

APPENDIX C – DATCOM Model

The following shows the DATCOM model utilized for the rigid body simulation of this research.

```
DIM FT
DERIV DEG
DAMP
PART

 $FLTCON WT=7000.0, LOOP=2.0,
       NMACH=1.0, MACH(1)=0.4,
       NALT=1.0, ALT(1)=0.0,
       NALPHA=20.0,
       ALSCHD(1)= -16.0, -8.0, -6.0, -4.0, -2.0, 0.0, 2.0, 4.0, 8.0, 9.0,
          10.0, 12.0, 14.0, 16.0, 18.0, 19.0, 20.0, 21.0, 22.0, 24.0,
       STMACH=0.6, TSMACH=1.4, TR=1.0$

 $OPTINS SREF=320.8, CBARR=6.75, BLREF=51.7, ROUGFC=0.25E-3$

 $SYNTHS XCG=21.9, ZCG=3.125,
       XW=19.1,  ZW=3.125,  ALIW=2.5,
       XH=39.2,  ZH=7.75,   ALIH=0.0,
       XV=36.0,  ZV=6.0,
       XVF=28.0, ZVF=7.4,
       SCALE=1.0, VERTUP=.TRUE.$

 $BODY NX=8.0,
     X(1)=0.0,1.0,2.7,6.0,8.8,28.5,39.4,44.8,
     R(1)=0.0,1.25,2.1,2.7,2.76,2.7,1.25,0.0,
     ZU(1)=3.5,4.3,4.8,5.5,7.4,7.4,6.5,5.7,
     ZL(1)=3.5,2.5,2.25,2.1,2.0,2.2,4.3,5.7,
     BNOSE=1.0, BLN=8.8,
     BTAIL=1.0, BLA=19.7,
     ITYPE=1.0, METHOD=1.0$

 $WGPLNF CHRDR=9.4,   CHRDTP=3.01,
       SSPN=25.85,  SSPNE=23.46,
       SAVSI=1.3,
       CHSTAT=0.25, TWISTA=-3.0,
       DHDADI=3.6,
       TYPE=1.0$

NACA W 5 23014
NACA H 4 0010  ! Citation is 0010 at root, 0008 at tip
NACA V 4 0012  ! Citation is 0012 at root, 0008 at tip
NACA F 4 0012   ! Guess it to be the same as vertical tail for Citation.

 $HTPLNF CHRDR=4.99, CHRDTP=2.48,
```

```
      SSPN=9.42, SSPNE=9.21,
      SAVSI=5.32,
      CHSTAT=0.25, TWISTA=0.0,
      DHDADI=9.2,
      TYPE=1.0$

 $VTPLNF CHRDTP=3.63, SSPNE=8.85,  SSPN=9.42, CHRDR=8.3,
      SAVSI=32.3,  CHSTAT=0.25, TYPE=1.0$

 $VFPLNF CHRDR=11.8, CHRDTP=0.0, CHSTAT=0.0, DHDADO=0.0,
      SAVSI=80.0, SSPN=2.3,  SSPNE=2.1, TYPE=1.0$

 $JETPWR NENGSJ=2.0,  AIETLJ=2.0,    THSTCJ=0.0,
      JIALOC=25.8, JELLOC=4.33,   JEVLOC=5.625,
      JEALOC=33.3, JINLTA=2.243,
      AMBTMP=59.7, AMBSTP=2116.8, JERAD=0.755$

CASEID TOTAL: Citation II Model 550 Aircraft (Simple)
```

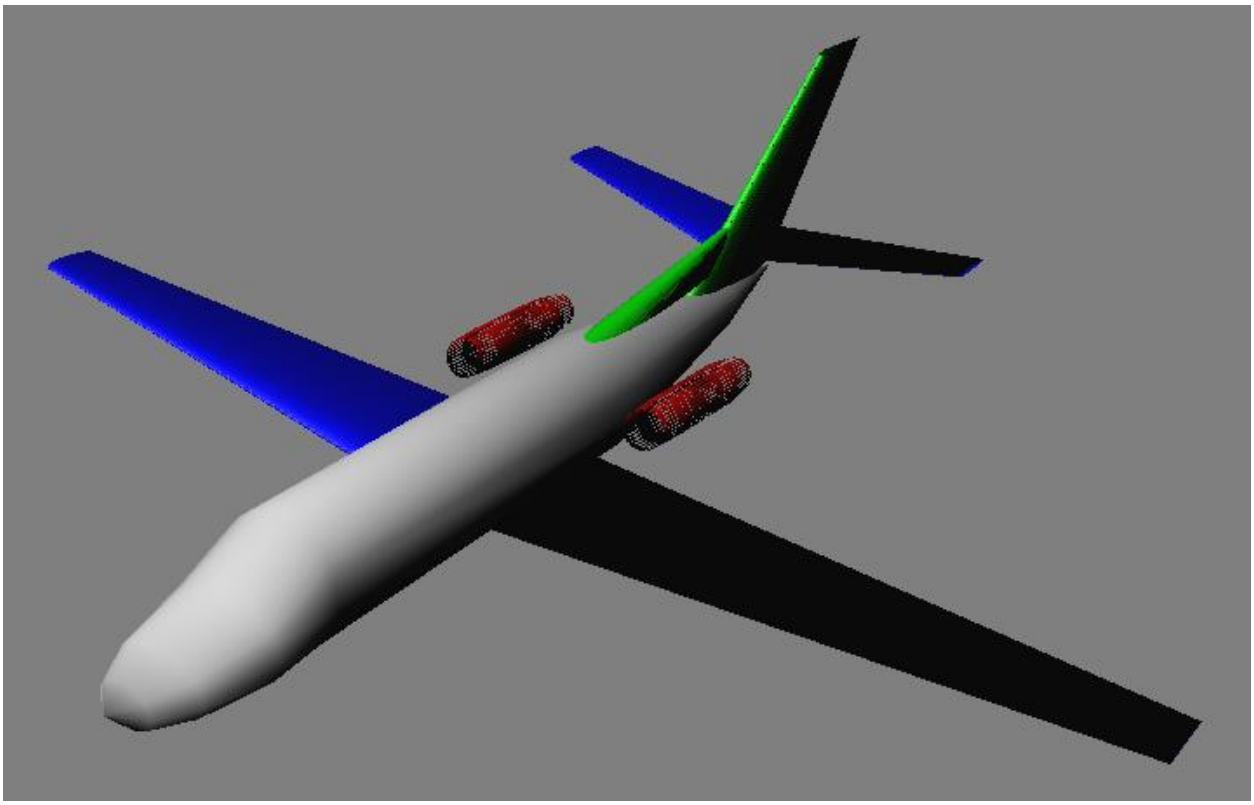

Figure 64: DATCOM AC3D Model Utilised for Rigid Body Simulation